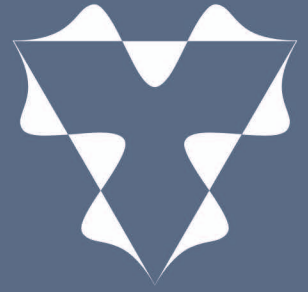
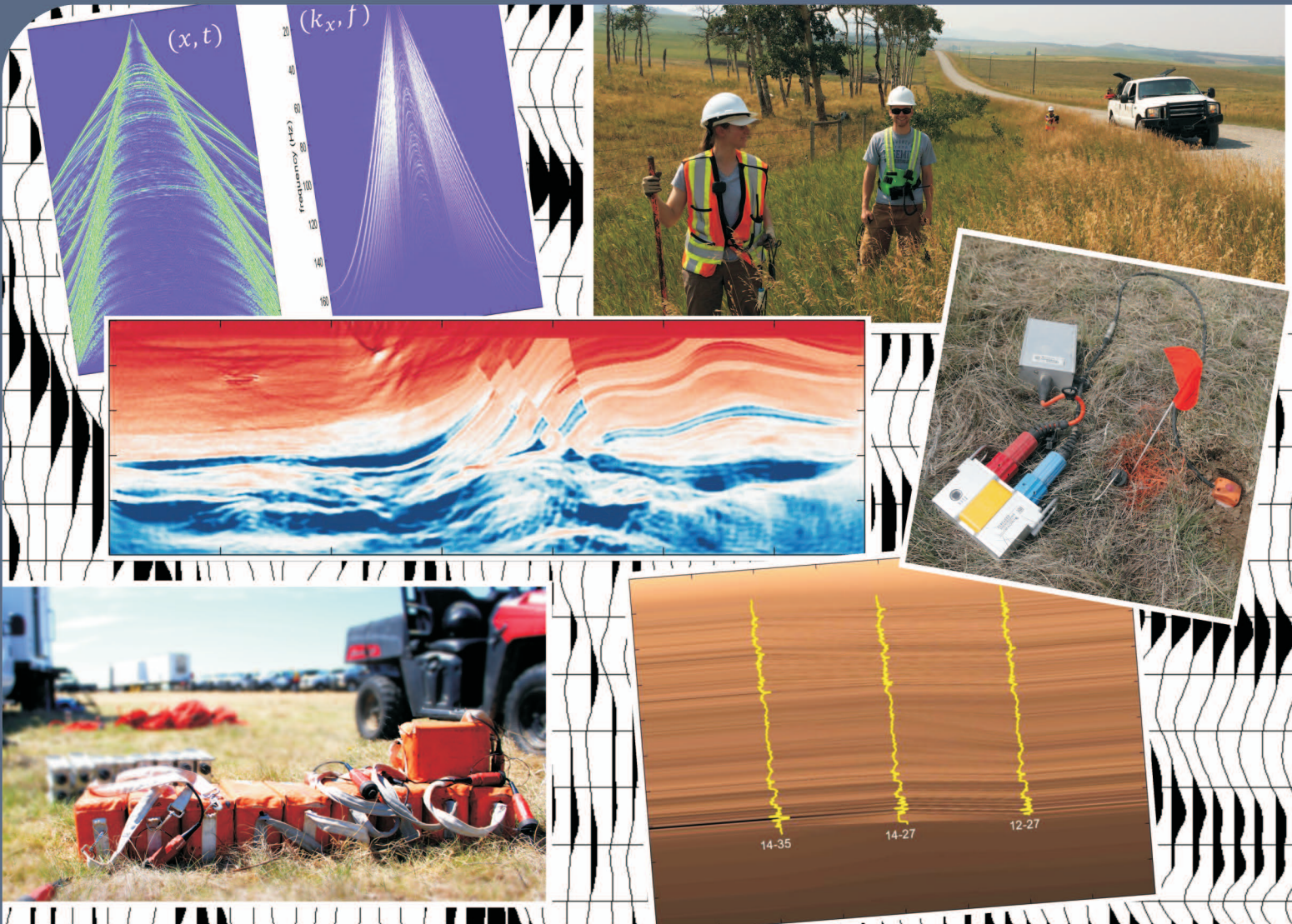


CREWES



CONSORTIUM FOR RESEARCH IN ELASTIC WAVE EXPLORATION SEISMOLOGY



2015 Sponsors Meeting

Banff Park Lodge Resort Hotel and Conference Centre

December 2nd - December 4th



Providing Advanced Seismic Imaging to the Geophysics Community
for 27 years



UNIVERSITY OF CALGARY
FACULTY OF SCIENCE
Department of Geoscience



Research Report 2015
Volume 27

In this volume...

Report Summaries

On the memory stick...

Complete Reports
Student Theses



UNIVERSITY OF CALGARY
FACULTY OF SCIENCE
Department of Geoscience

Notice of Intent to Publish

Please note that the authors of the research in this 27th Volume of the Abstract Book intend to publish or otherwise publically disseminate their full research papers in the coming calendar year. According to the contracts between the University of Calgary (CREWES) and each Sponsor, the University will make available to the Sponsor a copy of the proposed publication resulting from the CREWES Project prior to submission for publication. In the event that the Sponsor determines that Research Results within the proposed publication contain Sponsor Confidential Information, the Sponsor shall have thirty (30) days to notify the University in writing and the University shall remove Sponsor Confidential information prior to publication. This 30 day period shall be considered to have started at the end of this meeting (December 4, 2015). These full research reports are distributed on memory sticks at the CREWES annual meeting and are available on the CREWES website to all Sponsors and their employees.



CREWES Project faculty, staff and students, September 2015

Left to Right:

Front Row: Kevin Hall, Dave Henley, Helen Isaac, Kris Innanen, Scott Keating, Oliver Lahr, Raúl Cova, Michelle Montano, Adriana Gordon.

Second Row: Winnie Ajiduah, Heather Hardeman, Shahin Moradi, Bona Wu, Emma Lv, Gary Margrave, Shahin Jabbari, Jessica Dongas, Ali Fathalian, Marcelo Guarido de Andrade, Joe Wong, Bobby Gunning, Don Lawton

Back Row: Jian Sun, Tiansheng Chen, Davood Nowroozi, Junxiao Li, Sina Esmaeili, Sergio Romahn, Wenying Pan, Shahpoor Moradi, Khaled Al Dulaijan, Khalid Almuteri, Larry Lines, Andrew Mills, Tunde Arenrin, Eric Rops, Rafael Asuaje, Kennedy Nwafor, Laura Baird, Kevin Bertram

CREWES in 2015

Welcome to our 27th annual Sponsors meeting. In a climate of continued low oil prices and crises around the globe, we hope that you will find our meeting to be a welcome technical retreat. We realize that many of you traveled great distances to be here and we are committed to making the meeting worth your while. We ask you to relax and enjoy our presentations and to take advantage of the wonderful mountain setting of our meeting.

These are very challenging times for our industry and for applied geophysics in particular. Even in good economic times, the value of geophysics is questioned by some, and now in these times the need to provide positive answers to such value questions has become vital. We recognize this need and have tried our best to focus our efforts on those issues that seem most likely to increase the value of exploration seismology. Our selection of which topics to address has been strongly influenced by industry feedback both at our annual meetings and throughout the year. We hope you will feel motivated to provide comments and suggestions either directly to individual researchers or to CREWES leadership.

In the midst of this turmoil, CREWES is also transitioning leadership. With my retirement at the end of this year, Kris Innanen will become CREWES Director. I'm very grateful for the support you have shown us during my tenure and I hope you will continue that support under our new leadership. With a change in leadership there is always a change in perspective and this can be a very good thing. Please take time to meet our new Director and learn about his research interests while you communicate your priorities.

As is evident from our agenda, we have had a very active year and have managed to address a wide variety of topics. It is always uplifting to me to see the quality of the work that emerges each year, mostly from our students. I'm confident that the current downturn will soon transition into a renewal and that our industry will be grateful for the efforts of these young scientists. Your wisdom and experience will be warmly received as you hear about their work and provide commentary that could influence them for many years to come.

Again, we hope you will enjoy both the technical content and the fellowship of our meeting. Thank you very much for your support and attendance.

Calgary, Alberta
December, 2015

Gary Margrave
CREWES Director

Table of Contents

CREWES in 2015	i
Table of Contents	ii
2015 CREWES Sponsors	viii
CREWES Personnel	ix
Student Theses	xvi

Numerical modeling of elastic waves propagation in isotropic vertically inhomogeneous media.

Sitamai W. Ajiduah, Gary F. Margrave and P. F. Daley..... 1

3D Seismic Physical modeling for azimuthal variations of P-wave velocity

Khaled Al Dulaijan, Gary F. Margrave, and Joe Wong 2

Azimuthal velocity analysis of 3D seismic for fractures: Altoment-Bluebell field

Khaled Al Dulaijan*, and Gary F. Margrave 3

Full waveform inversion of Hussar synthetics

Babatunde Arenrin* and Gary Margrave..... 4

Going outside, acquisition and learning in the field

Kevin L. Bertram, Malcolm B. Bertram, Kevin W. Hall, Kristopher A.H. Innanen, Don C. Lawton and Joe Wong..... 5

AVO inversion through iteration of direct nonlinear inverse formulas

Tiansheng Chen and Kris Innanen 6

Processing converted-wave data in the tau-p domain: rotation toward the source and moveout correction

Raul Cova and Kris Innanen 7

Shear wave near-surface corrections in the tau-p domain: a case study

Raul Cova*, Xiucheng Wei and Kris Innanen 8

Phase correction of Gabor deconvolution

Tianci Cui and Gary F. Margrave..... 9

Seismic-to-well ties by smooth dynamic time warping

Tianci Cui* and Gary F. Margrave 10

Finite difference methods for orthorhombic media: perfectly reflecting and absorbing boundaries

P.F. Daley 11

* Presenter

Inversion of quasi-compressional ray travel time data for anisotropic parameters in a TI Medium using phase velocities	
P.F. Daley	12
Isotropic and transversely isotropic media: absorbing bottom boundary conditions	
P.F. Daley	13
Development and characterization of a geostatic model for shallow CO₂ injection	
Jessica M. Dongas and Don C. Lawton.....	14
Influence of color operator on Husky Hussar data	
Sina Esmaeili* and Gary F. Margrave.....	15
AVO modelling of linearized Zoeppritz approximations	
Ali Fathalian and Kris Innanen	16
Direct nonlinear inversion of viscoacoustic media using the inverse scattering series	
Ali Fathalian and Kris Innanen	17
Full waveform inversion using the PSPI migration: a convergence study	
Marcelo Guarido*, Laurence Lines, Robert Ferguson	18
Receiver statics of converted waves without stacking reflections: test with real data	
Saul E. Guevara, J. Helen Isaac, and Gary F. Margrave.....	19
Multicomponent seismic data analysis for interval rock properties in the Marcellus Shale	
Bobby J. Gunning* and Don C. Lawton	20
Preliminary interpretation of 3C-3D seismic data from an Athabasca oil sands field, Alberta	
Bobby J. Gunning, Don C. Lawton and Helen Isaac.....	21
Initial 3C-2D surface seismic and walkaway VSP results from the 2015 Brooks SuperCable experiment	
Kevin W. Hall*, J. Helen Isaac, Joe Wong, Kevin L. Bertram, Malcolm B. Bertram, Donald C. Lawton, Xuewei Bao and David W.S. Eaton.....	22
Using corrected phase to localize geological features in seismic data	
Heather Hardeman, Michael P. Lamoureux.....	23
3D or not 3D, that is the question: raypath interferometry in 3D processing	
David C. Henley*	24
Absorption in FWI – some questions and answers	
Kris Innanen.....	25

Direct measurement of near surface seismic body wave dispersion from uncorrelated vibratoseis data	
Kris Innanen.....	26
A nonstationary search parameter for internal multiple prediction	
Kris Innanen.....	27
Residual dependent FWI sensitivities based on direct nonlinear inverse scattering	
Kris Innanen.....	28
Time domain internal multiple prediction	
Kris Innanen*	29
3D3C seismic data at the Brooks experimental CO₂ injection site	
J. Helen Isaac* and Don C. Lawton	30
A little case study of an offset-dependent seismic response	
J. Helen Isaac and Don C. Lawton	31
Analysis of time-lapse difference AVO with the Pouce Coupe field data	
Shahin Jabbari, David D'Amico, Jeff Grossman, Brian H. Russell, Helen Isaac, and Kris Innanen.....	32
PS and SP converted wave reflection coefficients and their application to time-lapse difference AVO	
Shahin Jabbari and Kris Innanen.....	33
Extrapolation of low frequencies and application to physical modeling data	
Scott Keating and Kris Innanen	34
Interpolation of seismic data using a principal component analysis POCS approach	
Scott Keating and Kris Innanen	35
Nonstationary L₁ adaptive subtraction and application to inverse scattering multiple attenuation	
Scott Keating*, Jian Sun, Pan Pan, Kris Innanen	36
Second order, iterative least squares inversion of dispersive reflections	
Scott Keating, Kris Innanen	37
Preservation of AVO after migration	
Oliver Lahr and Gary F. Margrave	38
Tweaking minimum phase calculations	
Michael P. Lamoureux, Gary F. Margrave	39
New approaches to seismic monitoring at the Brooks Field Research Station	
Don Lawton*, Malcolm Bertram, Kevin Hall and Kevin Bertram	40

Azimuth ambiguity elimination for borehole imaging using 3D borehole RTM scheme	
Junxiao Li, Kris Innanen, Guo Tao, Laurence R. Lines and Kuo Zhang	41
Reflection extraction from sonic log waveforms using Karhunen-Loeve transform	
Junxiao Li, Kris Innanen, Guo Tao and Laurence R. Lines	42
Wave field simulation on 3D borehole dipole radiation	
Junxiao Li*, Kris Innanen, Kuo Zhang, Guo Tao and Laurence R. Lines	43
Utilizing PSSP Waves	
Laurence R. Lines* and Patrick F. Daley	44
Gabor nonstationary deconvolution for attenuation compensation in highly lossy dispersive media	
Kay Y. Liu, Elise C. Fear, and Mike E. Potter	45
Recording seismic on geophones within ground screws II	
Peter M. Manning, Eric Gallant, Kevin Hall.....	46
Intrinsic attenuation: removing the stratigraphic effect from attenuation measures	
Gary F. Margrave*, Sylvestre Charles (Suncor), and Hossein Aghabarati (Suncor).....	47
Post-stack iterative modeling migration and inversion (IMMI)	
Gary F. Margrave.....	48
Shear wave attenuation measurements from converted-wave VSP data	
Michelle C. Montano*, Don C. Lawton, and Gary F. Margrave.....	49
Finite difference modeling of the diffusive slow P-wave in poroelastic media	
Shahin Moradi, Don C. Lawton and Edward S. Krebs	50
Full viscoelastic waveform inversion: a mathematical framework	
Shahpoor Moradi* and Kris Innanen.....	51
Radiation patterns associated with the scattering from viscoelastic inclusions	
Shahpoor Moradi and Kris Innanen	52
Sensitivity analysis of viscoelastic full waveform inversion	
Shahpoor Moradi and Kris Innanen	53
Viscoelastic AVO equation updates: Born versus Aki-Richards approximations	
Shahpoor Moradi and Kris Innanen	54
A framework for full waveform modeling and imaging for CO₂ injection at the FRS project	
Davood Nowroozi, Donald C. Lawton.....	55

Full-waveform inversion in the frequency-ray parameter domain	
Wenyong Pan, Kristopher Innanen	56
FWI numerical test using Hussar dataset	
Wenyong Pan, Kristopher Innanen, Gary Margrave, Nassir Seed	57
Preconditioning for the Hessian-free Gauss-Newton full-waveform inversion	
Wenyong Pan, Kristopher Innanen, Wenyuan Liao	58
Recover low-frequency for full-waveform inversion via band-limited impedance inversion and projection onto convex sets	
Wenyong Pan, Kristopher Innanen, Gary Margrave, Scott Keating	59
Source-independent Hessian-free Gauss-Newton full-waveform inversion	
Wenyong Pan, Kristopher Innanen	60
Suppressing cross-talk for elastic FWI with multi-parameter approximate Hessian and its parameter-type approximation	
Wenyong Pan*, Kristopher Innanen	61
Effects of available long offset and random noise on simultaneous-AVO inversion	
Sergio Romahn and Kris Innanen	62
Repercussions of available long offset, random noise and impedance contrast on AVO analysis	
Sergio Romahn and Kris Innanen	63
Predicting heavy oil viscosity from well logs - testing the idea	
Eric A. Rops* and Laurence R. Lines	64
Predicting oil sands viscosity from well logs using an industry provided dataset	
Eric A. Rops and Laurence R. Lines	65
Visualizing inversion results with rock physics templates	
Brian Russell*	66
1.5D internal multiple prediction: physical modelling results	
Jian Sun, Kristopher A.H. Innanen, Pan Pan	67
2D internal multiple prediction in coupled plane wave domain	
Jian Sun*, Kristopher A.H. Innanen	68
AVO inversion with a combination of series reversion and Gauss-Newton iteration	
Jian Sun, Kristopher A.H. Innanen	69
Internal multiple prediction in the tau-p domain: 1.5D synthetic results	
Jian Sun, Kristopher A.H. Innanen	70

The Borga transform and some applications in seismic data analysis	
Todor I. Todorov and Gary F. Margrave	71
Field and numerical investigation of filtered m-sequence pilots for vibroseis acquisition	
Joe Wong and David Langton.....	72
Upgrading the CREWES seismic physical modeling facility	
Joe Wong*, Kevin Bertram, and Kevin Hall	73
Interpretation of a multicomponent walkaway vertical seismic profile data	
Bona Wu*, Don C. Lawton, and Kevin W. Hall	74
Porosity prediction using cokriging with multiple secondary datasets	
Hong Xu*, Jian Sun, Brian H. Russell, and Kris A. Innanen	75
Explosion source data analysis from a Jordanian quarry	
Matthew Yedlin*, Gary F. Margrave, and Yochai Ben Horin	76

2015 CREWES Sponsors

Acceleware	BHP Billiton Petroleum (Americas) Inc.
CGG	Chevron Corporation
ConocoPhillips	Devon Energy Corporation
Exxon Mobil Corporation	Geokinetics Inc.
Halliburton	INOVA Geophysical Equipment Ltd.
Nexen Energy ULC	Northwest Geology Institute, CNPC
Pemex	Petrobras
Petronas Carigali SDN BHD	Repsol, S.A.
Saudi Aramco	Sensor Geophysical Ltd. (a Global Geophysical Services, Inc. company)
Shell Canada Limited	Sinopec
Suncor Energy Inc.	Tullow Oil p.l.c.

Natural Sciences and Engineering Research Council of Canada (NSERC)
- Collaborative Research and Development Grant, #CRDPJ 461179-13

CREWES Personnel

LEADERSHIP

Gary F. Margrave, Director

Professor, Department of Geoscience, University of Calgary

B.Sc. Physics, 1975, University of Utah

M.Sc. Physics, 1977, University of Utah

Ph.D. Geophysics, 1981, University of Alberta

- Work Experience: Chevron Canada Resources, Chevron Geoscience Company

Kristopher A. Innanen, Associate Director

Associate Professor, Department of Geoscience, University of Calgary

B.Sc. Physics and Earth Science, 1996, York University

M.Sc. Physics, 1998, York University

Ph.D. Geophysics, 2003, University of British Columbia

- Work Experience: University of Houston

Don C. Lawton, Associate Director

Professor, Department of Geoscience, University of Calgary

B.Sc. (Hons. Class I) Geology, 1973, University of Auckland

Ph.D. Geophysics, 1979, University of Auckland

- Work Experience: New Zealand Steel Mining Ltd., Amoco Minerals (N.Z.) Ltd., Carbon Management Canada

Laura A. Baird, Program Manager

BA, History, 1992, University of Calgary

- Work Experience: Alberta Cancer Board, Department of Geoscience at the University of Calgary

Kevin W. Hall, Technical Manager

B.Sc. Geophysics, 1992, University of Calgary

M.Sc. Geophysics, 1996, University of Calgary

- Work Experience: Lithoprobe Seismic Processing Facility at the University of Calgary

ADJUNCT DIRECTORS

Laurence R. Lines

Professor and Interim Head, Department of Geoscience, University of Calgary

B.Sc. Physics, 1971, University of Alberta

M.Sc. Geophysics, 1973, University of Alberta

Ph.D. Geophysics, 1976, University of B.C.

- Work Experience: Amoco Production Research, Tulsa University, Memorial University of Newfoundland

ASSOCIATED FACULTY AND SCIENTISTS

Andreas Cordsen

Technical Advisor, CREWES, University of Calgary

M.Sc. Geology, 1975, Queen's University, Kingston

M.Sc. Geophysics, 1980, Dalhousie University, Halifax

- Work Experience: BEB, Esso Resources, Norcen Energy, GEDCO, Schlumberger

Michael P. Lamoureux

Professor, Department of Mathematics and Statistics, University of Calgary

Adjunct Professor, Department of Geoscience, University of Calgary

B.Sc. Mathematics, 1982, University of Alberta

M.Sc. Mathematics, 1983, Stanford University

Ph.D. Mathematics, 1988, University of California, Berkeley

- Work Experience: Farallon Computing, NSERC Canada

Roy O. Lindseth MC., FRSC

Technical Advisor, CREWES, University of Calgary

Doctor of Laws, Honoris Causa, 1978, University of Calgary

- Work Experience: Chevron; NSERC, Teknica Corporation; TCPL

Brian H. Russell

Adjunct Professor, Department of Geoscience, University of Calgary

B.Sc. Physics, 1972, University of Saskatchewan

Honours Certificate in Geophysics, 1975, University of Saskatchewan

M.Sc. Geophysics, 1978, University of Durham

Ph.D. Geophysics, 2004, University of Calgary

- Work Experience: Chevron Geoscience Company, Teknica Resource Development, Veritas Software Ltd., Hampson-Russell Software Ltd.

Robert R. Stewart

Cullen Chair in Exploration Geophysics, University of Houston

Adjunct Professor, Department of Geoscience, University of Calgary

B.Sc. Physics and Mathematics, 1978, University of Toronto

Ph.D. Geophysics, 1983, Massachusetts Institute of Technology

- Work Experience: Veritas Software Ltd., Gennix Technology Corp., University of Calgary

Xiucheng Wei

Technical Advisor, CREWES, University of Calgary

B.Sc. Geophysics, 1982, China University of Petroleum

M.Sc. Geophysics, 1992, China University of Petroleum

Ph.D. Geophysics, 1995, China University of Petroleum

- Work Experience: China National Petroleum Company (CNPC), China University of Petroleum (CUP), British Geological Survey (BGS), China Petroleum & Chemical Corporation (Sinopec)

Matt Yedlin

Associate Professor, Department of Electrical and Computer Engineering, University of British Columbia

B.Sc. Honors Physics, 1971, University of Alberta

M.Sc. Physiology, 1973, University of Toronto

Ph.D. Geophysics, 1978, University of British Columbia

- Work Experience: Conoco

RESEARCH STAFF, POST DOCS AND VISITING SCHOLARS

Kevin L. Bertram

Electronics Technician Certificate, 2005, Southern Alberta Institute of Technology

- Work Experience: Aram Systems Ltd.

Malcolm B. Bertram

B.Sc. Geology, Auckland, New Zealand

- Work Experience: GSI (Western Australia), Western Geophysics (Western Australia), Auckland University, University of Calgary.

Huaizhen Chen

B.Sc., Geophysics, 2010, China University of Petroleum

Ph.D., Geophysics, 2015, China University of Petroleum

Tiansheng Chen

B.Sc., Applied Geophysics, 2001, Daqing Petroleum Institute, China

M.Sc., Geophysics, 2003, China University of Petroleum

Ph.D., Geophysics, 2006, China University of Petroleum

- Work Experience: Petroleum Exploration and Production Research Institute, SINOPEC, China

Patrick F. Daley

B.Sc. Mathematics, 1974, University of Alberta

M.Sc. Physics 1976, University of Alberta

Ph.D. Geophysics, 1979, University of Alberta

- Work Experience: Independent contractor associated with research centres of major oil companies

Yu Geng

B.Sc. Information Engineering, 2005, Xi'an Jiaotong University

Ph.D. Information and Communication System, 2014, Xi'an Jiaotong University

- Work Experience: MILAB, IGPP, Department of Earth and Planetary Sciences, University of California, Santa Cruz

David C. Henley

B.Sc. Physics, 1967, Colorado State University

M.Sc. Physics, 1968, University of Michigan

- Work Experience: Shell Oil Co., Shell Canada Ltd

Helen Isaac

B.Sc. Mathematics, 1973, Imperial College, London

M.Sc. Geophysics, 1974, Imperial College, London

Ph.D. Geophysics, 1996, University of Calgary

- Work Experience: Phillips Petroleum Company, Hudson's Bay Oil and Gas, Canterra Energy, Husky, Fold-Fault Research Project at the University of Calgary

Joe Wong

B.Sc. Physics/Mathematics, 1971, Queen's University

M.Sc. Applied Geophysics, 1973, University of Toronto

Ph.D. Applied Geophysics, 1979, University of Toronto

- Work Experience: Ontario Ministry of the Environment, University of Toronto, JODEX Applied Geoscience Limited

GRADUATE STUDENTS

Winnie Ajiduah

B.Sc. Physics, University of Benin, Nigeria

M.Sc. Geophysics, University of Port Harcourt, Nigeria

- Work Experience: Shell Petroleum Development Company of Nigeria

Khaled Al Dulaijan

B.Sc. Geosciences, 2003, University of Tulsa, Oklahoma

M.Sc. Geophysics, 2008, University of Calgary

- Work Experience: Saudi Aramco

Khalid Almuteri

B.Sc. Geophysics, 2012, University of Houston

- Work Experience: Saudi Aramco

Babatunde Arenrin

B.Sc. Geophysics, 2005, University of Lagos, Nigeria.

M.Sc. Petroleum Geophysics, 2010, Imperial College London, UK.

- Work Experience: WesternGeco Norway.

Rafael Asuaje

B.Sc. Mechanical Engineering 2005, Kettering University, USA

M.Sc. Mechanical Engineering 2006, Kettering University, USA

- Work Experience: Faurecia Interior Systems.

Raúl Cova

B.Sc. Geophysical Engineering, 2004. Simon Bolivar University, Venezuela.

Graduate Diploma in Petroleum Studies, 2011. IFP School. Venezuela

- Work experience: PDVSA Intevep. Venezuela

Tianci Cui

B.Sc. Geophysics, 2013, China University of Petroleum (Beijing)

Jessica Dongas

B.Sc. Hons. Geological Sciences, 2013, Queen's University

- Work experience: Schlumberger – Carbon Services, Calgary

Sina Esmaeili

B.Sc. Physics, 2009, Science and Research University - Iran

M.Sc. Field Theory and Particle Physics, 2011, Science and Research University, Iran

Ali Fathalian

B.Sc. Applied Physics, 2001, University of Razi, Iran

M.Sc. Condensed Matter Physics, 2003, University of Razi, Iran

Ph.D. Condensed Matter Physics, 2007, University of Razi, Iran

Adriana Gordon

B.Sc. Geophysics 2015, Simon Bolivar University, Venezuela.

Marcelo Guarido de Andrade

B.Sc. Physics, 2006, University of São Paulo, Brazil

M.Sc. Geophysics, 2008, University of São Paulo, Brazil

- Work Experience: Schlumberger-WesternGeco (Houston) and Georadar Leventamentos Geofísicos S.A. (Brazil), Orthogonal Geophysics (Canada)

Bobby Gunning

B.Sc. Geophysics (first class honours), 2014, University of Calgary

- Work Experience: MEG Energy, Devon Energy, Canadian Natural Resources Limited

Heather Hardeman

B.Sc. Mathematics (summa cum laude), 2012, University of Montevallo, AL, USA.

M.A. Mathematics, 2014, Wake Forest University, NC, USA.

Shahin Jabbari

B.Sc. Mathematics applied in Physics, 1992, University of Tehran, Iran

M.Sc. Medical Physics, 1997, Tabriz University of Medical Sciences, Iran

M.Sc. Medical Physics, 2010, University of Calgary

- Work Experience: Encana Corporation, Sessional Instructor in the Department of Geoscience at the University of Calgary

Scott Keating

B.Sc. Honours Physics 2014, University of Alberta

Junxiao Li

B.Sc. Science of information and Computing (Geophysics), 2009, China University of Petroleum (Beijing)

Bachelor of Arts. English, 2009, China University of Petroleum (Beijing)

M.Sc. Geophysics, 2012, China University of Petroleum (Beijing)

Kay Yuhong Liu

- B.Sc. Electrical and Computer Engineering, 1996, Wuhan University, China
M.Sc. Electrical and Computer Engineering, 2005, University of Calgary, Canada
- Work Experience: CGG, Divestco Inc.

Siming (Emma) Lv

- B.Sc. Geophysics, 2015, China University of Petroleum (East China)

Oliver Lahr

- B.Sc. Pure and Applied Mathematics, 1988, University of Calgary
- Work Experience: Hampson-Russell Software Ltd.

Andrew Mills

- BSc Geophysics, 2014, University of Calgary
- Work experience: Nexen Energy

Michelle Montano

- B.Sc. Geophysics 2008, Simon Bolivar University, Venezuela
- Work experience: PDVSA Sismica Biellovenezolana, Daqing de Venezuela

Shahin Moradi

- B.Sc. Applied Physics, 2006, University of Razi, Iran
M.Sc. Geophysics, 2010, University of Tehran, Iran

Shahpoor Moradi

- B.Sc. Applied Physics, 2000, University of Razi, Iran
M.Sc. Theoretical Physics, 2002, University of Razi, Iran
Ph.D. Theoretical Physics, 2006, University of Razi, Iran

Davood Nowroozi

- B.Sc. Mining engineering, University of Tehran, 1996
M.Sc. Mining engineering, University of Tehran, 1999
- Work Experience: Geophysicist at National Iranian Oil Company

Wenyong Pan

- B.Sc. Computer and Software Engineering, 2009, China University of Geosciences (Beijing)
M.Sc. Geophysics, 2012, China University of Geosciences (Beijing)

Sergio Jorge Romahn Reynoso

- B. Eng. Geophysics, 2004, National University of Mexico
M.Sc. Exploration Geophysics, 2012, University of Leeds. U.K.
- Work Experience: PEMEX

Eric Rops

- B.Sc. Honors Geophysics, 2014, The University of Western Ontario (London Ontario)
- Work experience: Husky Energy, Sander Geophysics Ltd., Nexen-CNOOC

Jian Sun

B.Sc. Geophysics, 2009, Shandong University of Science and Technology, China
M.Sc. Geophysics, 2012, Shandong University of Science and Technology, China

Todor Todorov

B.Sc. Applied Geophysics, 1996, University of Mining and Geology, Bulgaria
M.Sc. Geophysics, 2002, University of Calgary
• Work Experience: Petro-Canada / SUNCOR Energy

Bona Wu

B.Sc., Applied Geophysics, 1999, Jianghai Petroleum Institute, China
M.Sc., Geophysics, 2006 China University of Petroleum
• Work Experience: CGGVeritas, Nexen Energy ULC

Kiki Xu

M.Sc. Computer Science, 2008, University of Calgary, Canada
• Work experience: Hampson-Russell Software Ltd.

Student Theses

The following theses are included with the CREWES 2015 Research Report:

Ph.D.	Xiaoqin (Jean) Cui	Seismic Forward Modeling of Fractures and Fractured Media Inversion
Ph.D.	Hassan Khaniani	Iterative Multiparameter Elastic Waveform Inversion Using Prestack Time Imaging and Kirchhoff approximation
M.Sc.	Pan (Penny) Pan	1.5D Internal Multiple Prediction: an Application on Synthetic Data, Physical Modelling Data and Land Data Synthetics
M.Sc.	Christopher Petten	Exploring Potential Applications of the Sharpe Hollow Cavity Model, the Gaussian Ball Source Model, and the Heelan Cylindrical Model in Modeling Explosive Pressure Sources

Numerical modeling of elastic waves propagation in isotropic vertically inhomogeneous media.

Sitamai W. Ajiduah, Gary F. Margrave and P. F. Daley

ABSTRACT

A method for calculation of complete theoretical seismograms for coupled P-Sv wave propagation in a vertically inhomogeneous media has been studied. Called the AMM method (for Alekseev-Mikhailenko), it is based on a combination of partial separation of variables via a finite Hankel transform over lateral coordinates and finite-differencing in time and depth. Results of theoretical seismograms for an isotropic vertically inhomogeneous model are presented in this paper and the effects of incidence angle and free-surface on component amplitudes are also investigated. Amplitudes from the AMM computations are compared with computations from the exact Zoeppritz equations for angles up to 60 degrees. All the computed amplitudes from AMM methods matched Zoeppritz amplitude at near vertical incidence up to 10 degrees (0.5km source-receiver offset). The P-P AMM and the P-P Zoeppritz amplitudes have the same trend for all pre-critical and post-critical angles; at the critical angle, Zoeppritz predicts an abrupt rise in amplitude while the AMM amplitudes show a gradual rise with a maximum beyond critical angle. The P-S amplitudes predicted from Zoeppritz matched with P-S AMM amplitudes only at near offset.

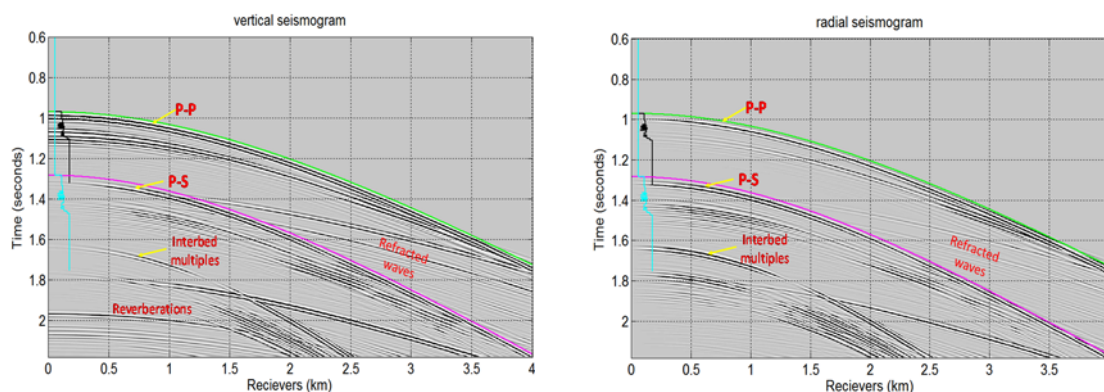


FIG. 1. Time-domain shot-gather for total vertical and horizontal component wavefields showing reflected events as well as refracted, converted waves and multiples. The black and cyan logs are the zero offset PP and PS two-way traveltime-velocity function.

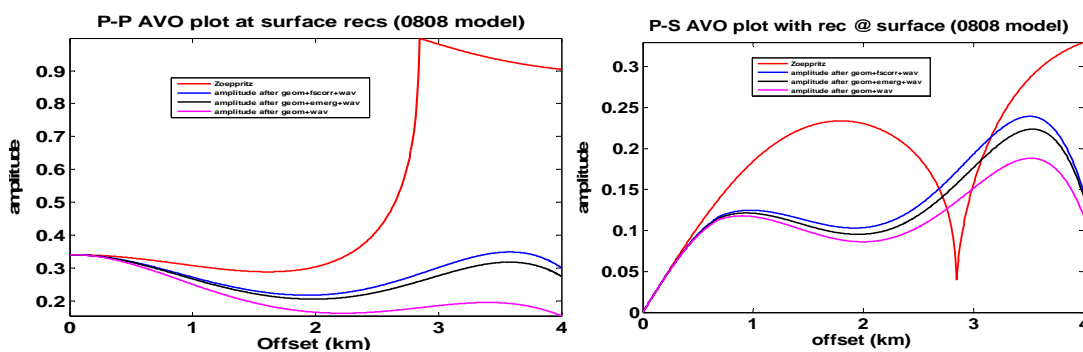


FIG. 2. P-P and P-S AVO amplitude plots before and after free-surface correction.

3D Seismic Physical modeling for azimuthal variations of P-wave velocity

Khaled Al Dulaijan, Gary F. Margrave, and Joe Wong

ABSTRACT

Information related to fracture orientation and intensity is vital for the development of unconventional hydrocarbons, such as tight sand gas and shale gas. Numerical modeling provides a valuable tool for geophysicists to test and validate their methodologies that provide them with information about reservoirs. Fractures make numerical modeling more complicated and introduce complexities that might even require geophysicists to validate their numerical models before using them to assess their methods. Alternatively, physical modeling provides a unique opportunity to test, validate, and develop methods for characterizing fractured reservoirs. This report utilizes seismic physical modeling to test a method for Velocity Variations with Azimuth (VVAz) based on the non-hyperbolic NMO equation for TI media that was derived by Grechka and Tsvankin (1998).

A three-layer model was built using vertically laminated Phenolic overlain by Plexiglas to represent a fractured reservoir overlaid by an isotropic overburden. HTI planes of phenolic have an orientation in northern half of the model that is orthogonal to HTI planes in southern half. A third layer of water is added to the model. 3D seismic data is acquired in patches. The data is processed with a surface-consistent amplitude and deconvolutions, so it can be used for amplitude analysis as well. Third reflector, in the CDP domain, is very weak due to attenuation of anisotropic phenolic and low fold of data. After sectoring the data, orientation and intensity of anisotropy is estimated by VVAz. Results of anisotropy orientation matches the physical model.

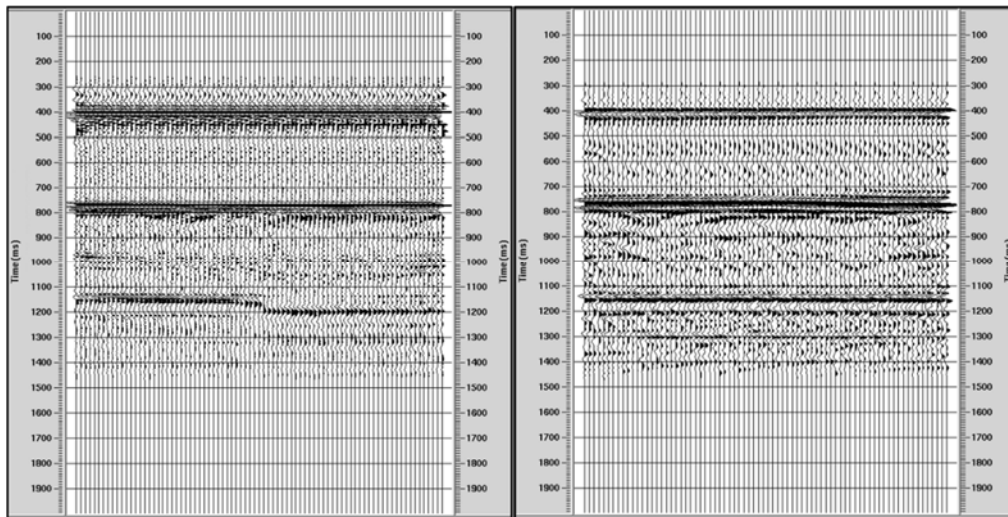


FIG. 1. CDP Stacks: an inline (left) and a crossline (right). The three strong reflectors are: top of plexiglas, top of phenolic and bottom of phenolic. HTI planes of phenolic have an orientation in northern half of the model that is orthogonal to HTI planes in southern half. CMP stacks are created using isotropic NMO velocities. From the geometry of the model, cross lines are always parallel to HTI planes. Crosslines are perpendicular to HTI planes in southern half of the model, as can be seen by the third reflector (bottom of phenolic).

Azimuthal velocity analysis of 3D seismic for fractures: Altomont-Bluebell field

Khaled Al Dulaijan*, and Gary F. Margrave

ABSTRACT

The 3D seismic data was acquired within Bluebell Field, the eastern portion of Altamont-Bluebell field in northeastern Utah. Altamont-Bluebell field is within the Uinta Basin, and is considered an unconventional reservoir in the sense that natural fractures act as fluid storage and conduits in the tight sandstones and carbonates. Information related to fracture orientation and intensity is vital for the development of such reservoirs. Therefore, this paper utilizes Velocity Variations with Azimuth (VVAz) to estimate the direction and intensity of fractured-induced anisotropy within one of the reservoirs, Upper Green River formation.

VVAz inversion method is applied based on the non-hyperbolic NMO equation for TI media that was derived by Grechka and Tsvankin (1998). Our code has been tested on a 3D physical modeling dataset and results are shown in another report. Isotropic NMO velocities are used along with azimuthally variant time residuals to estimate fast and slow NMO velocities and their direction. Hampson-Russel VVAZ has also been implemented and results are compared in the report.

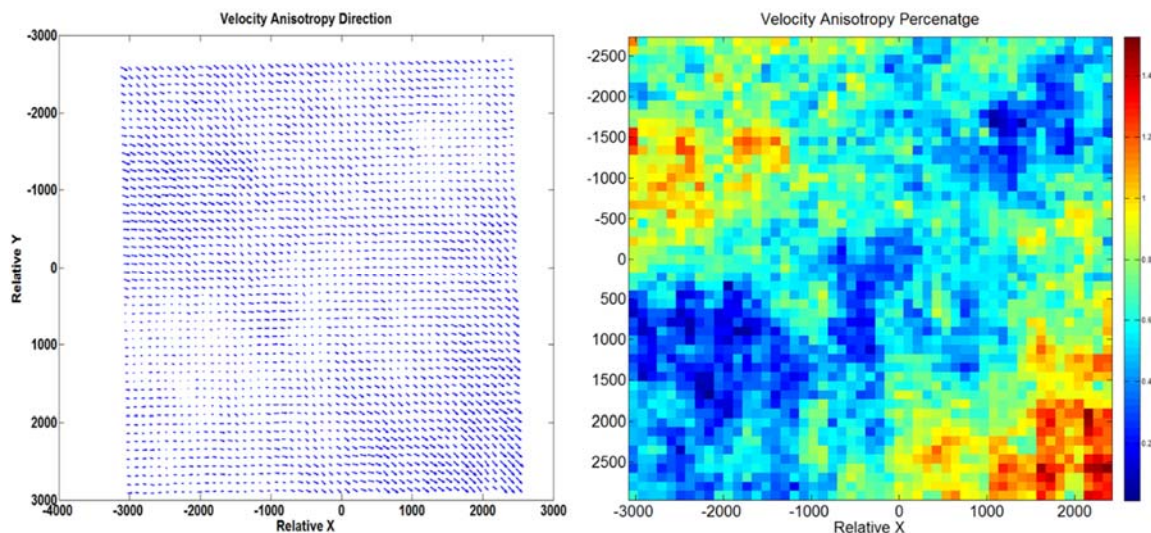


FIG. 1. VVAZ Results: Velocity Anisotropy Direction (left), and Velocity Anisotropy Percentage (right). X- and Y- coordinates are relative and referenced to VSP.

Full waveform inversion of Hussar synthetics

Babatunde Arenrin* and Gary Margrave

ABSTRACT

In this study, we present the result obtained from incorporating well log information into a conjugate gradient optimization scheme in Full Waveform Inversion (FWI). We test this approach on synthetic datasets generated using the three sonic logs from Hussar. Using formation tops to guide the interpolation, the sonic logs are interpolated to form the 2D velocity model used in this study. The initial velocity model for the inversion is a linear $v(z)$ velocity model. We adopt the conjugate gradient algorithm as described by Magnus R. Hestenes and Eduard Stiefel. Our results show that combining well information with conjugate gradient directions in FWI can save computational time, as well as getting a good inverted model after a few iterations. The inverted model shows encouraging results and this proves that the algorithm works well and can resolve thin beds in the model.

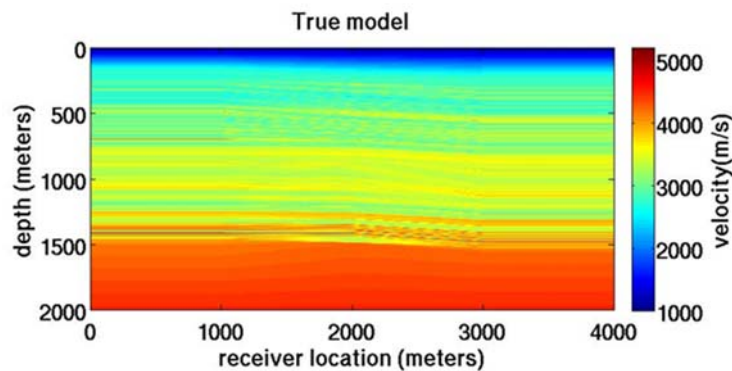


FIG. 1: True velocity model.

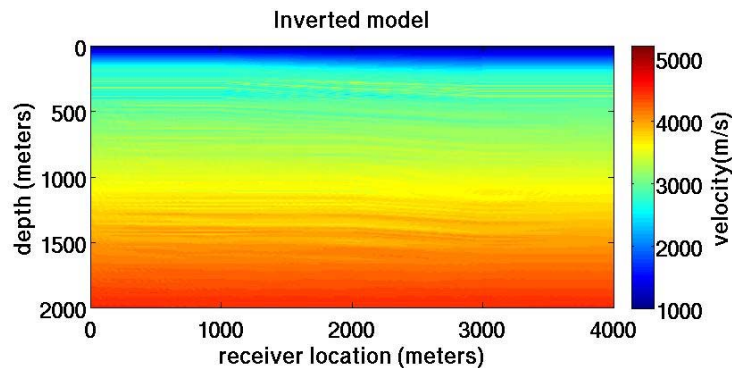


FIG 2. Inverted velocity model after 9 iterations.

Going outside, acquisition and learning in the field

Kevin L. Bertram, Malcolm B. Bertram, Kevin W. Hall, Kristopher A.H. Innanen, Don C. Lawton and Joe Wong

ABSTRACT

CREWES continues to perform actual seismic acquisition in the field using industry equipment. This opens up the possibilities of taking ideas from the minds of students and staff and taking them outside to try in real world situations. Students, staff and sponsors are able to see our equipment and suggest new methods in using it. CREWES data set are often created using this equipment. CREWES also brings some of this equipment and several support staff to the annual geophysics undergraduate field school. The Geophysics program at the University of Calgary is one of the very few that has access to commercial grade seismic equipment and has the opportunity for students to use it. For many students this is the first time that they actually observe and participate in the production of seismic data. This provides a much better understanding for these future geophysicists of how the environment affects data. This year CREWES assisted with a survey at the Brooks CMC test site, did a small demonstration at Earth Science for Society and aided with the annual geophysics field school.

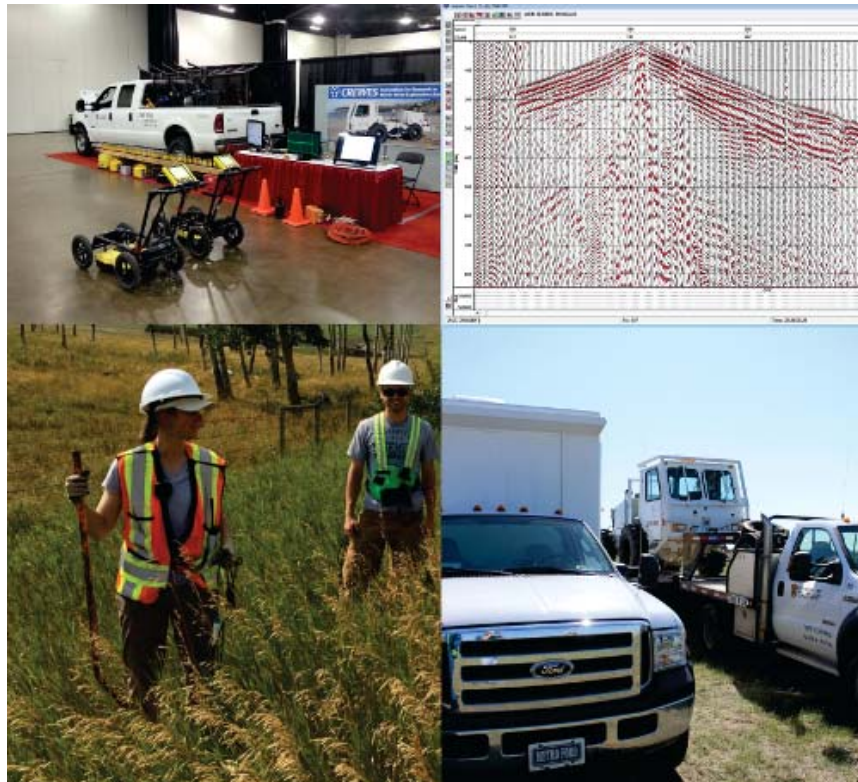


FIG. 1. Gathering data outside.

AVO inversion through iteration of direct nonlinear inverse formulas

Tiansheng Chen and Kris Innanen

ABSTRACT

Linear AVO inversion technique has been used widely in industry to invert elastic parameter. In this paper, we put forward a new inversion through iteration of direct nonlinear inverse formulas. Following the workflow presented by Innanen (Innanen 2011), I expand the reflection coefficient of PP wave and PS wave as function of elastic parameters contrast at third order. Those formulae can be used to invert elastic parameter by use of AVO series reversion method or Gauss-Newton iteration method. To solve the local convergence problem of Gauss-Newton iteration method, we introduce the first or second AVO series reversion result as the initial value. All of the experiments illustrate that reconstruction of contrasts from Gauss-Newton iteration of direct nonlinear inverse formulas is more accuracy and faster.

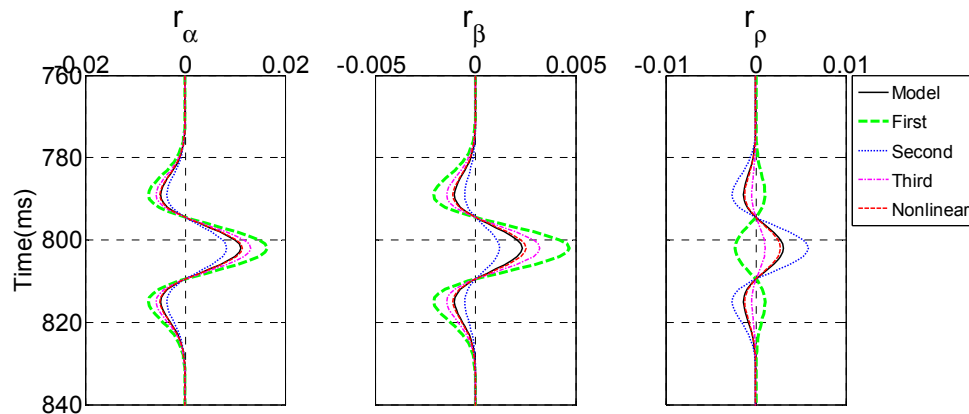


FIG. 1. (a) Input shot record containing two primaries and one multiple; (b) output of 1.5D space/time prediction, full record; (c) output of 1.5D space/time prediction, zero offset trace extracted (black original, blue prediction).

Processing converted-wave data in the tau-p domain: rotation toward the source and moveout correction

Raul Cova and Kris Innanen

ABSTRACT

The asymmetry of the converted-wave raypath is one of the main sources of complexity in the processing of multicomponent data. Such asymmetry is controlled by Snell's law, which also states that in an isotropic and flat layered medium the ray-parameter value p is preserved, even for converted-wave modes. In this study we propose processing converted-wave data in the ray-parameter domain as a more suitable framework for dealing with this type of waves. Here we address the problem of rotations toward the source in 2D media with dipping reflectors, converted-wave velocity analysis and NMO corrections. Results show that reversing the polarity of the traces to correct for the orientation of the horizontal components around the zero ray-parameter condition provides consistent polarities along all the events. Also, using an elliptical approximation to the PS-moveout in τ - p domain provides an alternative tool for velocity analysis and converted-wave moveout correction. Its implementation is very similar to the conventional processing in x - t domain. However, results show that in τ - p domain the information in shallow events can be fully exploited. The ability of shallow events to reach wider reflection angles, therefore larger ray-parameter values, makes them a good target for processing in τ - p domain. An accurate algorithm for the τ - p transformation is required to avoid introducing numerical artifacts. Here we noticed that the polarity reversals present in the converted-wave events are a new source of these artifacts. Efforts on developing a new τ - p algorithm able to account for these polarity reversals is needed to provide cleaner data for further processing.

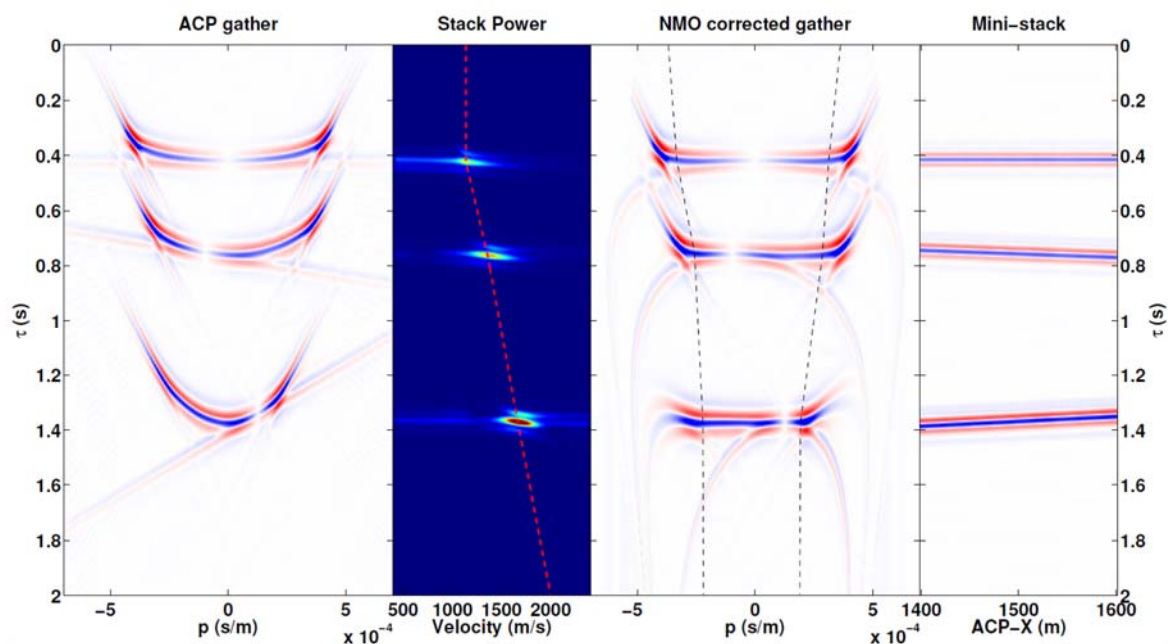


FIG. 1. Velocity analysis and NMO correction of converted-wave data in τ - p domain.

Shear wave near-surface corrections in the tau-p domain: a case study

Raul Cova*, Xiucheng Wei and Kris Innanen

ABSTRACT

Removing near-surface effects in the processing of 3C data is key to exploiting the information provided by converted waves. Receiver-side corrections may need a more accurate approach than source-side corrections due to the complex character of S-wave propagation in the near-surface. In this study a raypath-consistent approach is used to correct the S-wave near-surface effects. This is achieved by transforming the data sorted in receiver gathers to the τ - p domain and performing cross-correlation and convolution operations to capture and subtract the near-surface effects from the data. Results show that this processing improves coherency and stacking power of shallow and deep events simultaneously. Shallow events benefited most from this processing due to their wider range of reflection angles. We also show how the correction of receiver orientations based on reversing the polarity of one of the ends of the spread does not consider receiver stations offset due to obstacles during the acquisition. A full 2D rotation toward the source, as in 3D-3C processing, was applied in this study to account for irregularities in the acquisition geometry.

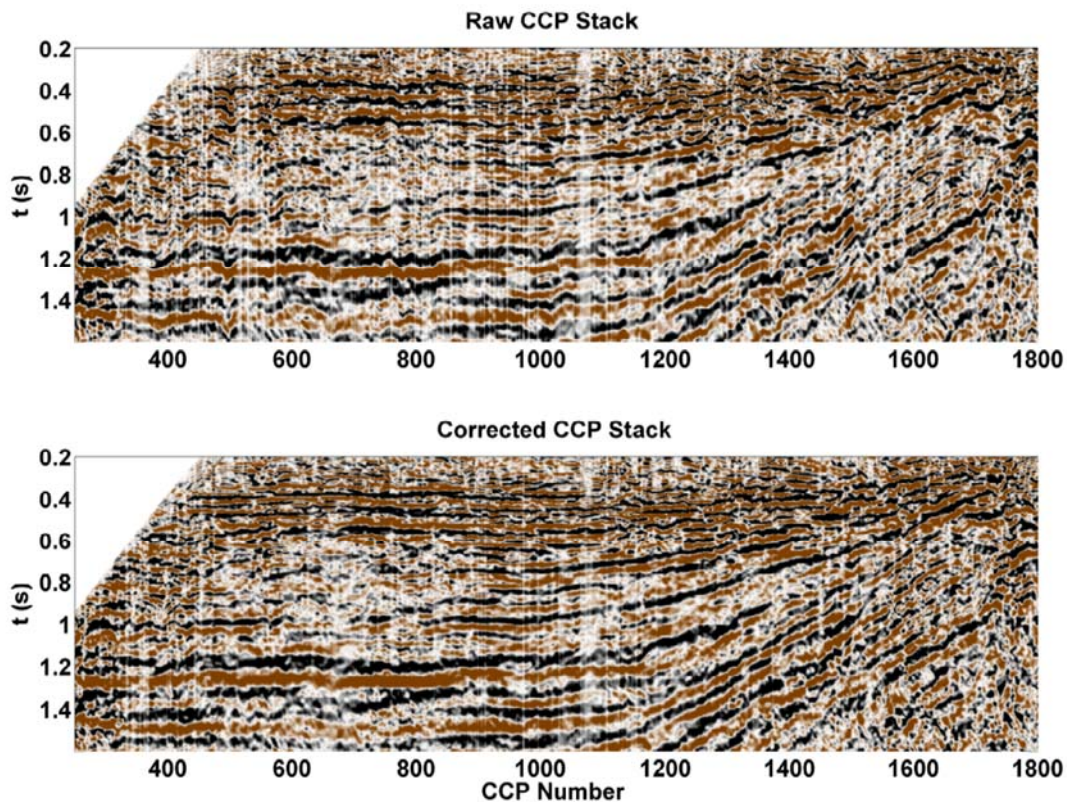


FIG. 1. Zoom view around CCP stations 500-1800 before (top) and after (bottom) removing near-surface effects.

Phase correction of Gabor deconvolution

Tianci Cui and Gary F. Margrave

ABSTRACT

Seismic data is always nonstationary due to ubiquitous anelastic attenuation modeled by the constant-Q theory. The stationary spiking deconvolution of stationary traces is extended to Gabor deconvolution of nonstationary traces, in which a seismic trace is decomposed into a time-frequency spectrum by the windowed Fourier transform and a nonstationary wavelet is estimated within each window. The amplitude spectrum of the nonstationary wavelet is accurately estimated by a smoothing process while its phase spectrum is calculated by the discrete Hilbert transform integrating within the seismic frequency band only. The Gabor deconvolved seismic trace ties the well reflectivity in amplitude and spectral content, but has phase being corrected respect to the seismic Nyquist frequency only. The phase error is the phase difference of the nonstationary wavelet with respect to the well logging frequency and the seismic Nyquist frequency. It can be calculated by knowing the Q values and the well logging frequency, to serve as a phase correction operator in the Gabor domain, which is equivalent to a time-variant residual drift time correction operator in the time domain. Without knowledge of Q or the well logging frequency, the residual drift time can be estimated by smooth dynamic time warping, which is more accurate than that estimated by time-variant crosscorrelation. The Gabor deconvolved nonstationary trace with phase or residual drift time correction ties the well reflectivity with little amplitude or phase errors.

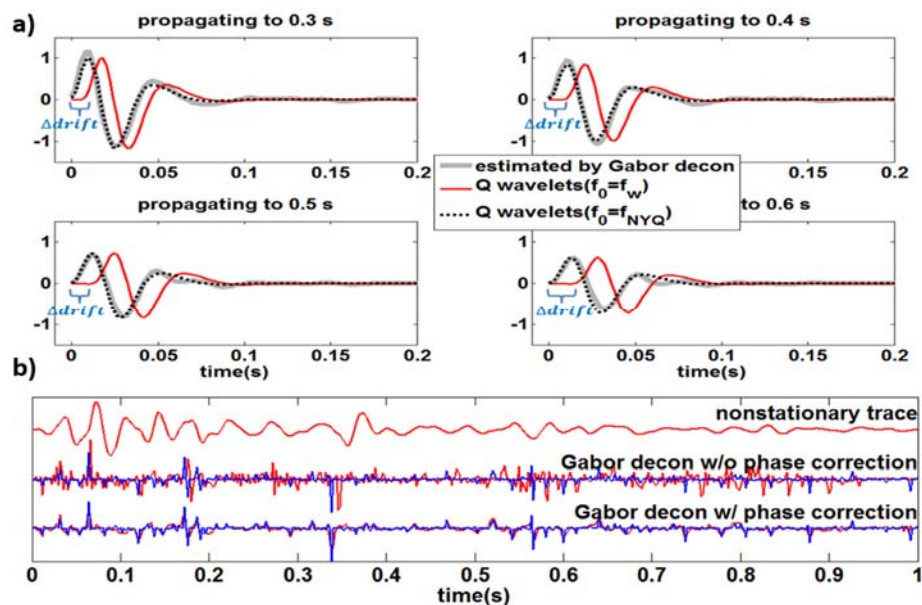


FIG. 1. a) The nonstationary wavelets propagating to different times estimated by Gabor deconvolution are consistent with the constant-Q theory modeled wavelets with respect to the well logging frequency, but appear earlier than the embedded wavelets with respect to the seismic Nyquist frequency by the amount of the residual drift time, which is indicated by the blue brackets. b) Gabor deconvolved nonstationary trace without or with phase correction compared to the known well reflectivity (blue).

Seismic-to-well ties by smooth dynamic time warping

Tianci Cui* and Gary F. Margrave

ABSTRACT

Without knowledge of Q or a check-shot/VSP survey, synthetic seismogram has to be manually stretched or squeezed to tie the seismic traces in practice, which is a tedious process and always involves human errors. Dynamic time warping (DTW) can reliably estimate the time shifts between two signals, but it returns unsmooth integer lags. The improved algorithm, smooth dynamic time warping (SDTW), can accurately estimate smooth time shifts, which are more realistic to represent the drift time in seismic-to-well ties. Taking the place of the interpretive stretch-squeeze process, SDTW is applied to estimate the time shifts between the synthetic seismogram and seismic traces of the Hussar field data. The estimated time shifts are used to calibrate the timing of the reflectivity instead of warping the synthetic seismogram, to reserve the embedded zero-phase wavelets but making the time calibration adequate only after two iterations. Both the residual drift time and overestimated sonic overburden cause these time shifts, which have similar slopes at the three well locations attributed from the flat subsurface geological structure in the Hussar area. The time-variant constant-phase difference and time-variant amplitude scalar function are calculated between the time calibrated synthetic seismogram and the seismic traces. They are linearly interpolated and extrapolated from the three wells to other CDP locations horizontally to rotate the phase and balance the amplitude of the whole seismic section. After seismic-to-well ties, the same well tops are tied to the same seismic events, making major seismic horizons easy to be identified. The bandlimited impedance inversion of the Hussar seismic data using a low-frequency cut-off of 3 Hz and a high-end frequency of 75 Hz is shown to be a good approximation to the subsurface properties. The second iteration of time calibration significantly reduces the percent errors around well 12-27 between the seismic inversion and well impedance, verifying better seismic-to-well ties.

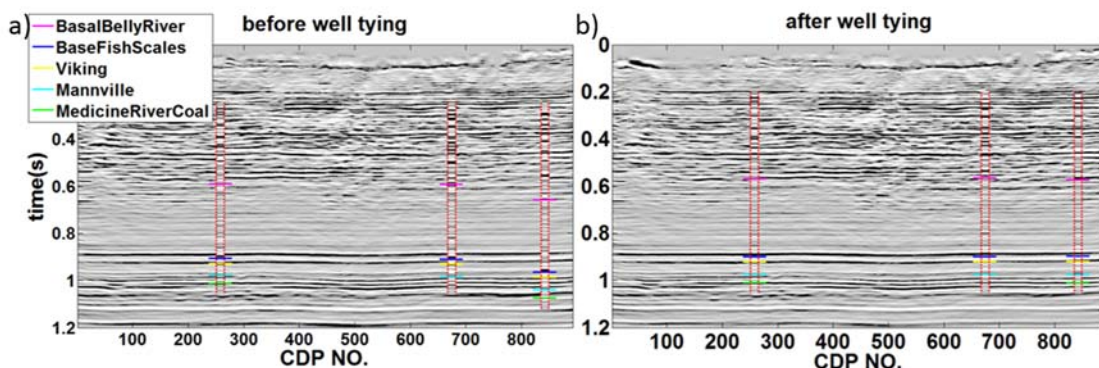


FIG. 1. a) The 2-D seismic section, on top of which are the untied synthetic seismogram plotted in the same gray level separated by the dotted red lines at each well location with the tops annotated. b) The final well tying results after two iterations of time calibration by smooth dynamic time warping.

Finite difference methods for orthorhombic media: perfectly reflecting and absorbing boundaries

P.F. Daley

ABSTRACT

An approach for the numerical solution of the forward problem for elastic wave propagation in a plane layered anisotropic (orthorhombic) elastic media is revisited. The introduction of an absorbing boundary at the model bottom is considered in this report. These boundary conditions are similar to those derived in Clayton and Engquist (1977). The stiffness coefficients (in Voigt notation), C_{ij} and the density, ρ , may vary arbitrarily with depth. The method discussed here employs finite Fourier transforms to temporarily remove the x and y coordinates resulting in a coupled system of three finite difference equations in the 3 Cartesian coordinate particle displacements in terms of depth (z) and time (t). The return to the (x, y, z, t) domain is done using a double inverse summation over the two horizontal wave numbers (k_x, k_y) . The absorbing boundary conditions are only considered for the model bottom as there are alternate methods for the free surface and side boundaries. The full elastic equations are not used at the model bottom, but rather their scalar approximations. This may appear highly suspect, but reasonable results have been obtained for less complex media types and it was thought that it should at least be investigated for this case.

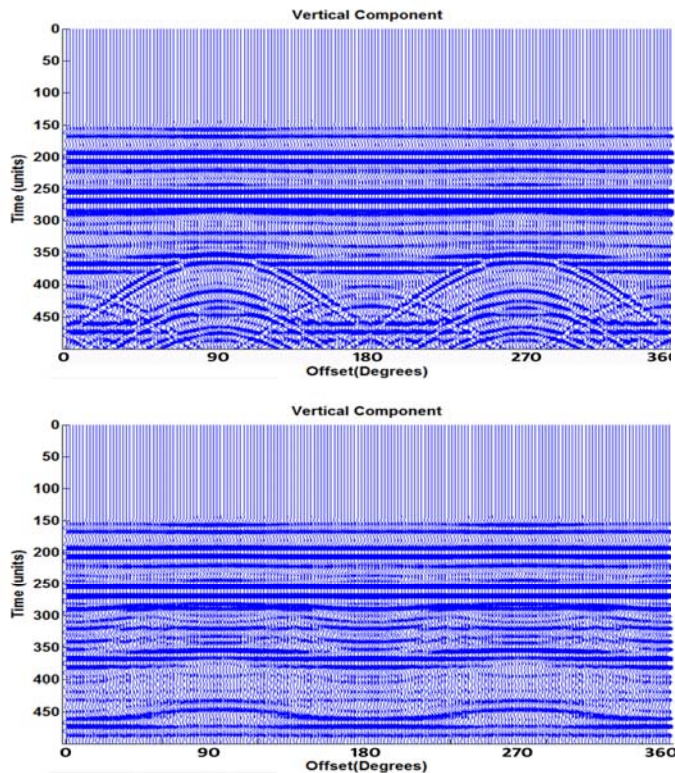


FIG. 1. Vertical component of displacement. In the top panel the perfectly reflecting pseudo-boundaries have been placed at distances where they will definitely produce unwanted arrivals during the time length of the synthetic. In the bottom panel these boundaries have been moved to distances where they cannot introduced unwanted reflected arrivals.

Inversion of quasi-compressional ray travel time data for anisotropic parameters in a TI Medium using phase velocities

P.F. Daley

ABSTRACT

Problems are encountered during the course of one's research on related topics. These are put on a list with promises made that one day, they will be revisited. The one discussed here was put on such a list four decades ago. It was visited a number of times during that time. However, there was always the problem of being unable to rederive the results presented in the paper. The specific work dealt with in this report is: [Section (4.3) *Computation of the Coefficients of Elasticity, Using the \mathbf{w} Surface (Gassmann, 1964)*]. As noted in the title, using ray travel times (the \mathbf{w} surface) the phase velocity is used to invert for the anisotropic parameters in a transversely isotropic (TI) medium. The exact phase velocities may be used to this end, given that the measured ray travel times have been acquired with reasonable accuracy. Apart from the exact phase velocities, the problem is set up so that approximate and linearized forms of the phase velocity may also be used. It should be further mentioned that the author is now able to derive the equations in the abovementioned section of the paper. As this is a fairly complex and lengthily undertaking, it will not be included here. A proper resolution with the formulae in the above paper was achieved. Consequently the equations given in that paper will be used in a moderately modified form. Only P -wave travel times are considered, as the qP and qS_V wave fronts are coupled so that the anisotropic medium parameters for both may be obtained using only P -wave data.

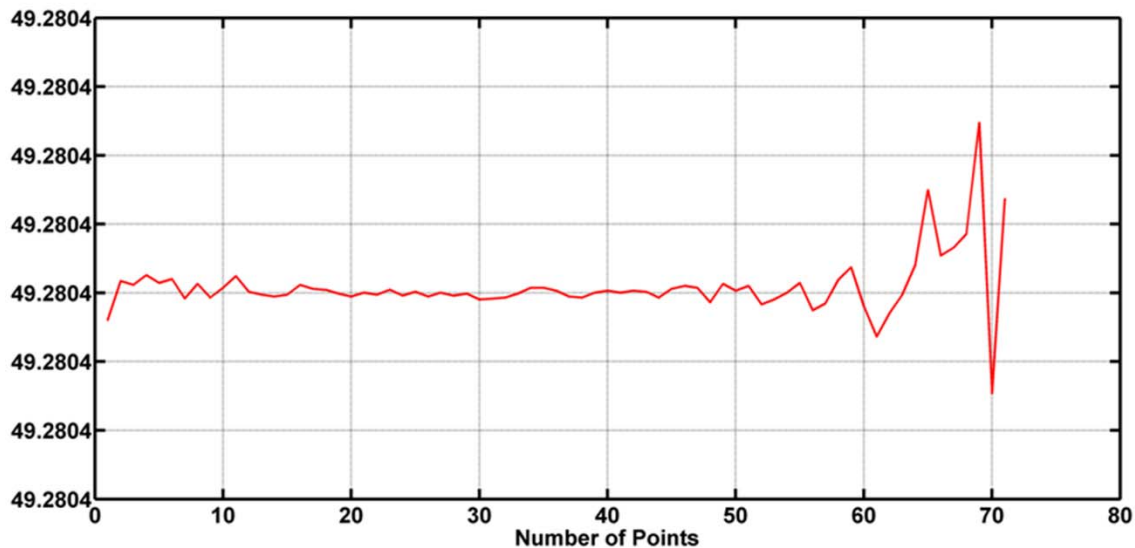


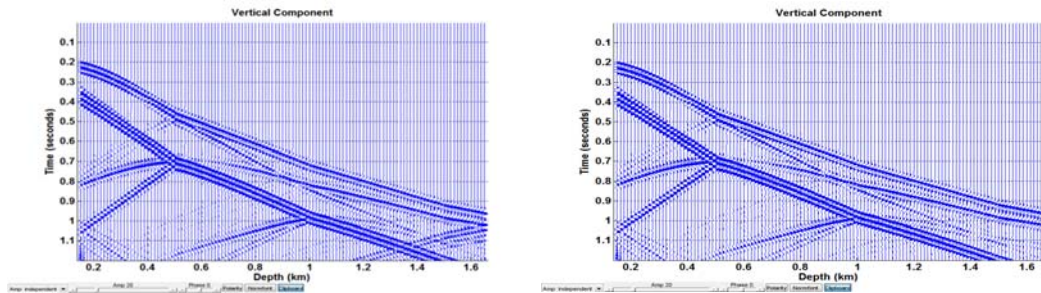
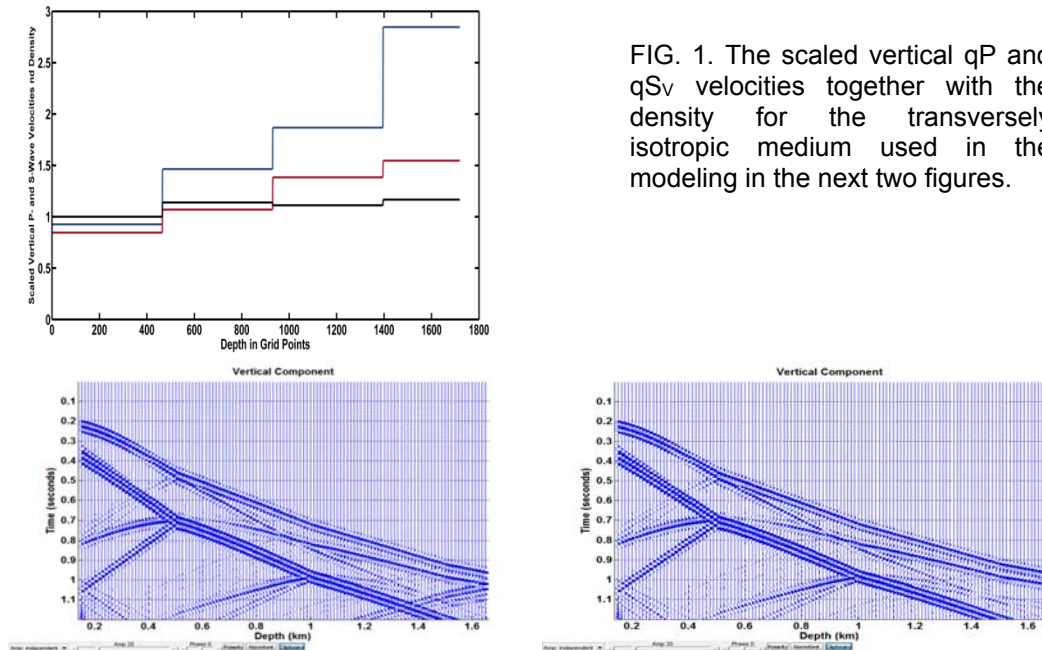
FIG. 1. $(A_{13}+A_{55})^2$ in the 13-plane for Olivine. The error is about $1.0e-07$. Once this quantity has been determined, the deviation from the elliptical, A_D may be computed. ($A_D = (A_{13}+A_{55})^2 - (A_{11}-A_{55})(A_{33}-A_{55})$).

Isotropic and transversely isotropic media: absorbing bottom boundary conditions

P.F. Daley

ABSTRACT

When using pseudo – spectral methods to reduce to the spatial dimensionality of the 2.5D coupled $qP-qS_V$ wave propagation problem in an isotropic or transversely isotropic (TI) medium to that in one spatial dimension and time, the introduction of an absorbing boundary, at least, at the model bottom is useful in the removal of spurious arrivals. The top model boundary is usually wanted in the numerical calculations and reflections from the model sides may be removed by a judicious choice of model parameters, which does not significantly increase the run time. In this report, a method similar to that presented in Clayton and Engquist (1977, 1980) and is derived for the coupled $P-S_V$ wave propagation problem in a transversely isotropic medium. Finite Hankel transforms are used to remove the radial coordinate (r) in what is assumed to be a radially symmetric medium. The problem that remains is a coupled problem in depth (z), where the anisotropic parameters may arbitrarily vary, in depth and time (t).



Development and characterization of a geostatic model for shallow CO₂ injection

Jessica M. Dongas and Don C. Lawton

ABSTRACT

A 25 sq. km static geomodel was updated for shallow injection into the 7 m thick Belly River Fm. at 295 m depth in Newell County, AB. Effective porosity and permeability were calibrated to six core lab analyses. A P10-50-90 framework was run to give conservative, typical, and optimistic scenarios of the reservoir's storage capacity. The regressional shoreline sandstone interval remains consistent across the study area giving a mean effective porosity of 11% and permeability of 0.57 mD. Dynamic simulation was completed on the P10-50-90 static cases for multiple injection scenarios, totaling 5000 t/CO₂ after a 5-year period. No significant variations existed in the results between the three static cases. The evolution of the CO₂ plume was observed at 1-year during injection and 5-years during injection, as well as the 1-year and 10-year mark for the post-injection period. The final 10-year post-injection result simulated a laterally extensive plume, expanding to 350 m in length and 20 m of vertical migration above the BRS Formation. The target interval proves as an ideal reservoir, and the seal interval demonstrates containment over a 10-year post-injection period. Uncertainties remain in the static and dynamic realm, and include reservoir, fracture, and capillary pressure, k_V/k_H ratio, and the relative $k_{CO_2-H_2O}$. Further work is being completed on a 1 km x 1 km layer cake case, and will be used as documentation as a step towards obtaining the injection license as part of Directive 051 from the Alberta Energy Regulator.

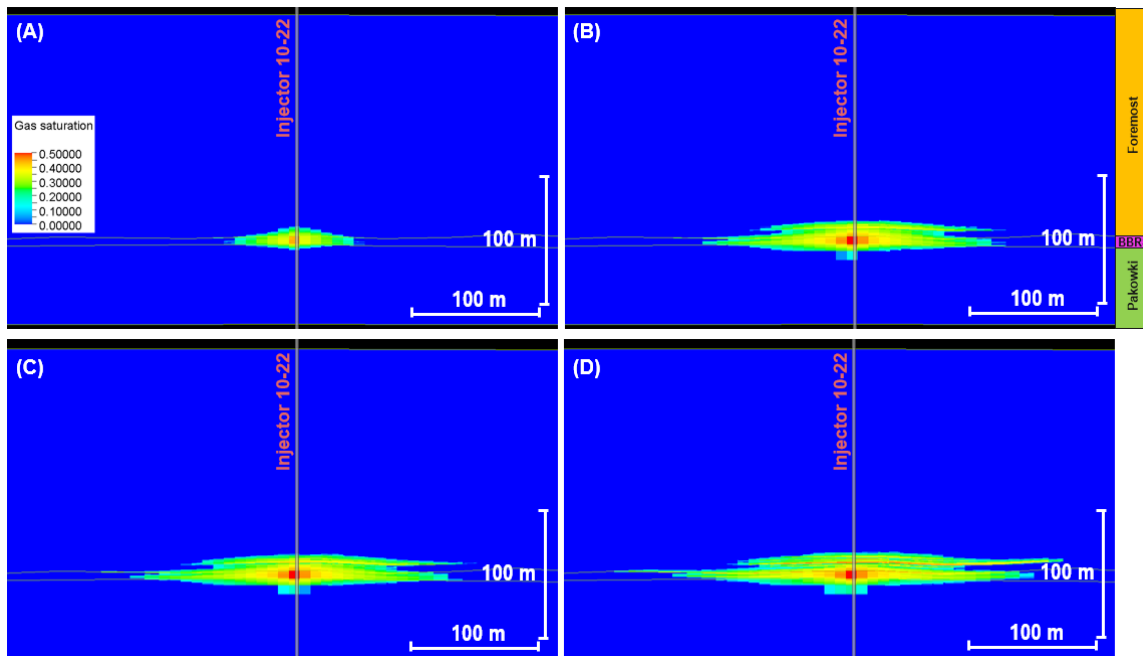


FIG. 1. The CO₂ saturation profile (E-W) for the P50 case of the heterogeneous model. (A) After 1-year of injection, (B) after 5-years of injection, (C) 1-year post-injection, and (D) 10-year post-injection. Modified from Lee (2015).

Influence of color operator on Husky Hussar data

Sina Esmaili* and Gary F. Margrave

ABSTRACT

The real seismic section, even after excellent data processing, is always very bandlimited, lacking both low and high frequencies. In this situation, recovering any of this bandwidth can be helpful. Especially, at the low frequencies, missing any of this information can effect remarkably the impedance estimation. Data that has been deconvolved will usually have a white spectrum whereas well logs show a roll off in spectral amplitude at the low frequencies that is called “color”. Using a color operator can restore this spectral color.

In this study, the effect of three different color operators on Husky Hussar data has been investigated. The results also are compared with the Colored Inversion method which is a popular way to compute a bandlimited impedance inversion with spectral color. These results demonstrate that using the color operator can improve the impedance results significantly.

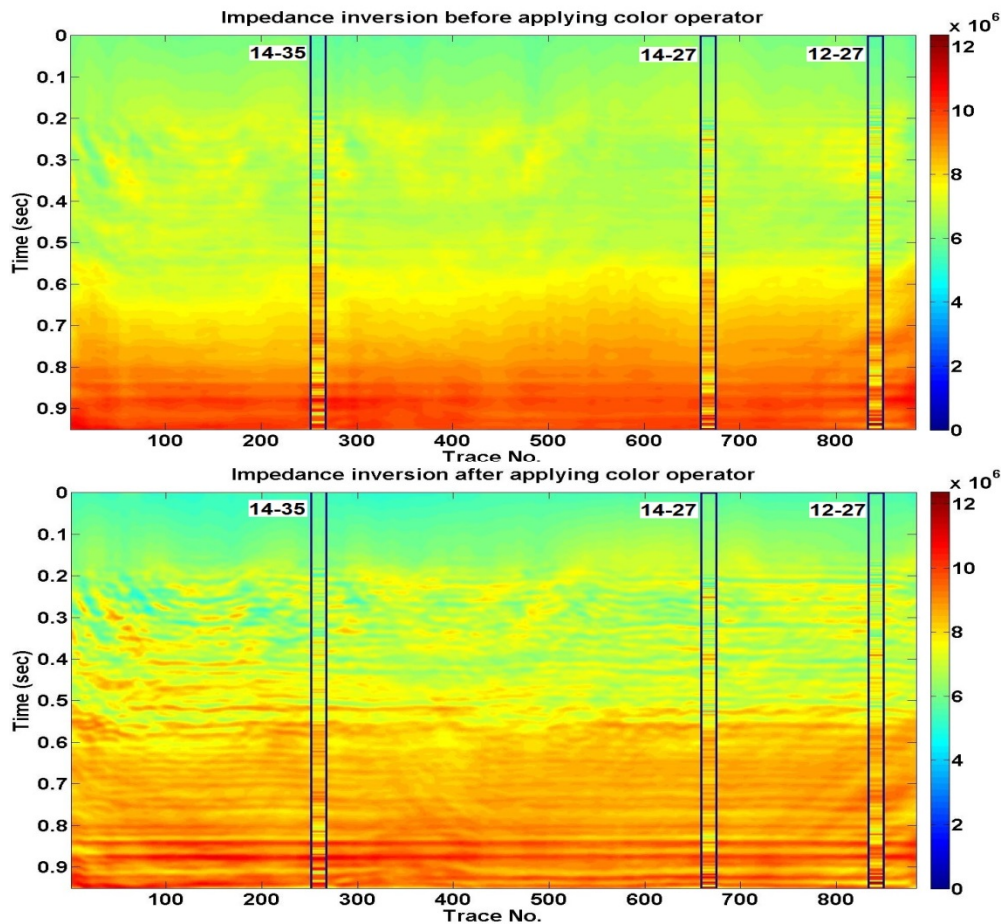


FIG. 1. The influence of color operator on impedance inversion of Husky Hussar seismic data. For both cases the low frequency contents is included in the seismic data and the high frequency components are inputted with BLIMP algorithm.

AVO modelling of linearized Zoeppritz approximations

Ali Fathalian and Kris Innanen

ABSTRACT

The reflection coefficients are investigated for the various approximation on Zoeppritz equation and the results compared with the exact solution. There some deviations near critical angles that for larger layer contrasts and larger angle of incidence these deviation are significant. Also, the effect of γ parameter on forward modelling is investigated. When the contrasts between the layers of model is larger, the γ parameter has more influence on forward modelling.

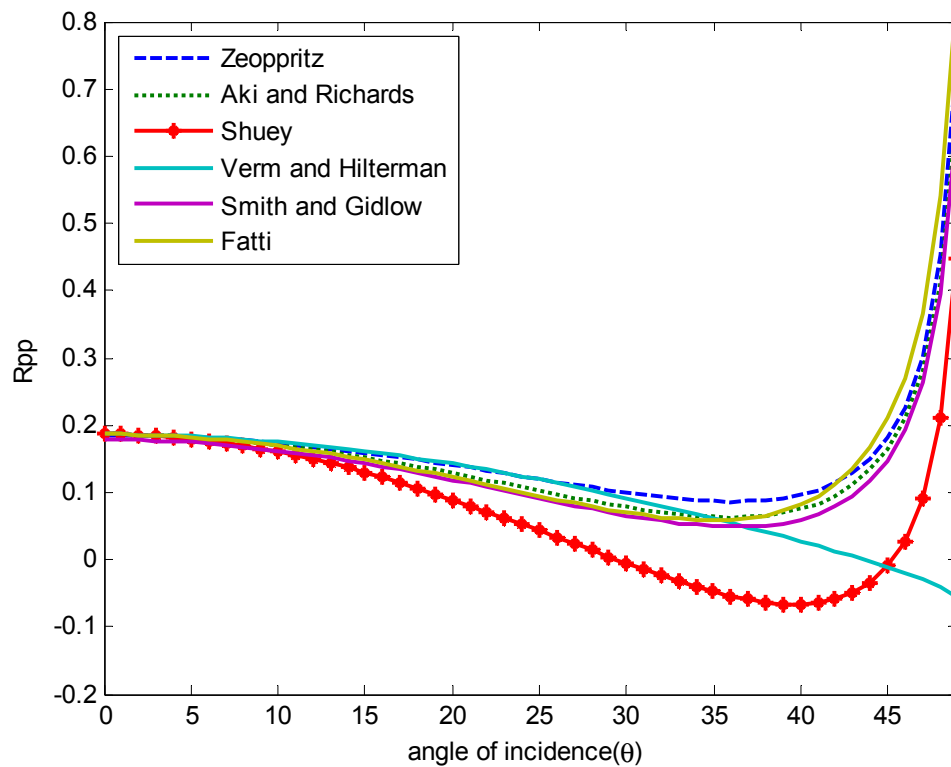


FIG. 3. Illustrate the reflection coefficients (R_{pp}) for different approximations using model 3 in Table 1.

Direct nonlinear inversion of viscoacoustic media using the inverse scattering series

Ali Fathalian and Kris Innanen

ABSTRACT

The objective of seismic exploration is obtaining structural subsurface information from seismic data by recording seismic wave motion of the ground. The recorded data have a non-linear relationship with the property changes across a reflector. In this work, the multi-parameter multi-dimensional direct non-linear inversion is investigated based on the inverse scattering task-specific sub-series. The result is direct and non-linear and has the potential to provide more accurate and reliable earth property predictions for larger contrast and more complex. The inverse scattering method has a direct response for imaging and inversion problems for a large contrast and a multi-dimensional corrugated target. We are derived the direct non-linear inversion equation for three parameter viscoacoustic cases. Numerical tests show that non-linear inversion results provide improved estimates in comparison with the standard linear inversion. When the non-linear term add to linear term the recovered value of parameters are much closer to the exact value.

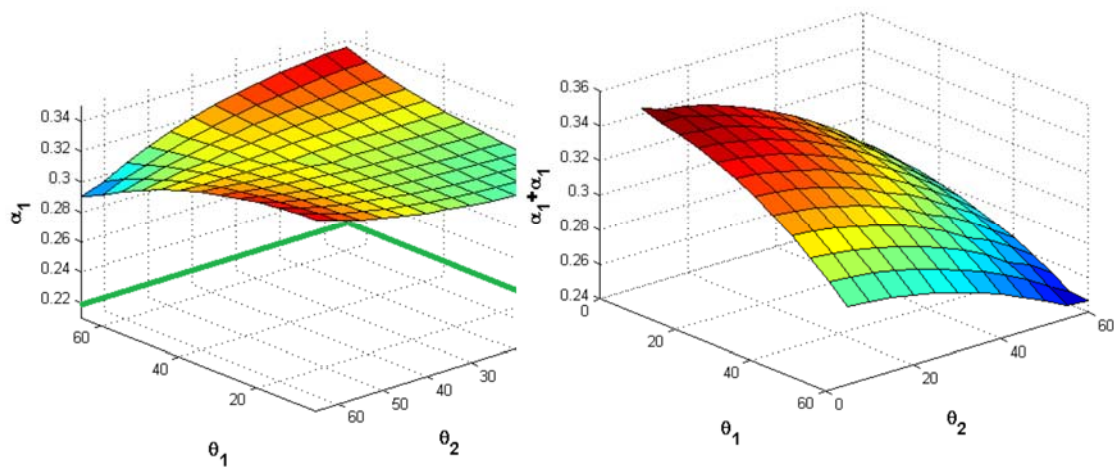


FIG. 3. Recovered parameter from the normal incidence for α . The exact value of α is 0.22. The linear approximation α_1 (a) and the sum of linear and first non-linear $\alpha_1 + \alpha_2$ (b).

Full waveform inversion using the PSPI migration: a convergence study

Marcelo Guarido*, Laurence Lines, Robert Ferguson

ABSTRACT

A full waveform inversion (FWI) routine using PSPI migration with a deconvolution imaging condition was tested on an acoustic synthetic 2D survey using the Marmousi model and the inverted P-wave velocities are, in the worst case, promising. The model update is computed by averaging monochromatic scaled gradients at each iteration and the resulting model is an improvement of the one obtained in the previous work (Guarido et al., 2014). We tested different starting models to check the routine behavior and, as expected, better the initial model, better will be the migration of the residuals and the model update, resulting in higher resolution velocity inversion. The conjugate gradient was included in the routine, building more precise gradients and increasing the quality of the inverted model. Impedance inversion by trace integration was applied in the model update (gradient) showing promising results, mostly related to the inversion of thicker layers, but it still requires improvement.

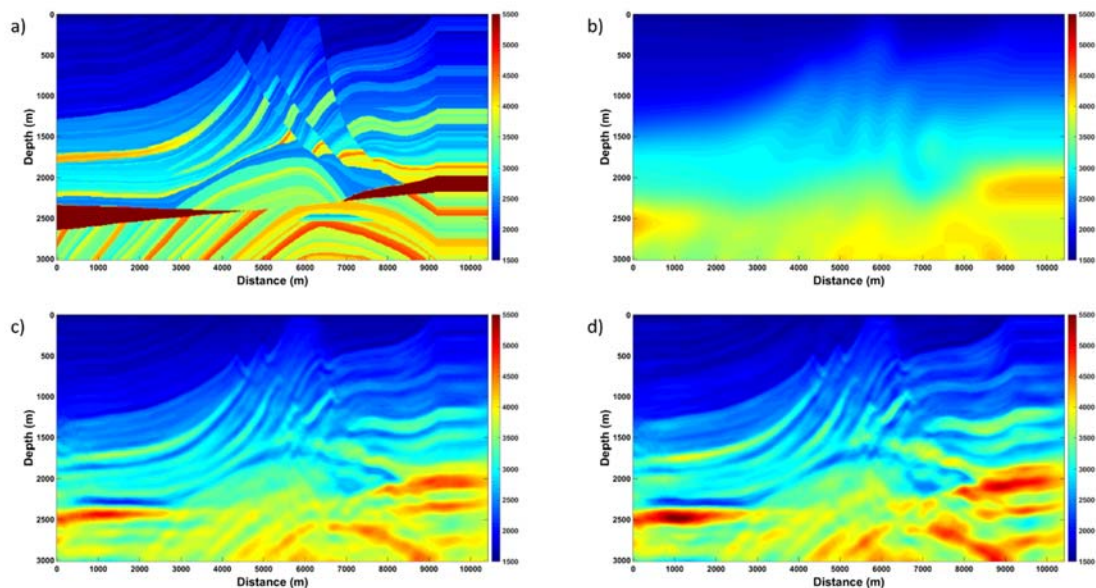


FIG. 1: FWI using PSPI migration: a) is the Marmousi model, b) is the initial guess, c) is the inverted model using classic gradient and d) is the inverted model using the conjugate gradient.

Receiver statics of converted waves without stacking reflections: test with real data

Saul E. Guevara, J. Helen Isaac, and Gary F. Margrave

ABSTRACT

The most popular method for receiver statics correction of converted wave (*PS*-wave) requires stacked Common Receiver Stacks (*CRS*) and thus a stacking velocity model (V_C). A new method that does not require V_C is proposed. This method obtains the differential delay between adjacent common receiver gathers (*CRG*) by cross-correlation of corresponding traces. Thus, it is automatic and does not require identification of a guide horizon. This report presents a test of this method with a 2D 3C seismic line from the Spring Coulee Survey, 2008. Strengths, promise and current shortcomings can be identified.

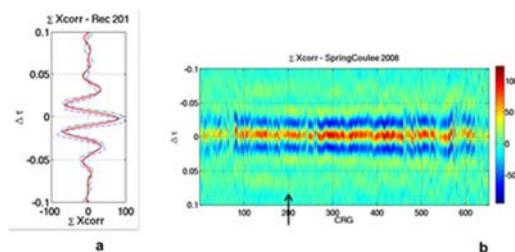


FIG. 1. The cross-correlations between traces of adjacent CRGs are summed and the maximum is the delay between them; (a) summation result for three adjacent CRGs; (b) summation result for all the receivers. The arrow shows the location of (a).

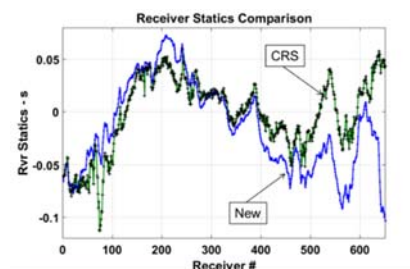


FIG. 2. Comparison of the receiver statics solution of the new method and the receiver final statics with the CRS method.

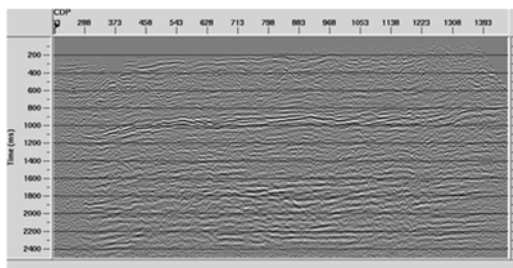


FIG. 3. Stacked section of the *PS*-wave with just elevation receiver statics applied.

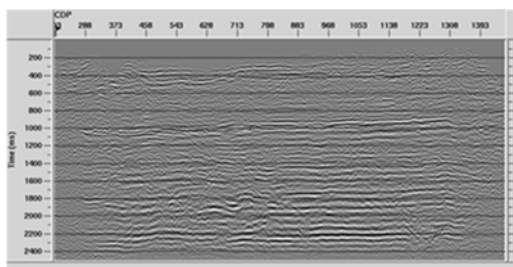


FIG. 4. Stacked section of the *PS*-wave after applying the receiver statics with the new method and a first velocity analysis.

Multicomponent seismic data analysis for interval rock properties in the Marcellus Shale

Bobby J. Gunning* and Don C. Lawton

ABSTRACT

The Devonian Appalachian Basin in the Northeast United States holds vast reserves of hydrocarbons. The Marcellus Formation is a black shale that contains one of the world's largest unconventional tight gas plays. In this paper, a three-component 3D seismic dataset acquired in Northeast Pennsylvania, near the New York border, is used to assess V_p/V_s in the Marcellus Formation. A general seismic interpretation and a more specific interval rock property analysis is performed. The mildly dipping, East-West trending thrust fault structure in the Marcellus and surrounding formations is explained. Interval V_p/V_s ratios are found for several of the important intervals in the Appalachian Basin, and potential sweet spots for hydrocarbon generation are speculated. A correlation between anisotropy and high V_p/V_s ratio was found.

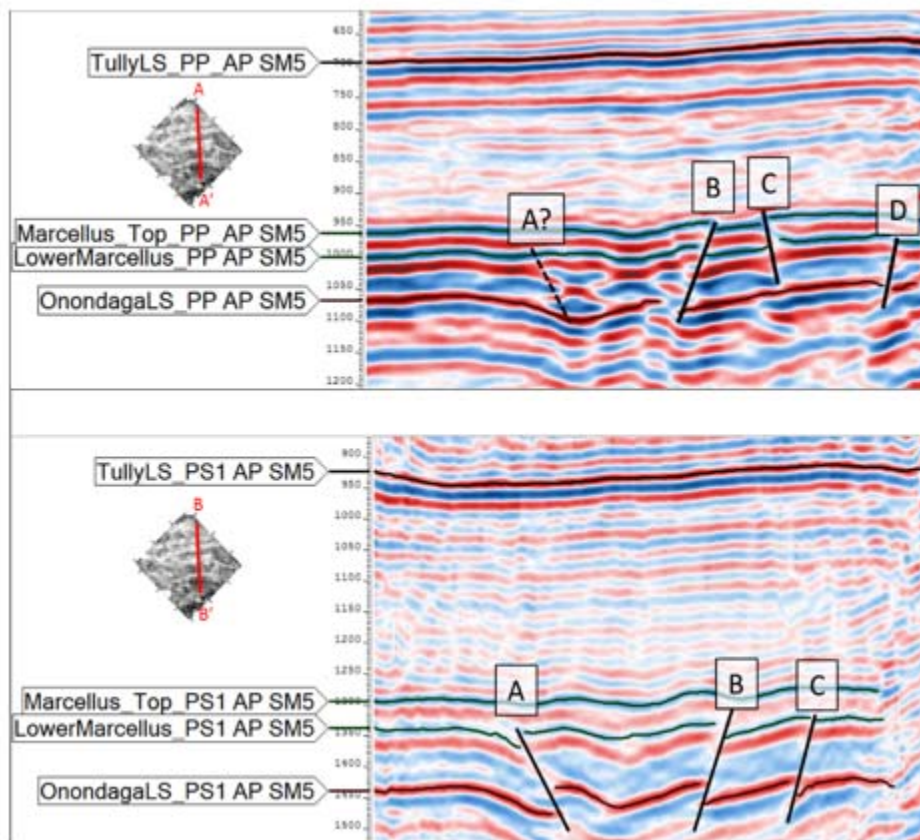


FIG. 1. PP (top) and PS1 (bottom) seismic cross section examples displaying the variability of structure between the two data types.

Preliminary interpretation of 3C-3D seismic data from an Athabasca oil sands field, Alberta

Bobby J. Gunning, Don C. Lawton and Helen Isaac

ABSTRACT

Oil sands in the Athabasca region constitute a major hydrocarbon deposit in northern Alberta. In this project, a multicomponent 3D seismic dataset provided by Canadian Natural Resources Limited is used to study the rock column in the Athabasca Oil Sands region. The initial data consists of fully processed PP seismic data, and three-component raw seismic data. The PP data is used for an initial, full volume interpretation including: picking several pervasive reflection horizons, well log analysis and post-stack impedance inversion. The raw three component data has begun processing and will eventually be processed into PP, PS1 and PS2 seismic volumes.

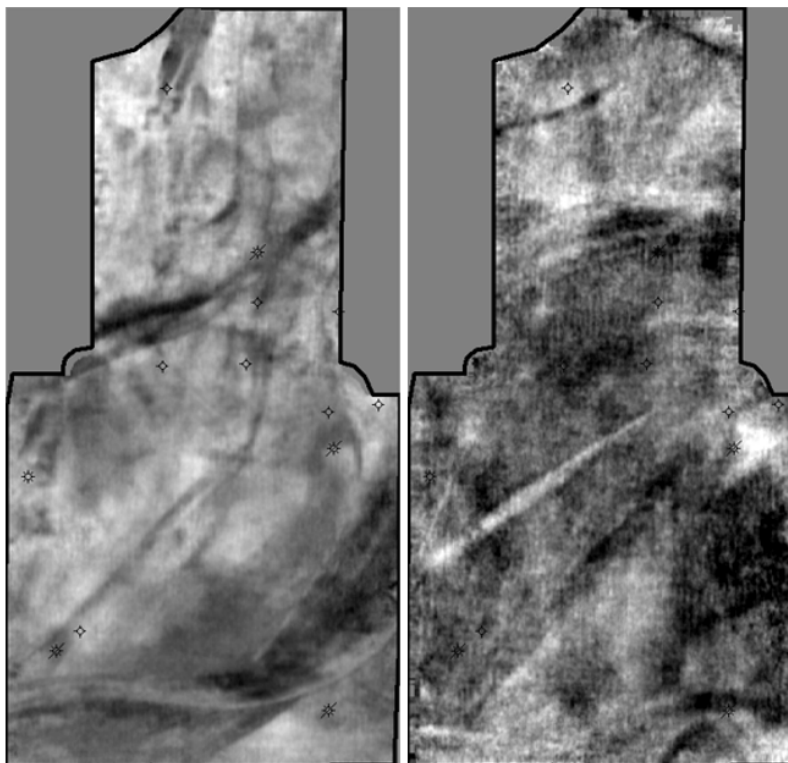


FIG. 1. Example stratal slices through variable fluvial geology in the Athabasca Oil Sands. The southern channel in the left figure shows channel movement patterns with an obvious thalweg and point bar sequences. The right hand figure displays more complex fluvial geomorphology but certain sedimentary boundaries are interpretable.

Initial 3C-2D surface seismic and walkaway VSP results from the 2015 Brooks SuperCable experiment

Kevin W. Hall*, J. Helen Isaac, Joe Wong, Kevin L. Bertram, Malcolm B. Bertram, Donald C. Lawton, Xuewei Bao¹ and David W.S. Eaton¹

ABSTRACT

A 3C walkaway VSP and surface seismic experiment was conducted at the Containment and Monitoring Institute (CaMI) Field Research Station (FRS) in May of 2015 (Figure 1). Two parallel NE-SW receiver lines were laid out with one line centered on well CMCRI COUNTESS 10-22-17-16, and the other offset 100 m to the northwest. Both receiver lines had single-component SM-24 geophones at a 10 m receiver spacing. In addition, the receiver line centered on the well had three-component SM-7 geophones at a 10 m receiver spacing. A three-component ESG SuperCable was deployed in the well at three different levels, giving receiver positions in the well from 106 to 496 meters depth at a 15 m spacing.

Two source lines were acquired three times, once for each tool position in the well. The source was an IVI EnviroVibe sweeping from 10-200 Hz over 16 s. The NE-SW source line had a Vibe Point (VP) every 10 m, offset to the NW of the surface receiver locations, for a walkaway VSP. A semi-circular source line with a radius of 400 m and a VP every five degrees was acquired for a velocity tomography study. Finally, the NE-SW source line was re-acquired using a variety of M-sequence sweeps as the SuperCable was removed from the well. This report presents a first look at the data and some early results.

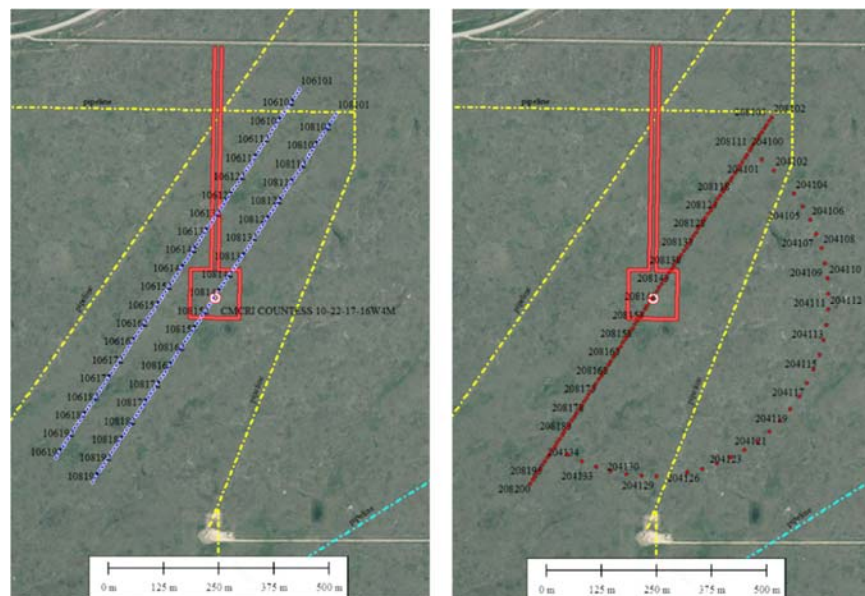


FIG. 1. Map of survey area. Vibe points are red dots, receiver points are blue dots, pipelines are yellow/cyan dash-dot lines, and the well location is a red bulls-eye. North is up. Photo courtesy of Newell County, Alberta.

¹ Microseismic Industry Consortium

Using corrected phase to localize geological features in seismic data

Heather Hardeman, Michael P. Lamoureux

ABSTRACT

We consider the time-frequency analysis method, basis pursuit. We look specifically at the phase attribute produced from the results of running basis pursuit on various data sets. We explore the numerical results of derivative of the corrected phase attribute proposed in (Han, et al.,2015) on other geological data sets. We consider the phase attribute provided by other spectral decomposition methods, continuous wavelet transform and synchro-squeezing transform, and apply the derivative of the corrected phase process to these attributes. We end with a comparison of the results for basis pursuit to those of continuous wavelet transform and synchro-squeezing transform.

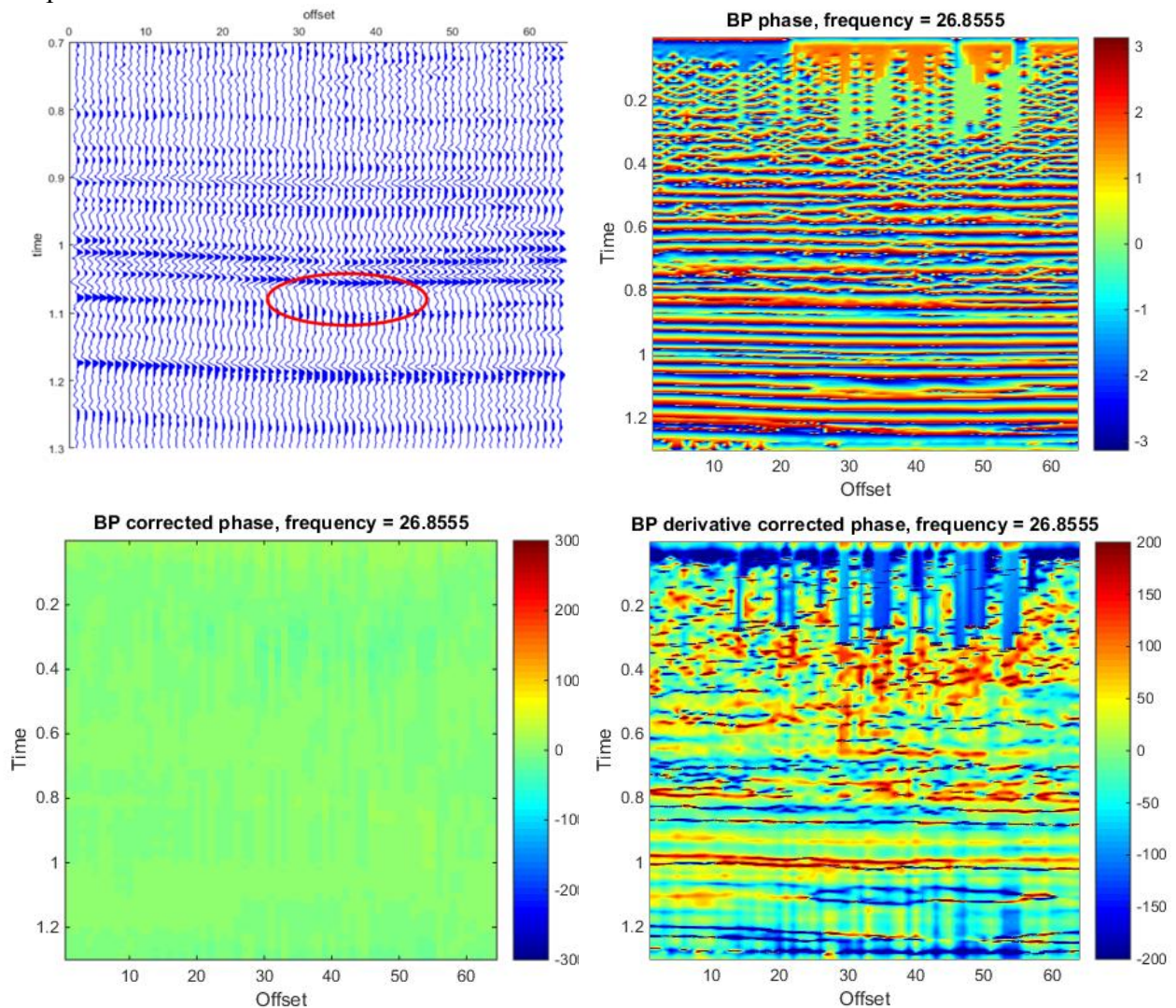


FIG. 1. The post-stack data of CREWES Blackfoot data set (upper left). The phase attribute produced by basis pursuit for the CREWES Blackfoot data set at approximately 26 Hz (upper right). The corrected phase attribute produced by basis pursuit for the CREWES Blackfoot data set at approximately 26 Hz (lower left). The derivative of the corrected phase curves for the Blackfoot data set at approximately 26 Hz (lower right).

3D or not 3D, that is the question: raypath interferometry in 3D processing

David C. Henley*

ABSTRACT

Raypath interferometry is a processing technique designed to find and apply surface corrections to seismic data where the near-surface layer properties invalidate the usual surface-consistency assumption. It can also be used on data where surface-consistency is not violated, where it can sometimes improve reflection resolution.

To apply raypath interferometry to 2D data, the source gathers are transformed into a domain where raypath is parametrized by a coordinate of the transformed ensemble. This process is straightforward for 2D datasets; but extending the concept to 3D requires further consideration. We explore here some of the possibilities and illustrate one approach which seems promising. Utilizing the surface azimuth between source and receiver locations, we demonstrate one possibility for extending raypath interferometry to 3D by extending the 2D ‘surface function’ introduced in 2D raypath interferometry to a 3D function of surface location, raypath parameter, and azimuth. We show a way to transform 3D data into a raypath domain using the radial trace transform. We then demonstrate the creation of a 3D ‘reference wavefield’ and show that raypath interferometry, even in 3D, can be implemented as a single cross-correlation and inverse-filter application, just as in the 2D case. We show that various trace ensembles extracted from the corrected 3D data have reduced short-wavelength residual statics compared to the same ensembles extracted from the raw data, hence encouraging us in our 3D approach.

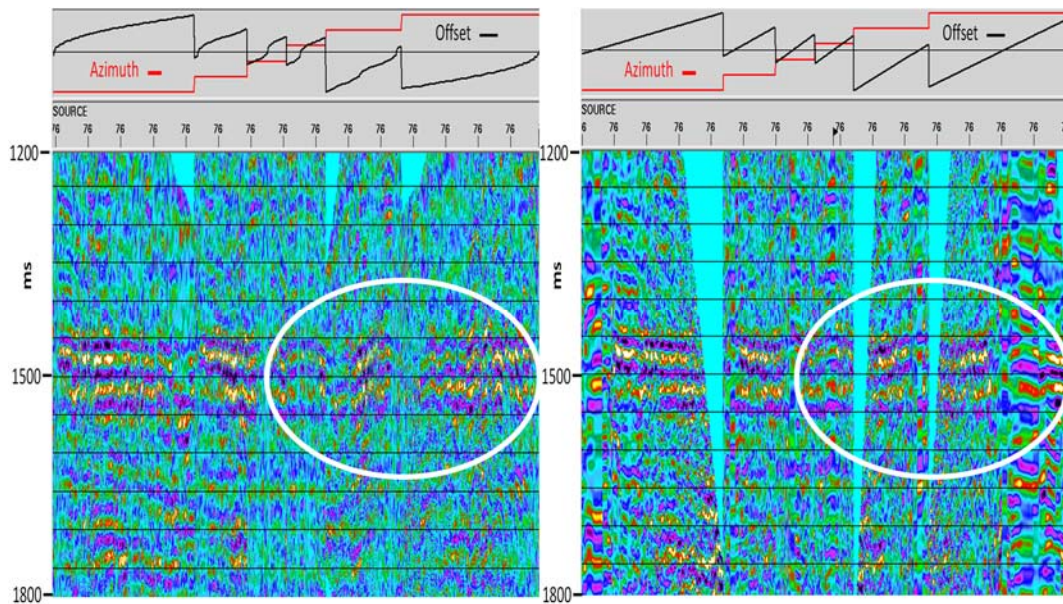


FIG. 1. Uncorrected 3D traces on the left, traces corrected by raypath interferometry on the right. Short-wavelength trace-to-trace jitter (statics) greatly reduced, in spite of inexact inverse RT transform.

Absorption in FWI – some questions and answers

Kris Innanen

ABSTRACT

In this short note we cover two questions concerning the inclusion in seismic FWI of an attempt to solve simultaneously for elastic and anelastic geological properties, i.e., Q_P and Q_S as well as (say) V_P , V_S and ρ . The first question is whether or not to do so: anecdotally (and incorrectly), attenuation parameters have been suggested to be unimportant to FWI, since they dominate at high frequencies and FWI is primarily concerned with low. The second is really several questions: where in the mechanisms of FWI (e.g., within the machinery of the gradient and the various approximate Hessians), are the tasks we normally associate with Q contained? Is there a component of the Hessian operator tasked with Q compensation, for instance.

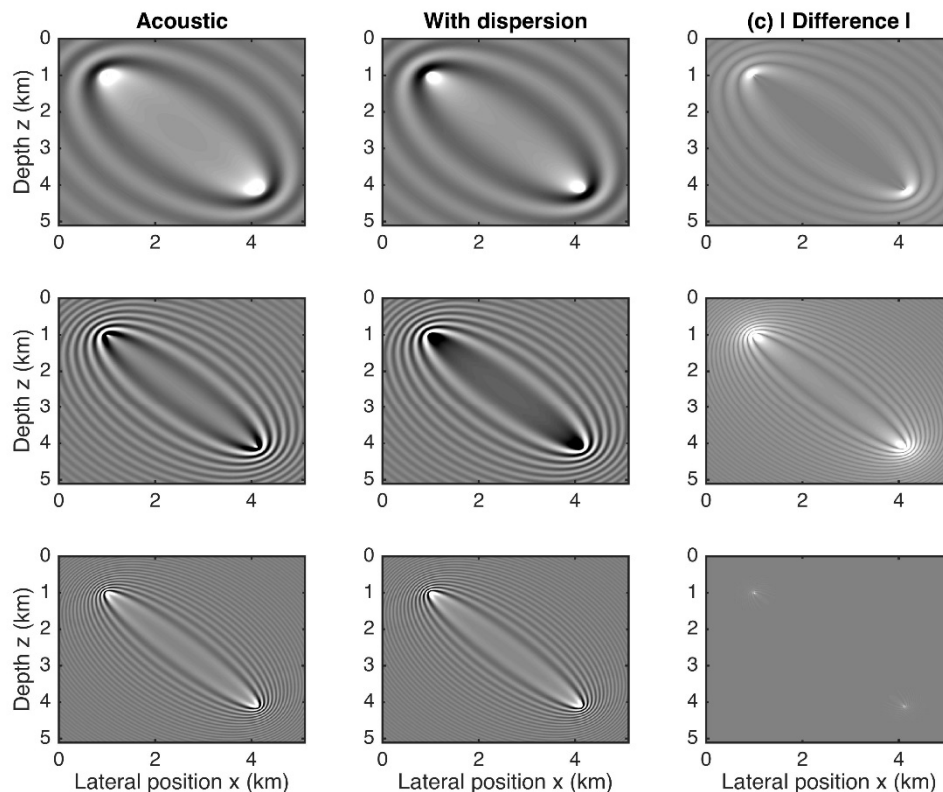


FIG. 1. Comparison of FWI sensitivities in homogeneous 2D media. Left column: acoustic sensitivities for low (top), medium (middle) and high (bottom) frequencies; middle column: dispersive sensitivities for low, medium and high frequencies; right column: absolute value of the differences between the left and middle columns. The “brightness” of the top right relative to the bottom right is telling: because of the dispersion which accompanies all attenuation phenomena, the effect on FWI of incorrectly assuming acousticity is much stronger for *low* frequencies than intuition may suggest.

Direct measurement of near surface seismic body wave dispersion from uncorrelated vibroseis data

Kris Innanen

ABSTRACT

The propensity of geological volumes, particularly in the near surface, to cause seismic body waves to propagate dispersively is a serious impediment to FWI. Anelastic parameters, like Q_P and Q_S , can appear as unknowns in tractable seismic inverse algorithms, provided the associated dispersion laws are known. However, general attenuation factors with arbitrary variability in space and frequency cannot be solved for. If a FWI scheme solves for elastic and anelastic properties given an accurate prior knowledge of the dispersion law, we will require a flexible and unconstrained procedure for determining this law; one which occurs relatively early in the processing flow. An example of such a procedure is illustrated in this paper, based on picked arrival times from the Gabor spectra of uncorrelated vibroseis sweeps measured in a walkaway VSP experiment. Estimating phase velocity as the ratio of the source/receiver ray path length to the departure/arrival time difference of each frequency in the sweep, a remarkably consistent set of $V_P(f)$ estimates are derived for 20 depth levels between 76m and 116m depth. Calibrating these to match group velocities measure with standard time domain slopes, a range between roughly 500m/s and 2000m/s, from 10Hz to 70Hz is calculated. The curves are sigmoidal, with a negative curvature that does not match with standard logarithmic models.

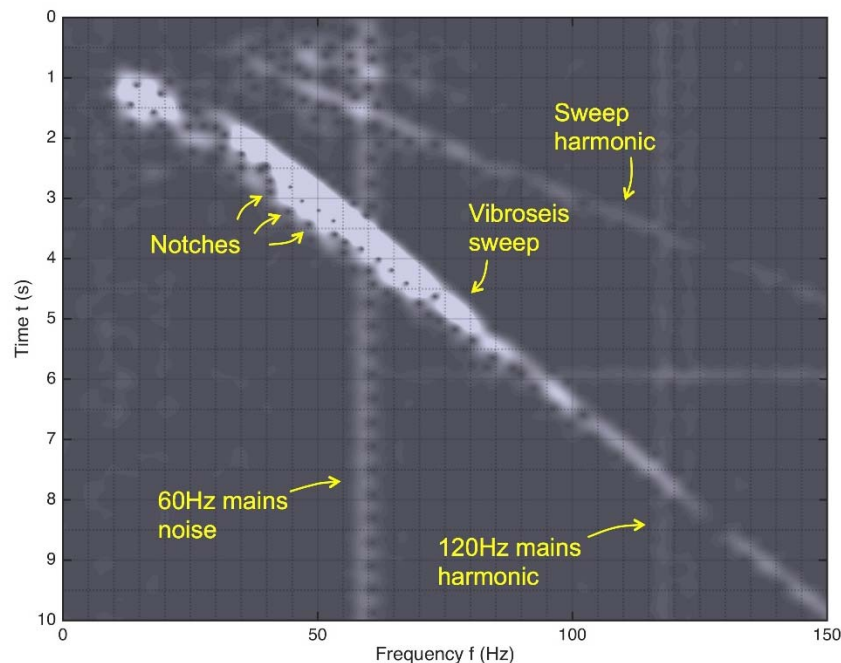


FIG. 1. Gabor spectrum of a single uncorrelated trace (depth $z_g=76\text{m}$, offset $x_s=320\text{m}$). Notches, mains noise and harmonics, and sweep and harmonic are labelled. The event labelled “vibroseis sweep” is analyzed in this study.

A nonstationary search parameter for internal multiple prediction

Kris Innanen

ABSTRACT

With the internal multiple prediction algorithm re-formulated in terms of the output time, the opportunity arises for the search limiting parameter to be varied according to some schedule $\epsilon(t)$. Any prior knowledge suggesting that within a single trace *this* output time requires aggressive prediction, but *that* output time requires cautious prediction, can be used to guide an appropriate selection of $\epsilon(t)$. Here we will consider two fairly obvious types of criterion for selection: data driven selection strategies and strategies driven by geological prior knowledge. 1D and zero offset synthetic and physical modelling lab data are used to find situations where the precision of predictions is increased beyond what would be available given any single fixed ϵ parameter. The promising results are suggestive that a much broader study of selection strategies for ϵ as functions of time, frequency, offset, lateral wavenumber, source and receiver horizontal slownesses, etc., is warranted.

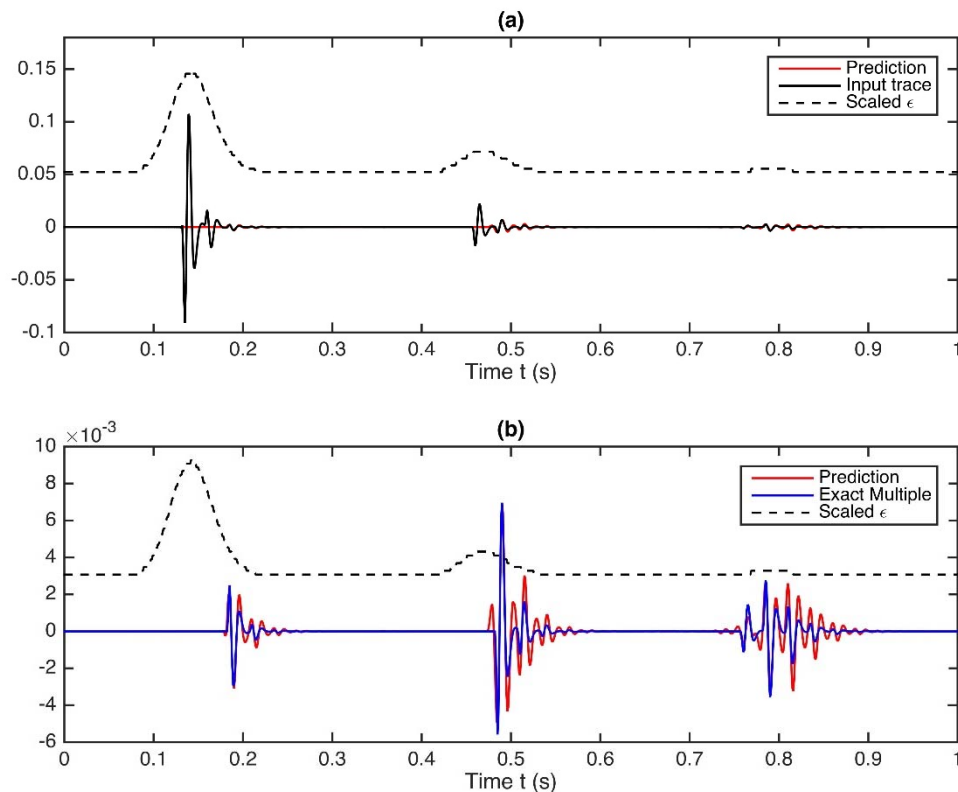


FIG. 1. The consequences to prediction of a data driven time-variant $\epsilon(t)$. (a) Input trace (black) vs prediction (red). Primary subevents near 0.2s and 0.5s are very close together. (b) Prediction (red) using an $\epsilon(t)$ determined from the Hilbert envelope of the trace (dashed black line), compared against the exact multiple (blue).

Residual dependent FWI sensitivities based on direct nonlinear inverse scattering

Kris Innanen

ABSTRACT

Nonlinear, residual dependent FWI sensitivities are the outgrowth of the observation that certain direct nonlinear procedures, available in special case environments/schemes, such as AVO inversion or 1D/1.5D direct nonlinear inverse scattering imaging and inversion, have no FWI generalization – they cannot be found as special cases of any standard FWI procedure. In order to derive general FWI schemes that reduce in this way, an extension of some kind is required to our ideas of FWI sensitivity. A proposal from 2014, namely that the sensitivities be created by varying not the current model iteration, but the forthcoming iteration, is pursued in this paper to confirm that this approach correctly reduces to an existing 1D normal incidence direct nonlinear imaging and inversion scheme, previously derived from inverse scattering considerations.

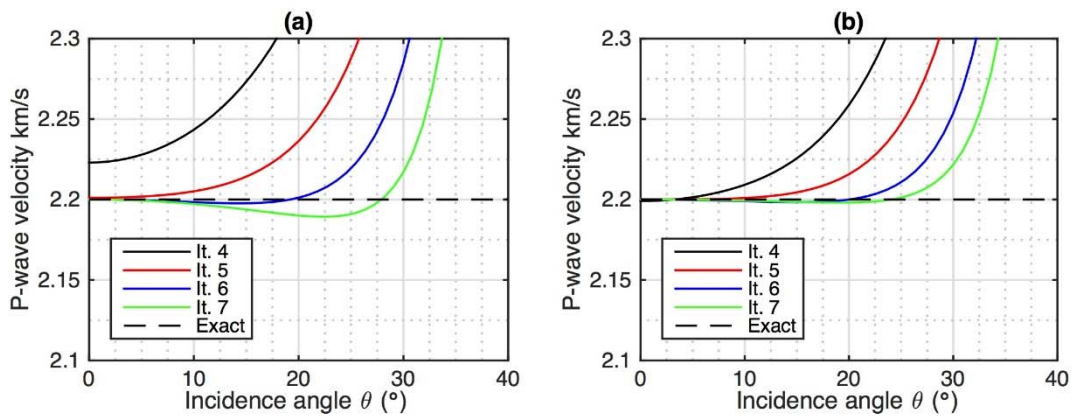


FIG. 1. Example of a “missing FWI procedure”. (a) FWI generalizes iterative linear AVO inversion when reconstructing a single elastic boundary from reflection data. However, at high angle iteration can lead to instability (green curve). (b) AVO inversion can be carried out using iterative nonlinear AVO inversion, wherein a direct nonlinear inverse formula is repeatedly used. This provides enhanced convergence and stability in principle. However, there is no standard FWI procedure generalizing this. Generalizations require some extension of the normal definition of sensitivities.

Time domain internal multiple prediction

Kris Innanen*

ABSTRACT

The standard 1.5D internal multiple prediction algorithm generates output in the (k_g, f) domain. Through some manipulation versions in the (k_g, t) and (x_g, t) domains are derived, along with the 1D time domain formula. Algorithms for calculating the predictions in these domains centre on partial convolutions in vertical time or pseudodepth. This is implemented by forming masking matrices to overlie standard dispersion or convolution matrices. The result are some intuitive codes which produce very clean predictions, even in the presence of gathers prior to deconvolution.

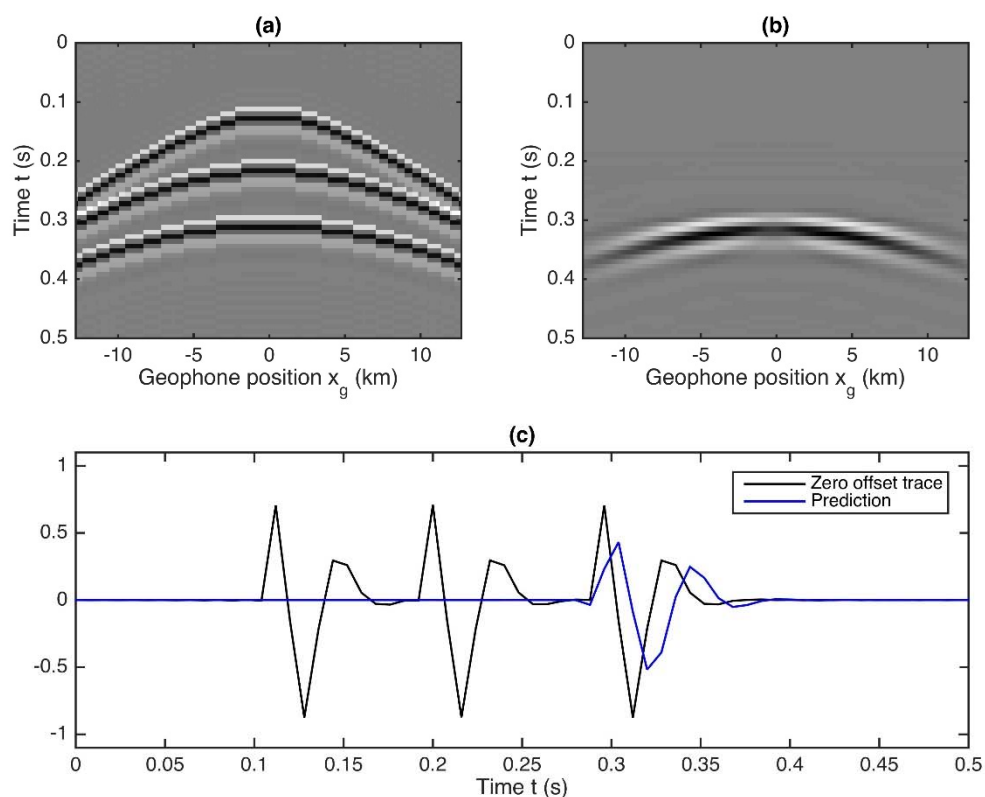


FIG. 1. (a) Input shot record containing two primaries and one multiple; (b) output of 1.5D space/time prediction, full record; (c) output of 1.5D space/time prediction, zero offset trace extracted (black original, blue prediction).

3D3C seismic data at the Brooks experimental CO₂ injection site

J. Helen Isaac* and Don C. Lawton

ABSTRACT

We processed and interpreted a 1 km² baseline 3D3C seismic survey acquired in May, 2014, at the Field Research Station near Brooks in Southern Alberta. This area is the site of planned experimental CO₂ injection into shallow Upper Cretaceous sandstones and where various technologies for monitoring the behaviour of the injected gas and cap rock integrity will be assessed. One of these technologies is timelapse 3D3C seismic data.

Processing of the PP and PS seismic data included noise attenuation and signal enhancement processes, Gabor deconvolution and post-stack time migration. After processing the PP and PS seismic data, we tied them to well logs using synthetic seismograms. We interpreted and mapped several key horizons on the PP and PS 3D data and registered the two data volumes. V_p/V_s was calculated from the registered horizon times for three intervals and also derived for the data volume through a joint PP-PS post-stack inversion.

We intend to compare these results to those obtained from monitor 3D3C surveys obtained after CO₂ injection.

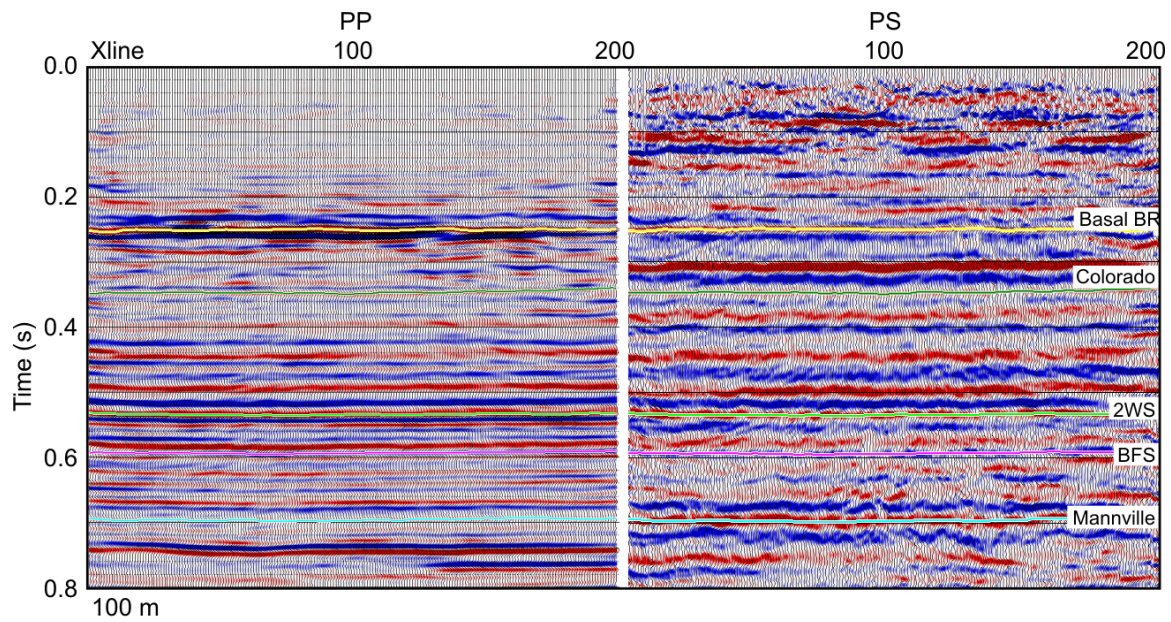


FIG. 1: Registered PP and PS data displayed together in PP time. The registration is based upon correlation of the annotated horizons, which were identified by correlation of the seismic data with synthetic seismograms created from sonic logs from a nearby well.

A little case study of an offset-dependent seismic response

J. Helen Isaac and Don C. Lawton

ABSTRACT

A small baseline 3D3C seismic survey was acquired in May, 2014, at the Brooks Field Research Station (FRS) in Southern Alberta. This area is of interest for planned experimental CO₂ injection, initially into the Basal Belly River sandstone at 295 m. We created PP and PS synthetic seismograms from dipole sonic and density logs acquired in a well 8 km away to enable us to identify the reflectors seen on the processed seismic data, especially in the shallow zone of interest. Subsequently we derived a shear sonic log from a compressional sonic log to tie the seismic data with synthetic seismograms from a well at the FRS site.

The high amplitude positive response (peak) at the top of the Upper Cretaceous Milk River Formation sandstone on the default normal incidence synthetic seismogram does not match that of the PP seismic data, which has a weak response. The Zoeppritz equations predict a high amplitude reflection coefficient at zero-offset, a decrease in amplitude with increasing offset and a change in polarity at an incidence angle of 35°, or about 250 m, resulting in a low amplitude stacked response for this high impedance sandstone. The character of the Milk River reflection on the seismic data stacked with all offsets matches the stacked offset synthetic seismogram while the character of the Milk River reflection on the seismic data stacked with only the near offsets matches the normal incidence synthetic seismogram. The seismic character of the PS data matches that of the PS synthetic seismogram.

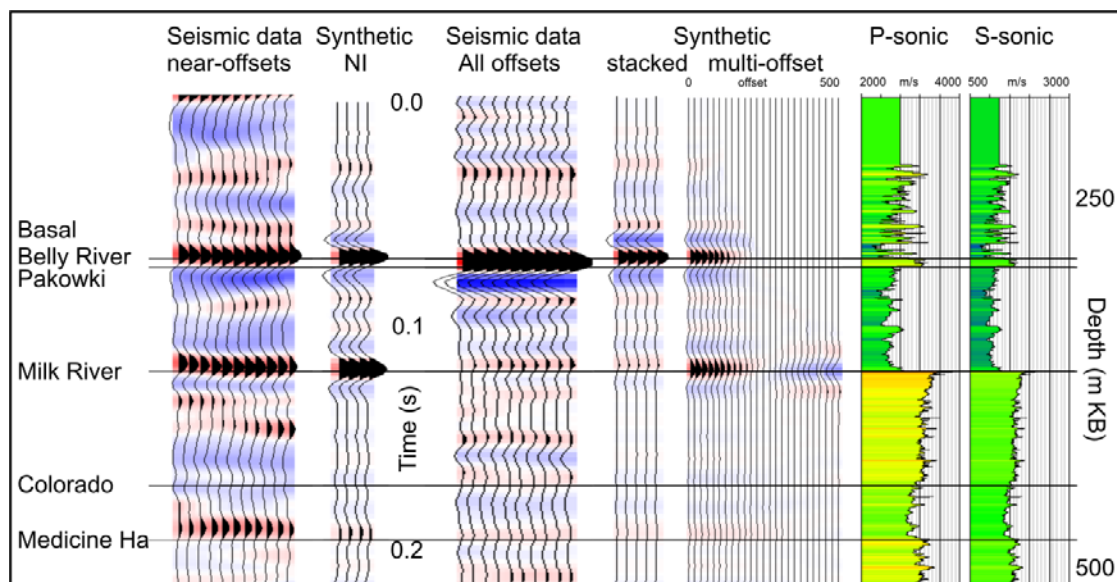


FIG. 1: Character ties for the top of the Milk River Formation, which is a high impedance sandstone. The near-offset seismic stack ties the Normal Incidence synthetic seismogram while the seismic data with all offsets ties the stacked multi-offset synthetic seismogram created from the P sonic and derived S sonic for well 07-22-017-16W4M.

Analysis of time-lapse difference AVO with the Pouce Coupe field data

Shahin Jabbari, David D'Amico, Jeff Grossman, Brian H. Russell, Helen Isaac, and Kris Innanen

ABSTRACT

Time-lapse seismology is a cost-effective approach for monitoring the changes in the fluid saturation and pressure over a period of time in a reservoir, in which multiple seismic surveys are done at different time intervals and then compared to see reservoir changes. A multicomponent time-lapse seismic data set was acquired during hydraulic fracturing of two horizontal wells in the unconventional Montney Reservoir at Pouce Coupe Field in the Peace River area by Talisman Energy Inc. In this study, we analyze this data to validate derived linear and nonlinear theoretical results for the time-lapse amplitude versus offset (AVO) difference during the change in a reservoir from the baseline survey relative to the monitor survey. We first generate the well tie to determine the location of the reservoir on the seismic data at the Montney Formation. Synthetic logs for P- and S- wave velocities and density are then generated for the monitor survey. Analyzing this data set at the baseline and monitor surveys shows that the linear approximation is good enough to estimate time-lapse AVO difference. This is consistent with the fact that the Pouce Coupe data set has a low baseline contrast between the cap rock and reservoir and a low time-lapse contrast from the baseline survey to the time of the monitor survey. The upper layer of the Montney Formation or Doig, with a larger baseline contrast, is also analyzed to evaluate the theoretical results.

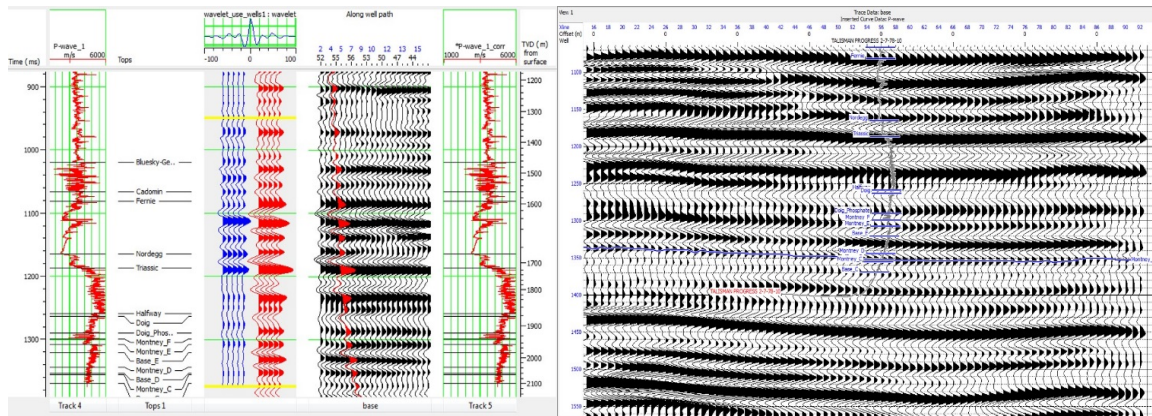


FIG. 1: Left panel: Vertical well tie with baseline P-wave seismic. Right panel: Estimating the horizon times on the seismic section by tying synthetic in Left panel to the baseline seismic data.

PS and SP converted wave reflection coefficients and their application to time-lapse difference AVO

Shahin Jabbari and Kris Innanen

ABSTRACT

Multicomponent time-lapse amplitude variation with offset (AVO) may improve approximating time-lapse difference data. The difference data during the change in a reservoir from the baseline survey relative to the monitor survey are described for converted waves. We defined a framework for the difference reflection data, $\Delta R_{PS}(\theta)$, and $\Delta R_{SP}(\phi)$, in order of physical change or baseline interface contrast and time-lapse changes. A framework for linear and nonlinear time-lapse difference data are formulated using amplitude variation with offset (AVO) methods. The nonlinear higher order terms represent corrections appropriate for time-lapse problems especially for large contrasts cases. We conclude that in many plausible time-lapse scenarios the increase in accuracy associated with higher order corrections is non-negligible for converted wave. Furthermore the third order approximation terms in difference data emphasizes on the difference between exact $\Delta R_{PS}(\theta)$, and $\Delta R_{SP}(\phi)$.

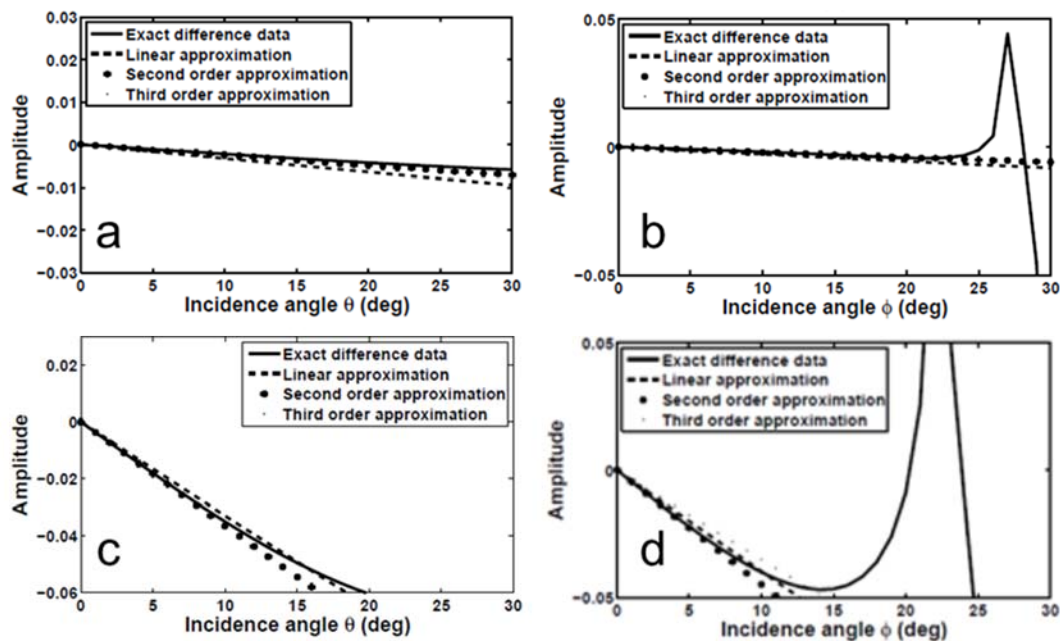


FIG. 1: $\Delta R_{PS}(\theta)$ (a and c) and $\Delta R_{SP}(\phi)$ (b and d) for the exact (Solid line), linear (- - -), second order (+++), and third order approximation (...). In (a) and (b) data set used by Landrø (2001) are applied. In (c) and (d) data used by Veire (2006) are applied.

Extrapolation of low frequencies and application to physical modeling data

Scott Keating and Kris Innanen

ABSTRACT

A projection onto convex sets (POCS) based frequency extrapolation is tested on 1D synthetic and physical modeling data sets, with the goal of obtaining sufficient low frequencies for inversion. The effects of both noise and available frequency band are also investigated. The addition of noise is found to restrict the effectiveness of our inversion in recovering small impedance changes. Broad frequency ranges at high frequency are shown to produce similar results after extrapolation as small frequency ranges at low frequency. Application to physical modeling data met with moderate success, but offered substantive improvements in the inversion as compared to that of the original band-limited data.

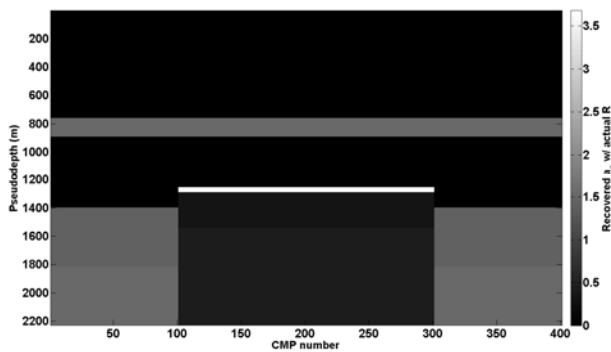


FIG. 1. Impedance inversion given the exact physical modeling parameters.

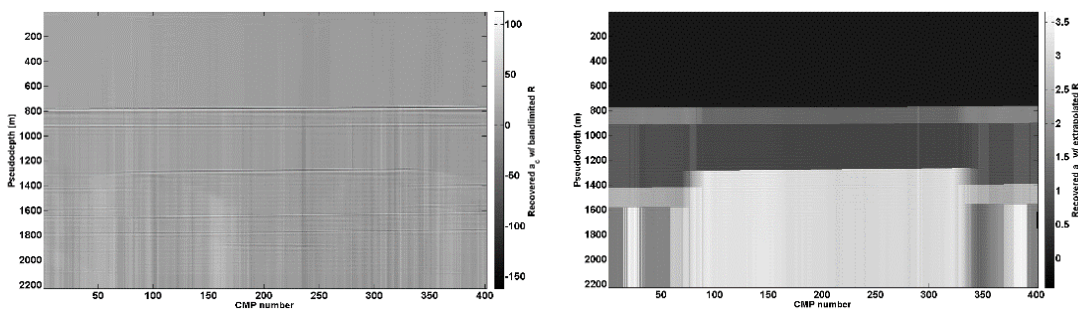


FIG. 2. Left: Impedance inversion result using the measured physical modeling data without frequency extrapolation. Low frequencies are lacking in the measured data, leading to a lack of absolute impedance changes in the result. Right: Impedance inversion using the measured physical modeling data after frequency extrapolation. While significant artifacts and other problems remain, there is significant improvement over the pre-extrapolation result.

Interpolation of seismic data using a principal component analysis POCS approach

Scott Keating and Kris Innanen

ABSTRACT

Projection onto convex sets, or POCS, is a simple, straightforward method of interpolation which hinges on a few basic assumptions. In order to better fulfill these assumptions, a type of POCS is proposed in which a projection onto principal components is the transform used. This method is shown to be effective both on simple synthetic data, as well as on real VSP data. The problem of acquiring the relevant principal components is addressed by using nearby intact data, and other methods are proposed if this should prove impractical. Partially incomplete data are shown to provide adequate principal components for interpolation in some cases.

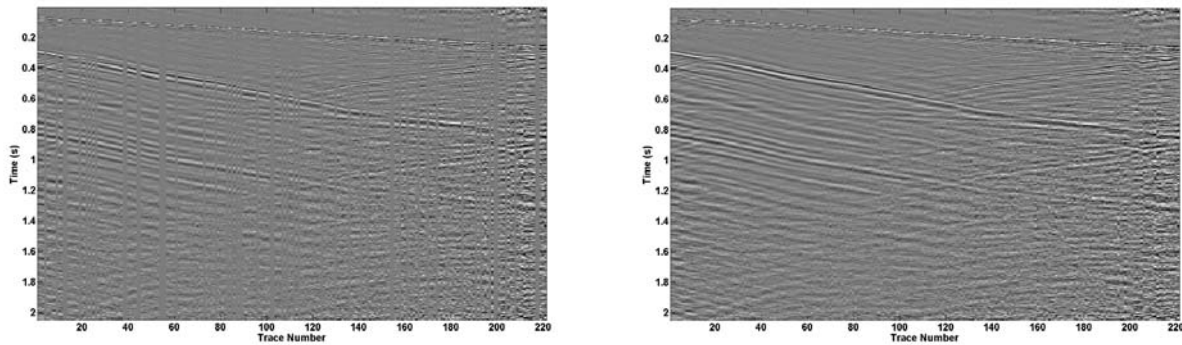


FIG. 1. Left: Shot gather for VSP data with 30% of traces removed. Right: Data after PCA POCS interpolation, using principal components of nearby, incomplete shot gathers.

Nonstationary L_1 adaptive subtraction and application to inverse scattering multiple attenuation

Scott Keating*, Jian Sun, Pan Pan, Kris Innanen

ABSTRACT

A method for adaptive subtraction in conjunction with internal multiple prediction by inverse scattering series is investigated. An L_1 , nonstationary adaptive subtraction is found to minimize mistaken matching to primaries while still allowing for a large degree of multiple removal. This adaptive subtraction is tested on both synthetic and physical modeling data. The method proves to be effective, and avoids unwanted matching to primaries.

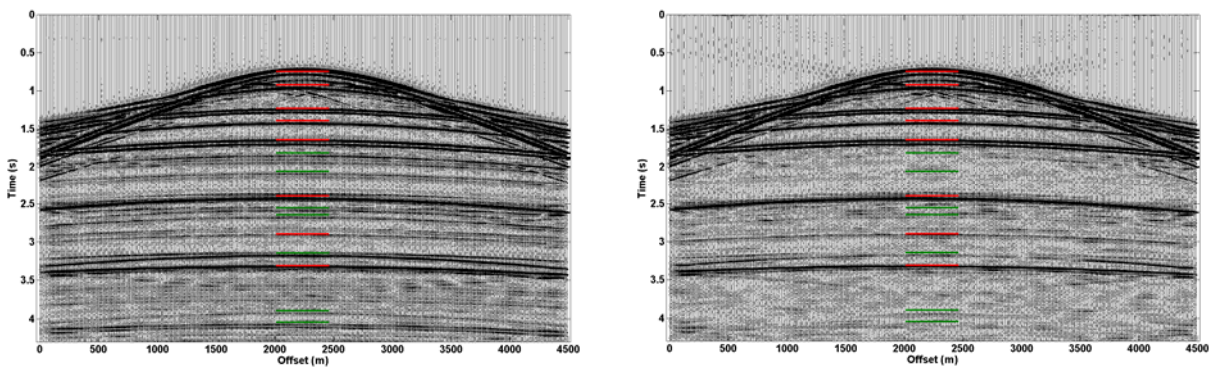


FIG. 1. Left: Synthetic shot record for a nearly 1.5 velocity model with absorbing surface. Primaries are highlighted in red, some notable internal multiples in green. Right: Shot record after L_1 nonstationary adaptive subtraction. Multiples are notably attenuated, while primaries are not.

Second order, iterative least squares inversion of dispersive reflections

Scott Keating, Kris Innanen

ABSTRACT

A second order, iterative least squares approach to anacoustic inversion is presented and tested. Results are compared to linearized inversions, and failure regions and their causes are explored. While the second order approach offers improvement over the linearized approach, problems associated with very low and high Q are caused by other factors and are not greatly improved by the second order inversion.

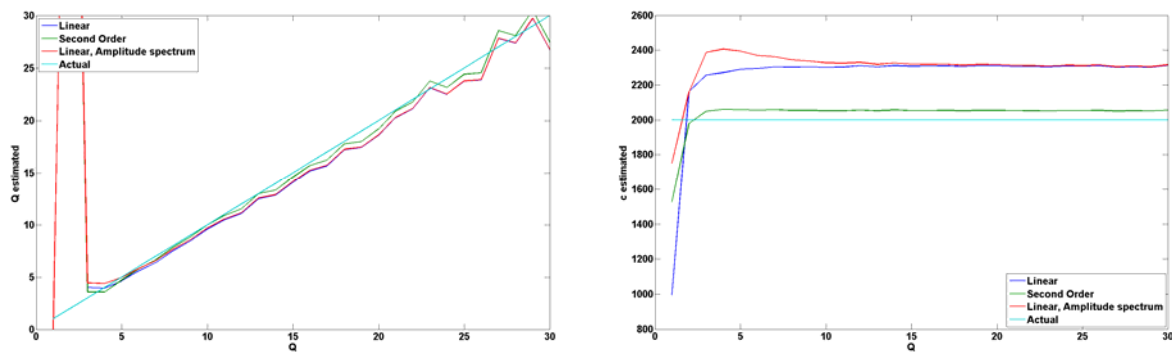


FIG. 1. Estimated Q (left) and velocity c (right) as a function of actual Q for a simple synthetic test. Red and dark blue are two different linear approximations, green is the result with a second order approximation. Light blue indicates the true model values. While the second order approximation provides a better recovery of both Q and velocity, it does not improve the low Q failure, nor the high Q noisiness, which have other causes.

Preservation of AVO after migration

Oliver Lahr and Gary F. Margrave

ABSTRACT

Choice of migration algorithms and seismic acquisition techniques are two contributing factors of how well Amplitude Variation with Offset (AVO) data is preserved. In this report, these effects are investigated using synthetic Common Offset Vectors (COV gathers), the 3D extension of Common Shot gathers. These gathers were created from a 2D synthetic data set that is comprised of the three different AVO classes occurring at different horizontal layers. They vary in terms of shot and receiver line spacing, and thus can be seen as different types of decimation of an actual seismic survey. To mitigate the effect of this decimation, i.e. seismic acquisition footprint, they were then migrated using Kirchhoff migration. It was the purpose of this report to quantify the results of these migrations, i.e. to see how well the Zoeppritz plot of the AVO anomalies pictured here, could be reproduced for the input data shown in the well logs and associated table below for each of the different COV gathers.

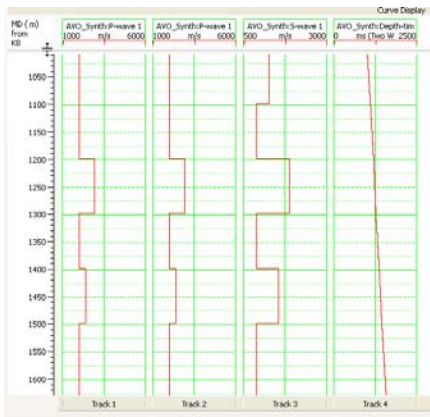
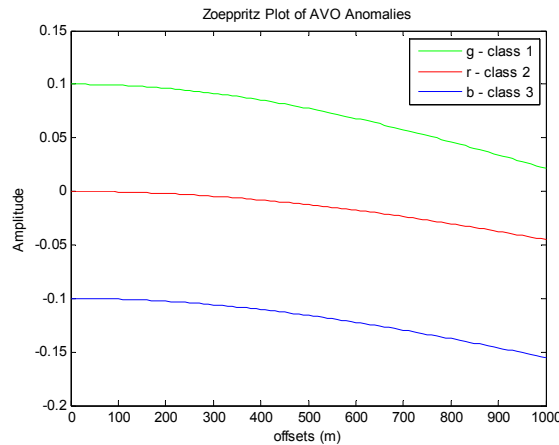


Table 1. Layer Parameters.

Class	α_1 /[m/s]	β_1 /[m/s]	ρ_1 /[kg/m ³]	α_2 /[m/s]	β_2 /[m/s]	ρ_2 /[kg/m ³]
1	2000	879.88	2400	2933.33	1882.29	2000
2	2000	879.88	2400	2400	1540.05	2000
3	2000	879.88	2400	1963.64	1260.04	2000
4	2000	1000	2400	1598.77	654.32	2456.43

Tweaking minimum phase calculations

Michael P. Lamoureux, Gary F. Margrave

ABSTRACT

The minimum phase characterization of impulsive seismic sources is an essential step in the deconvolution process, to remove source signature with appropriate phase. Calculation of the minimum phase equivalent of a given signal is numerically sensitive, given the presence of logarithmic singularities in certain algorithms.

We propose a simple over-sampling in the frequency domain that accommodates the singularity, and show with a few examples that the performance is improved.

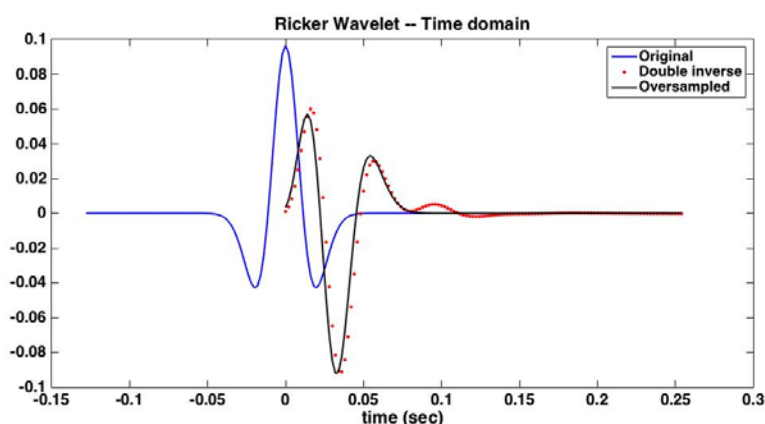


FIG. 1. Oversampling moves the min-phase waveform forward.

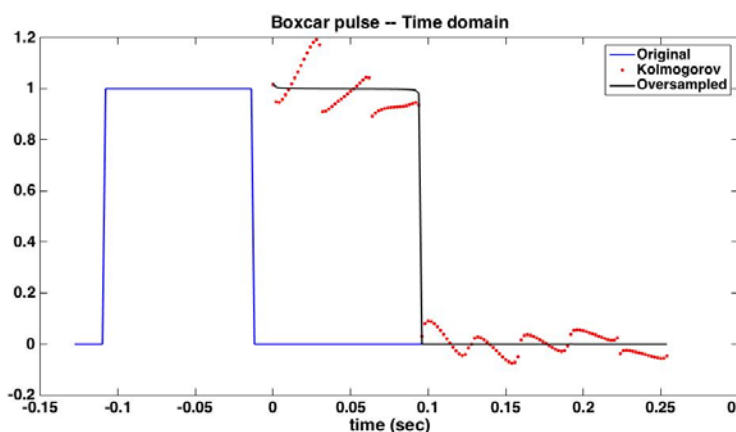


FIG. 2. Oversampling gives a better reconstruction of the boxcar, compared to the standard Wiener-Kolmogorov method.

New approaches to seismic monitoring at the Brooks Field Research Station

Don Lawton*, Malcolm Bertram, Kevin Hall and Kevin Bertram

ABSTRACT

The Containment and Monitoring Institute (CaMI) Field Research Station (FRS) is being developed by CMC Research Institutes, Inc. and the University of Calgary in Newell County, Alberta. The goal of this research station is to develop and calibrate various technologies for monitoring fluid injection and cap rock behaviour at depths of 300 m and 500 m below surface. The project has an emphasis on CO₂ detection thresholds at these relatively shallow depths, but is also focussed on understanding and monitoring understanding shallow gas (CO₂ and CH₄) migration, particularly fugitive gas emissions. The specific objectives being assessed at the FRS are sensitivity of monitoring systems for early detection of loss of conformance and in mapping temporal changes in cap rock that may lead to loss of containment. The FRS is being constructed on lands southwest of Brooks, Alberta, and the 2.5 km² site will operate for at least 10 years. Construction has begun on an array of wells, sensing stations, and surface facilities that will be monitoring fluid injection and cap rock behaviour.

Seismic monitoring is advancing rapidly with time-lapse or 4D seismic surveys, but these are expensive and the time interval between repeated, conventional seismic surveys may temporally alias the geological changes taking place in the reservoir. There is now a move towards not only permanent receiver arrays, but also permanent seismic sources. These may operate continuously, or with a rapid repeat time which may enable trigger events to be detected in the subsurface. Some of these technologies include fibre optic distributed acoustic sensing (DAS) and fixed seismic sources. Plans are in place to install some of these systems at the FRS. Figure 1a shows the FRS surface layout. Buried fibre-optic cable will be laid in a SW-NE trench, and integrated fibre optic packs will be installed in the monitoring wells. We also plan to install one or more new fixed, rotary sources at the site, similar to that shown in Figure 1b.

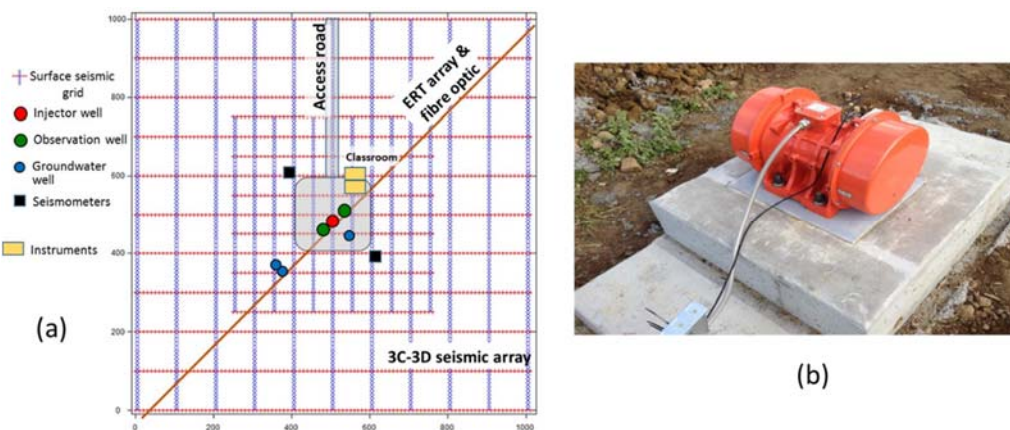


FIG 1. (a) Surface layout of the CaMI.FRS monitoring site; (b) permanent, rotary seismic source (courtesy Barry Freifeld, LBNL).

Azimuth ambiguity elimination for borehole imaging using 3D borehole RTM scheme

Junxiao Li, Kris Innanen, Guo Tao, Laurence R. Lines and Kuo Zhang

ABSTRACT

The azimuth ambiguity has been an issue ever since the beginning of borehole acoustic reflection imaging. The reason of this imaging authenticity indistinguishability occurring not only in the borehole reflection imaging but also in seismic imaging is due to the intrinsic defect of the 2D data processing that treats recorded real data as a 2D data set, which inevitably leads us to take for granted that the data (which actually may be from every possible direction of underneath formations) is only from one direction. The 4-C dipole acoustic well logging technique is then applied to solve the azimuth ambiguity problem by analyzing the azimuthal information contained in the recorded shear wave signals. Thereafter, the migration procedure is carried out to get the imaging result. In this paper, the 3D reverse time migration in the borehole environment is proposed and applied in the simulated data set with a similar source and receiver system as sonic scanner tool developed by Schlumberger. The result shows the directional information of the structures outside the borehole can be directly obtained.

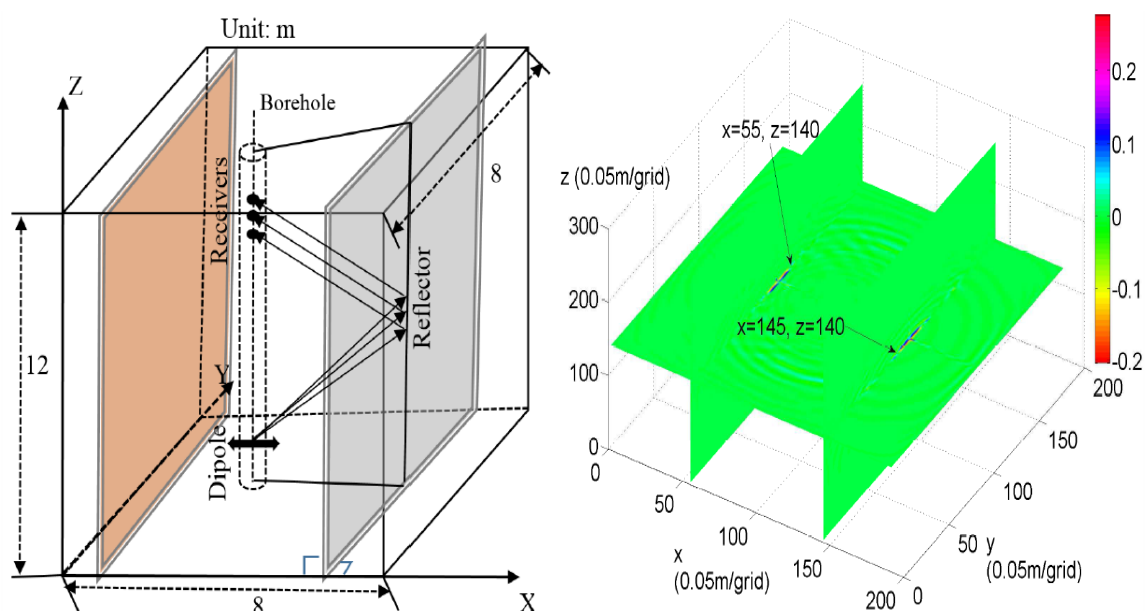


FIG. 1: 3D profile of the VTI model with a dipole source and 8 evenly spaced hydrophones (Left) and its imaging result for one shot by borehole RTM.

Reflection extraction from sonic log waveforms using Karhunen-Loeve transform

Junxiao Li, Kris Innanen, Guo Tao and Laurence R. Lines

ABSTRACT

Sonic reflection logging, a recently developed borehole geophysical scheme, is in principle capable of providing a clear view of structures up to 40 m away from well site theoretically. Under acoustic well logging conditions, reflected wave signals used in sonic reflection logging are generally lost in the full waveform records, hidden by the dominant direct waves (direct P- and S- waves, and the Stoneley wave). It is critical, therefore, to effectively extract the reflection signals from the acoustic full waveforms in acoustic reflection well logging data processing. The Karhunen-Loeve (KL) transformations combined with a band limiting filter is used to extract reflections of interest out of dominant direct waves. Based on energy difference of each wave component, the direct Stoneley wave, S wave and P wave are to be eliminated separately from high to low energy component. Therefore, the extracted reflections can then be used in migration so as to get a clear image of the structures outside borehole.

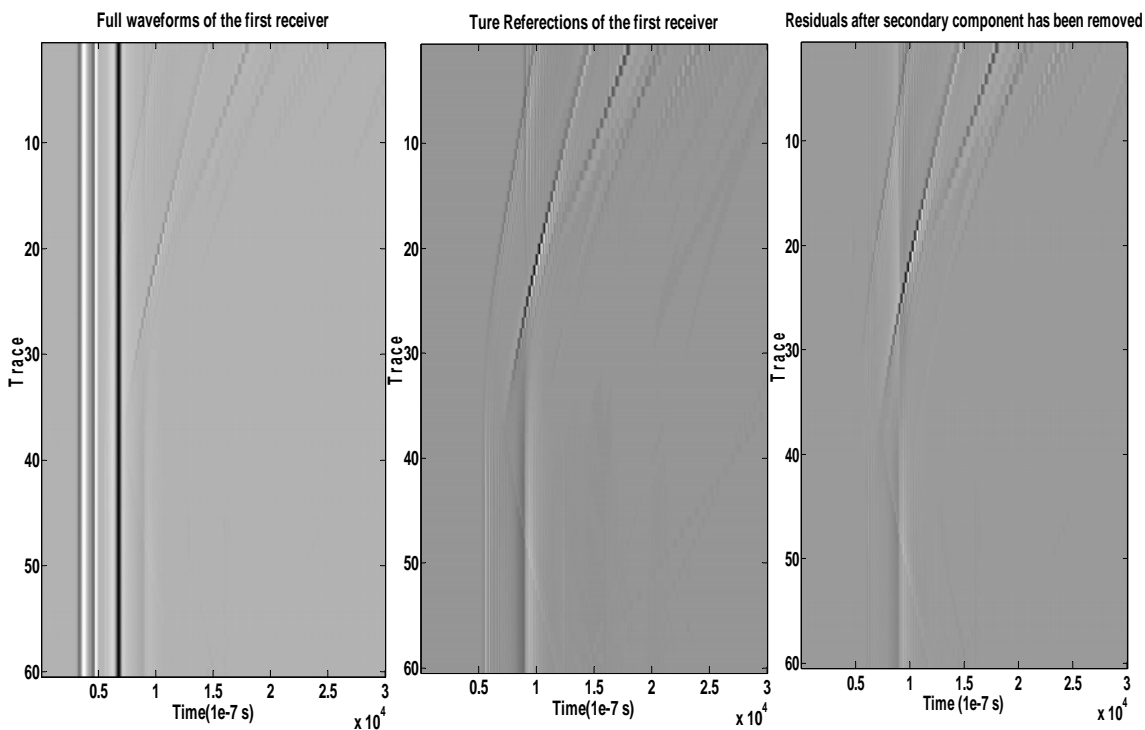


Fig. 1: Received full waveform when the dip angle is 45 degree (Left), theoretical refecation signals after the direct signals have been removed (Middle) and residuals after secondary component has been removed by KL transform (Right).

Wave field simulation on 3D borehole dipole radiation

Junxiao Li*, Kris Innanen, Kuo Zhang, Guo Tao and Laurence R. Lines

ABSTRACT

Wave simulation in borehole environment is crucial for characterization of the waveforms traveling through the borehole, recorded by the receivers, leaking away outside borehole and reflecting from geological structures outside borehole. In order to mitigate this directional ambiguity, a dipole acoustic reflection imaging is developed. In this paper, a 3D elastic staggered-grid finite difference method for both isotropic and anisotropic media is discussed for the bore hole acoustic wave simulation. A hybrid perfectly matched layer is proposed which removes the artificial reflections from the computational regions. A numerical simulation of radiation, reflection and multipole reception of the elastic waves in the presence of a dipole source is proposed, for azimuthal detection, to characterizing the relationship between S wave polarization and the offset between the source and receivers as well as the angle of the source and reflector. The results show the amplitude change of S-S reflection is related to the incident angle to the reflector. Its maximum amplitude occurs as the incident angle reaches to a critical angle, which can then be used to calculate the total propagation distance of the S-S wave. As a result, the critical angle as well as the SH wave velocity of the second layer outside the bore hole can thus be determined.

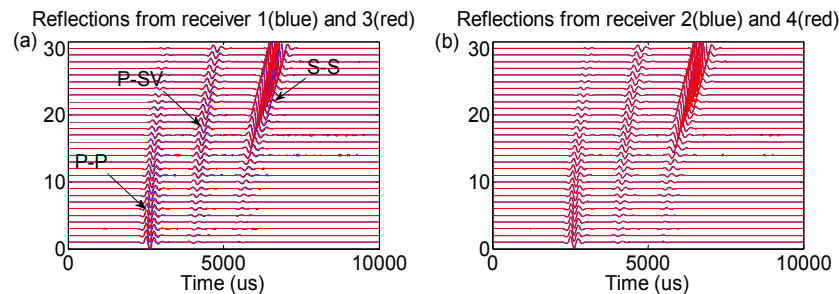


FIG.1: (a) Received reflections of receiver 1 (red) and receiver 3(blue); (b) and (d) Received reflections of receiver 2 (red) and receiver 4 (blue).

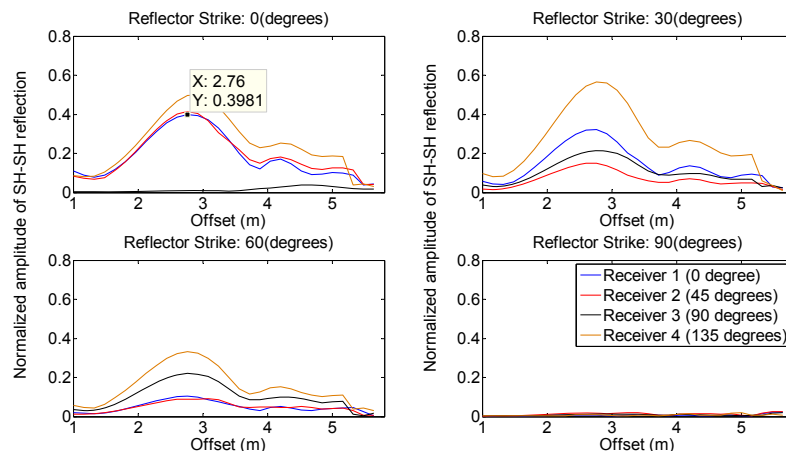


FIG.2: Cross-plot of normalized amplitude versus different receiver offsets in VTI medium.

Utilizing PSSP Waves

Laurence R. Lines* and Patrick F. Daley

ABSTRACT

While the interpretation of reflected P-waves on seismic data remains the main vehicle for seismic interpretation, there are other signals in seismic reflection recordings that can be fully utilized in seismic inversion. There are reflection signals that are due to the conversion of P-wave energy to S-wave energy in transmission followed by conversion from S-wave to P-wave upon reflection. These waves, known as PSSP waves, have significant amplitude and normal moveout (NMO), and are seen on reflection records at wide offset. We model PSSP waves by ray tracing and finite-difference wave equation computations. While PSSP amplitudes are essentially zero at normal incidence for flat reflectors, their energy is considerable at larger offsets. Also, the PSSP energy for non-flat reflectors will generally be nonzero at zero offset. In addition to identification of the PSSP modes, there is the challenge of utilizing this energy for estimation of seismic velocities. While the NMO for PSSP arrivals allows it to be suppressed through stacking in imaging P-wave reflections, it is feasible that full waveform inversion could be implemented for utilizing the PSSP energy as useful signal rather than treating it as undesirable “noise”.

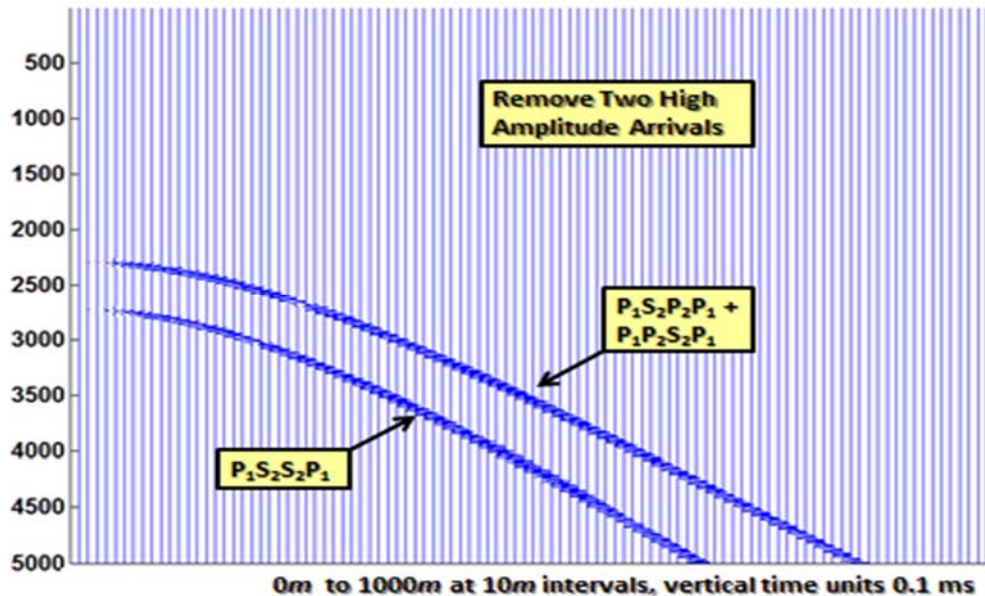


FIG. 1 Amplitudes of converted modes such as PSSP, PSPP, and PPSP as computed by ray-reflectivity modeling of Daley and Krebs (2015) for Long Lake model in this paper. Range of traces is from 0-1000 m at time intervals of 10m. Vertical time samples in units of 0.1 ms. These converted wave arrivals can be used to be improve seismic inversions.

Gabor nonstationary deconvolution for attenuation compensation in highly lossy dispersive media

Kay Y. Liu, Elise C. Fear, and Mike E. Potter

ABSTRACT

Gabor nonstationary deconvolution was developed in the field of Seismology to compensate for attenuation loss, correct phase dispersion, and produce images with high resolution. Compared to seismic waves, a stronger attenuation and dispersion effect is observed in microwave frequency electromagnetic (EM) waves, especially with the propagating medium that has high loss and high dispersion, such as human body tissues. In the microwave image, it is displayed as a characteristic blurriness or lack of resolution that increases with time/distance. To produce microwave images with high resolution, there is a strong need for a technique that is able to compensate for the energy loss and correct for the wavelet distortion. Therefore, the Gabor algorithm is proposed to deal with the nonstationarity in EM wave propagation and attenuation.

Gabor deconvolution is essentially based on the assumption that the anelastic attenuation of seismic waves can be described by a constant Q theory. Our study reveals that the same definition of Q as in seismic can also be used to characterize EM wave propagation and attenuation. Even though the Q for EM waves is not constant over the microwave frequency of interest; however, a new parameter Q^* , which is closely related to Q , can be approximated as constant for highly lossy dispersive human body tissues. Q and Q^* might be different in the order of magnitude; however, these quantities describe the attenuation and dispersion in the same manner.

Our test results indicate that the Gabor nonstationary deconvolution is able to sufficiently compensate for attenuation loss and correct phase dispersion for EM waves that propagate through high lossy dispersive media. It can work effectively where a constant Q^* approximation is achieved.

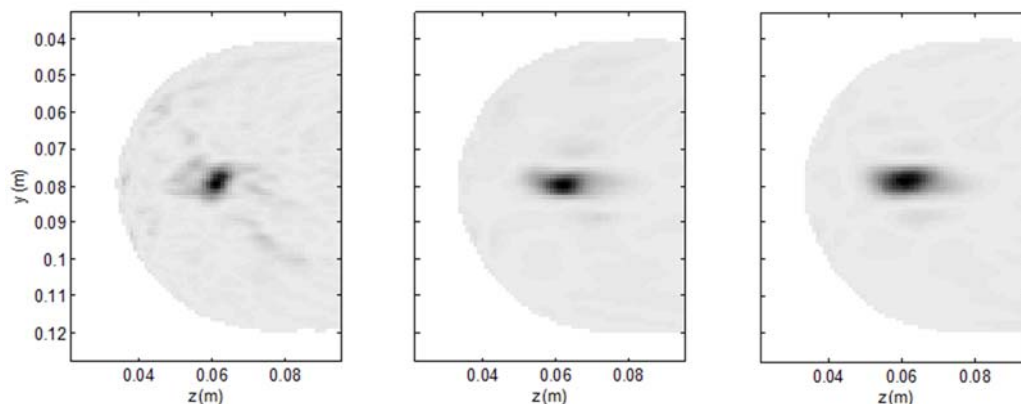


FIG. 1. Time focusing at the location of the maximum response in the image. The images are sliced through the yz plane of a 3D image volume. From left to right, the images are reconstructed using Gabor nonstationary deconvolution as preconditioning, using stationary deconvolution as preconditioning, and without deconvolution.

Recording seismic on geophones within ground screws II

Peter M. Manning, Eric Gallant, Kevin Hall

ABSTRACT

Seismic records were obtained from geophones installed within devices known as ground screws, normally used as bases for small buildings. The data were acquired along with other records at CREWES' Priddis test site in November/2014. Analysis is basically a comparison between the records and surface geophones at the same recording stations, and some ground screw records show clear advantages in signal to noise ratios. A patent on this type of recording is held by Ross Huntley.

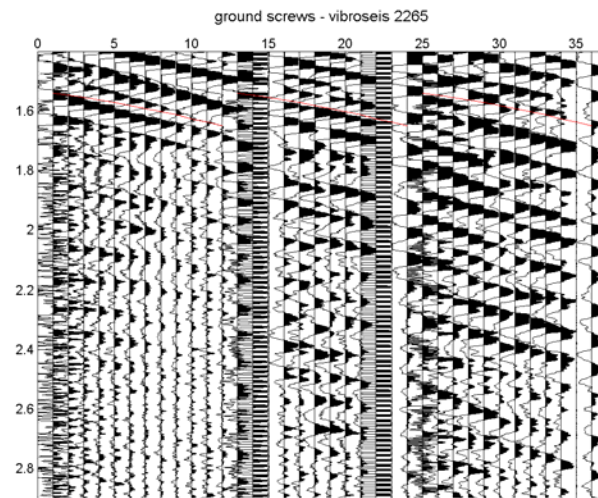


FIG. 1. Vibroseis data from source point 265 and recorded from ground screws. This record is plotted at high gain to see the signal at these long offsets.

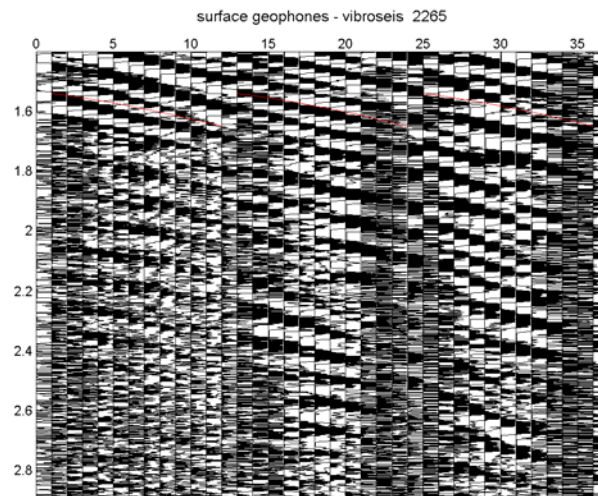


FIG. 2. Vibroseis data recorded from conventional surface geophones and with the same gain. Compare to the Figure above.

Intrinsic attenuation: removing the stratigraphic effect from attenuation measures

Gary F. Margrave*, Sylvestre Charles (Suncor), and Hossein Aghabarati (Suncor)

ABSTRACT

Estimates of attenuation computed from seismic data are inherently composed of two parts: a local intrinsic effect, and a nonlocal stratigraphic effect. The former is a property of the rock that the wave is transiting through and represents actual loss of wave energy to heat. The latter is a wave interference due to the cumulative effect of short path multiples occurring along the transmission path. It is often desirable to estimate intrinsic attenuation as a reservoir parameter as it may indicate reservoir quality. However, attenuation measurements from seismic data will always consist of both intrinsic and stratigraphic effects so the isolation of the former requires the estimation of the latter. We investigate the possibility of using a visco-acoustic 1D synthetic VSP driven by finely sampled well information to estimate the stratigraphic attenuation. We then use these estimates to isolate the intrinsic attenuation from a zero offset VSP. We show that well-log sampling of 0.3048m in depth is sufficient to estimate the stratigraphic effect; however, the unavoidable occurrence of an unlogged overburden means that the magnitude of the estimate will always be too small. The estimates of total attenuation on a real VSP are made on the separated downgoing wavefield. Intrinsic attenuation then follows by subtracting the stratigraphic component, estimated from the synthetic VSP, from the measured total attenuation. Our estimates of intrinsic attenuation fail to show the theoretically expected monotonically increasing behaviour. Among the possible reasons for this are the imperfect nature of VSP wavefield separation, problems with receiver and sonic coupling in the borehole, the aforementioned unlogged overburden, and mode-converted scattered waves that are not included in the visco-acoustic approximation. These are topics for future research.

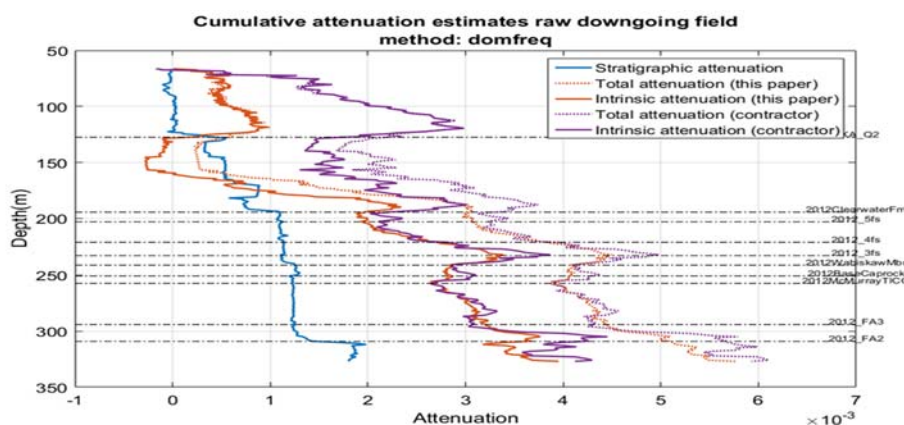


FIG. 1. The application of the estimated stratigraphic attenuation to measured total attenuation. Two alternate estimates of total attenuation are shown as dotted lines. Both were calculated on the downgoing field a real VSP, one by the contractor (purple) and the other by us (orange). The solid orange and purple lines are estimates of intrinsic attenuation formed by subtracting the estimated stratigraphic attenuation from the corresponding estimate of total attenuation.

Post-stack iterative modeling migration and inversion (IMMI)

Gary F. Margrave

ABSTRACT

The possibility of a post-stack process resembling full-waveform inversion (FWI) is investigated. As generalized by the IMMI concept, this implies an iterative process of modeling, migration, and inversion all done in the post-stack domain. To test this idea, a detailed stratigraphic p-wave velocity model was created by interpolating between 3 sonic logs from the Hussar dataset. The overburden (upper 200m) was created with smooth lateral and vertical gradients, and the underburden (1.55km to 2km depth) has similar smooth gradients while the detailed stratigraphy is contained in the 200m-1.55km interval. The wells were placed at 1km, 2km, and 3km distances along the line, the interpolation was guided by picked formation tops, and the resulting velocity model was created on a 2.5m square grid (2D). Using acoustic finite-difference modeling, 60 shot records were created at even intervals along the 4km line. The data were then processed with gain, f-k filter, normal-moveout removal, and stack to create a conventional CMP stack. Then, an IMMI process of exploding reflector modeling, post-stack migration, and matching to known impedance at a presumed well was employed. The exploding reflector modeling was chosen for its simplicity compared to the modeling and processing of all 60 shots in each iteration. The migration was a post stack depth migration, and the matching to well control was conducted using a single simulated well at coordinate 1000m. It was assumed that the overburden (upper 200m) velocity was known through tomography or refraction statics and it was further assumed that the velocity was known in detail at the well from 200m to 1.55km depth. The starting model contained the true overburden and then a simple linear gradient from the base of the overburden to a presumed-known basement velocity of 4500m/s. Shown below is the result after 11 iterations during which the maximum frequency allowed into the process was gradually increased from 10 to 60 Hz. At each step in the iteration, the depth migration at the well was scaled to approximately match the well velocity and this scaling was then applied to the entire migration. While a better result is desired, the process appears to be both feasible and worthwhile.

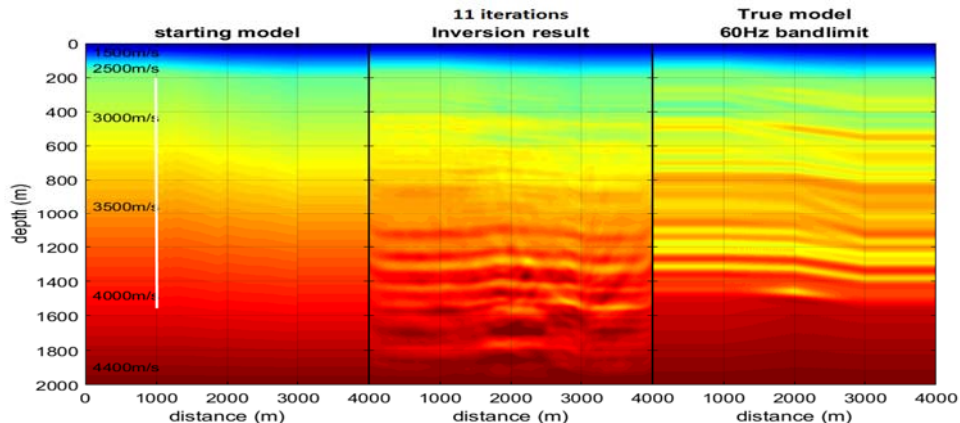


FIG. 1. The result of 11 iterations of post-stack IMMI. The lowest frequency was always zero while the maximum frequency followed the schedule: $f_{max} = 10, 15, 20, 25, 30, 35, 40, 45, 50, 55, 60$ (Hz). The white line is the simulated well location at which velocity is assumed known.

Shear wave attenuation measurements from converted-wave VSP data

Michelle C. Montano*, Don C. Lawton, and Gary F. Margrave

ABSTRACT

Shear wave attenuation can be measured from down-going shear waves in VSP data. However, direct down-going shear waves are not always easy to identify in the VSP data. One problem associated with these waves is that after a short distance, they lose a significant part of their bandwidth and energy because the direct shear waves have to travel through the near surface (Fig. 1a) which results in severe attenuation. If we want to estimate reliable Q_S values along the borehole receivers, this may be a problem. An alternative method to estimate Q_S is through exploiting converted-wave (P-S) reflections. In this case, the downward seismic wave-field travels as a P-wave and reflects as an S-wave. As a result, the initial S-wave at the conversion point has the same bandwidth as the incident P-wave. This enables us to obtain more reliable Q_S estimations along the borehole. Q_S values were estimated from VSP converted-wave data using the spectral-matching method. These values were computed from a walk-away VSP and conveyed into a single value at zero-offset by using the QVO method. Q_S values determined range from 20 to 50, suggesting a strong attenuation for the shear waves. Moreover, we were able to compare Q_S/Q_P versus V_P/V_S to understand the rock properties of the study area (Fig. 1b).

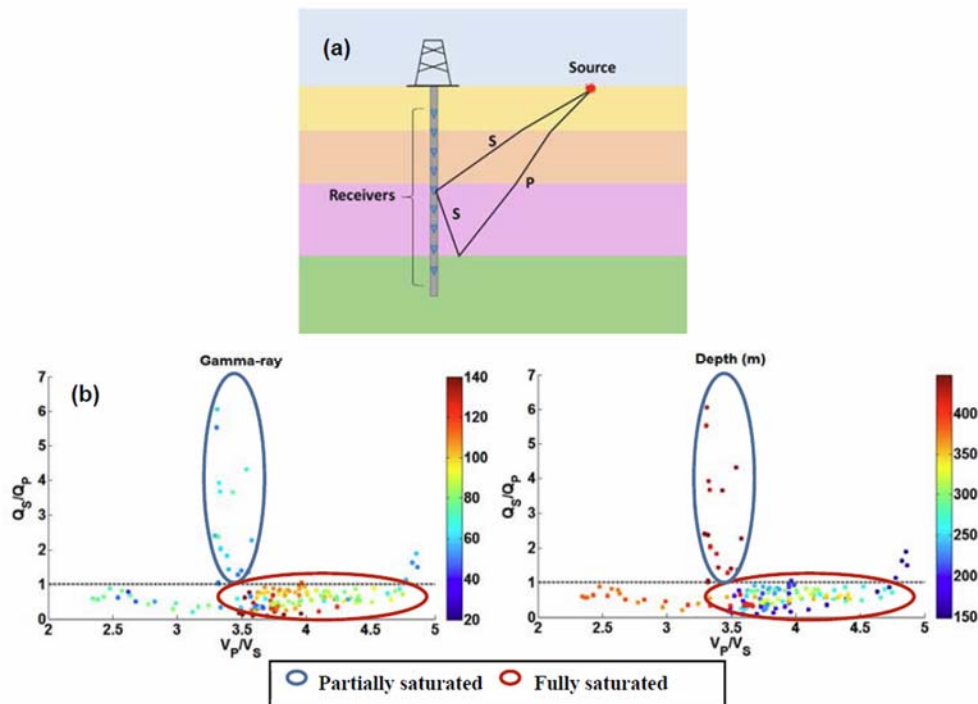


FIG. 1. (a) Down-going shear waves and converted-waves travelling through the borehole receivers. Seismic attenuation ratio versus velocity ratio scatter-plot. (b) Q_S/Q_P versus V_P/V_S coloured by gamma-ray and receiver depth.

Finite difference modeling of the diffusive slow P-wave in poroelastic media

Shahin Moradi, Don C. Lawton and Edward S. Krebs

ABSTRACT

Biot's theory of poroelasticity predicts the presence of a slow P-wave in a fluid saturated medium due to the relative movement of the pore fluid with respect to the rock matrix. The slow P-wave, is highly diffusive in seismic frequencies and thus will not be observed in seismic data. However, in the case of zero fluid viscosity, this wave is a non-diffusive mode that travels through the medium. In this report both diffusive and non-diffusive modes are modeled using a previously developed finite-difference algorithm. It seems that in a uniform homogenous medium the amount of amplitude loss due to wave conversion in the diffusive case is very close to the one in the non-diffusive case. This shows that although the diffusive P-wave is not a traveling mode, it exists in the medium but dissipates quickly. The slow P-wave is particularly important where gas exists in the form of separate patches in the pore fluid. In those cases the wave conversions to the slow P-wave may dissipate a considerable amount of energy. Modeling wave propagation in such media is useful in monitoring studies for CO₂ sequestration.

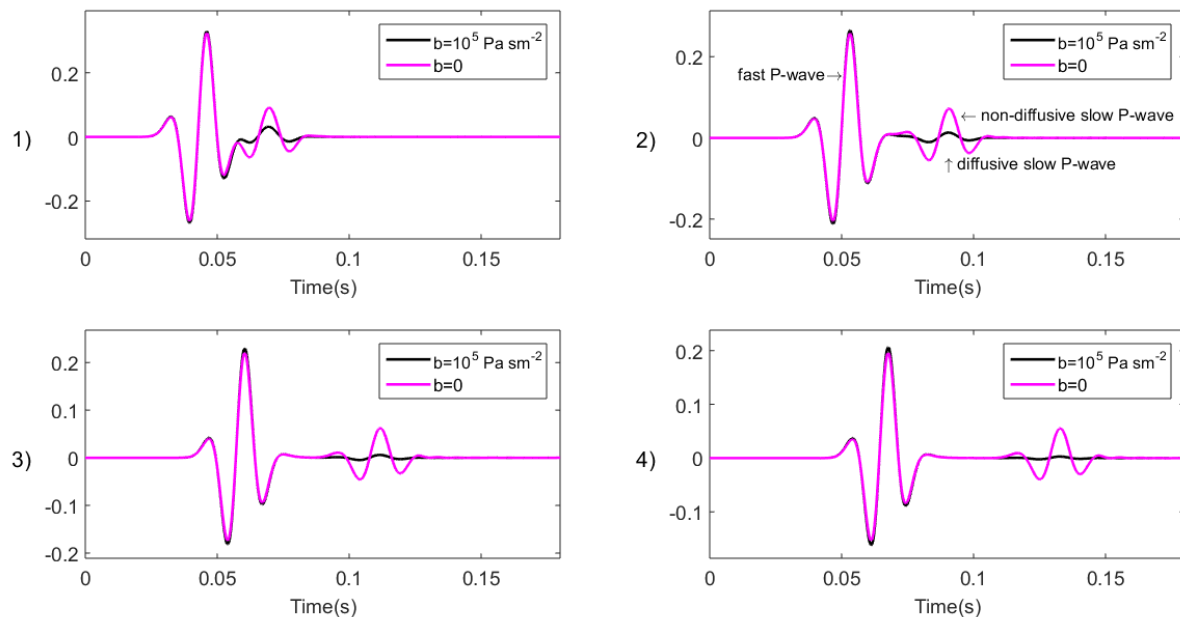


FIG. 1. Traces from the vertical particle velocities of the solid in poroelastic media for two values of $b=0$ and $b=10^5 \text{ Pa sm}^{-2}$, where b (mobility constant) is the ratio of the fluid viscosity to the rock's permeability. The slow P-wave in the case of nonzero mobility dissipates quickly while in the case of zero mobility does not change through time. Furthermore, the similarity of the fast P-wave amplitude in both cases implies that the dissipated amount of energy in non-diffusive mode is close to the one in the diffusive mode. Therefore, when the mobility is not zero, although the slow P-wave is not observed, it exists as a diffusion mode and dissipates the energy of the wave.

Full viscoelastic waveform inversion: a mathematical framework

Shahpoor Moradi* and Kris Innanen

ABSTRACT

We analyzed the mathematical framework of full viscoelastic waveform inversion in time domain. First we showed that how perturbations in density, relaxation function and stress generate the scattered wave. This is called the Born approximation, which is the single scattering assumption describing the relationship between the perturbations in reference medium with the scattered wave field. By inserting the changes in density, relaxation function and stress in wave equation, we arrive at a wave equation governed the scattered wave with new sources. Perturbations in density act as point force and perturbations in relaxation function and stress act as moment tensor source. By having the sources and using the retarded Green's tensor we can obtain the integral equation for the solution of the scattered wave. This integral equation can be expanded to extract the five Frechet kernels for density, unrelaxed bulk modulus and shear modulus, and the differences between the relaxed and unrelaxed modulus. By applying the adjoint operation we invert the aforementioned five parameters in terms of forwarded and backscattered wave field in time. Backscattered wave field is obtained by using the integral equation including the multiplication of advanced Green's tensor on the forward scattered wavefield. We also obtained the Jacobian transformations that relate the five viscoelastic parameters based on density and relaxation functions in terms of model parameters density-velocity-quality factor and density-impedance-quality factors.

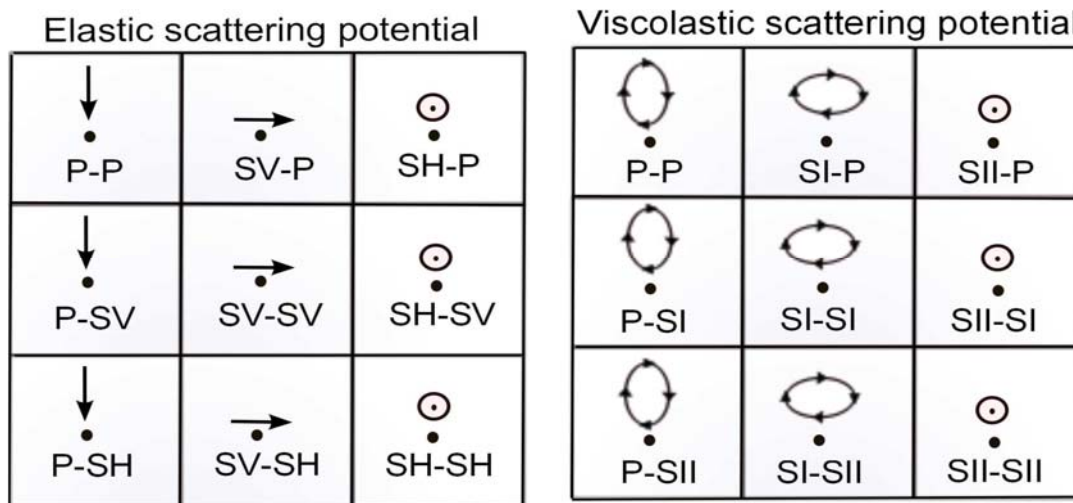


FIG. 4. Left figure illustrates the components of scattering potential for scattering from elastic perturbations. Arrows indicate the polarization of the incident waves, P-, SV, and SH-waves have linear polarizations. Right figure illustrates the components of scattering potential for scattering from elastic and anelastic perturbations. Polarization for P- and SI-waves is elliptical whereas for SII-wave is linear.

Radiation patterns associated with the scattering from viscoelastic inclusions

Shahpoor Moradi and Kris Innanen

ABSTRACT

We obtained the radiation patterns associated with the scattering of seismic waves from five viscoelastic inclusions; density, P- and S-wave velocities and quality factors for P- and S-waves. We show that the polarization and slowness of viscoelastic waves are complex. Basically the radiation patterns from elastic and anelastic inclusions are given by the scattering potentials which are the amplitude of the spherical scattered waves from scatter points. We show that the scattering potentials are complex functions of averages in phase and attenuation angles.

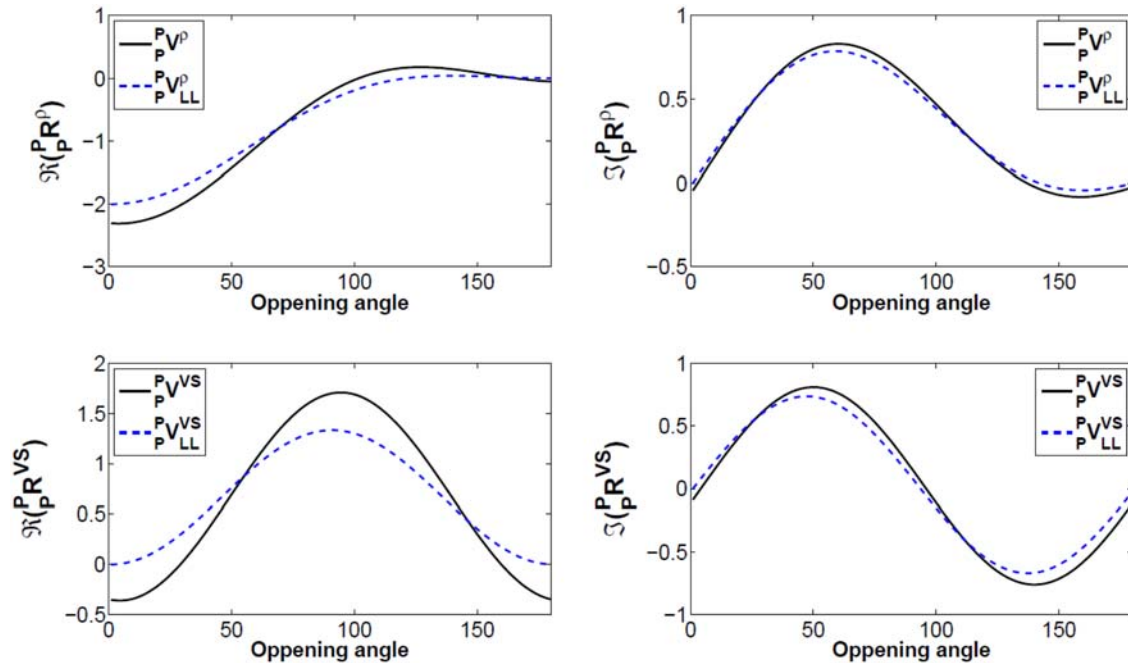


FIG. 1. Digram illustrating the real and imaginary of density and S-wave velocity terms of P-to-P scattering potential for $Q_P = 5$ and $Q_S = 4$ and attenuation angles $\delta_P = \delta_S = 70^\circ$. The solid line refers to the arbitrary attenuation and dash line refers to the low-loss case.

Sensitivity analysis of viscoelastic full waveform inversion

Shahpoor Moradi and Kris Innanen

ABSTRACT

Fréchet kernels for FWI of multicomponent data for a linear isotropic viscoelastic media are derived by using the Born approximation applied to the Green's integral solution of the wave equation. The kernels that also called scattering potentials are the functions of opening angle between the incident and scattered waves and attenuation angle that characterized the maximum direction of the attenuation. Sensitivities of the full recorded viscoelastic wave-field are obtained in three types of model parametrization, density-velocity-quality factor, $[\rho, V_P, V_S, Q_P, Q_S]$, density-impedance-quality factor $[\rho, Z_P, Z_S, Q_P, Q_S]$, and density-Lamé parameter-quality factor, $[\rho, \lambda, \mu, Q_P, Q_S]$. We also study the radiation patterns of point sources and moment tensor sources, among them, a dipole and double couple sources in a viscoelastic medium, this analysis can be used for the inversion of the seismic sources in an attenuative medium.

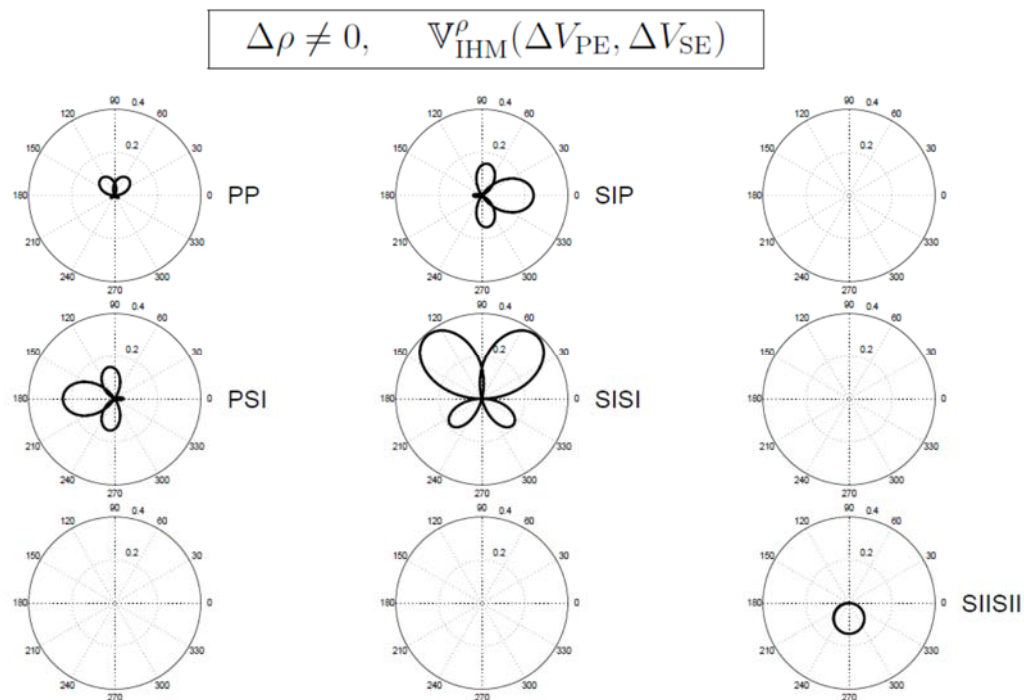


FIG. 1. Anelastic-inhomogeneous part of viscoelastic sensitivity matrix parameterized by $(\rho; V_{SE}; V_{PE})$ for density diffractor for the five scattering modes P-P, P-SI, SI-P, SI-SI and SI-SI. These patterns are generated by the inhomogeneous waves scattered from density scatterers in an attenuative background. In the absence of anelasticity in reference medium or in the case of homogeneous waves these terms are vanished.

Viscoelastic AVO equation updates: Born versus Aki-Richards approximations

Shahpoor Moradi and Kris Innanen

ABSTRACT

Anelastic properties of reservoir rocks are important and sensitive indicators of fluid saturation and viscosity changes due (for instance) to steam injection. The description of seismic waves propagating through viscoelastic continua is quite complex, involving a range of unique homogeneous and inhomogeneous modes. This is true even in the relatively simple theoretical environment of amplitude-variation-with-offset (AVO) analysis. For instance, a complete treatment of the problem of linearizing the solutions of the lowloss viscoelastic Zoeppritz equations, to obtain an extended Aki-Richards approximation (one that is in accord with the appropriate complex Snell's law) is lacking in the literature. Also missing is a clear analytical path allowing such forms to be reconciled with more general volume scattering pictures of viscoelastic seismic wave propagation. Our analysis, which provides these two missing elements, leads to approximate reflection and transmission coefficients for the P- and types I S- waves as formulated by Borchardt. These involve additional, complex, terms alongside those of the standard isotropic-elastic Aki-Richards equation. The extra terms are shown to have a significant influence on reflection strengths, particularly when the degree of inhomogeneity is high. The particular AVO forms we present are finally shown to be special cases of potentials for volume scattering from viscoelastic inclusions.

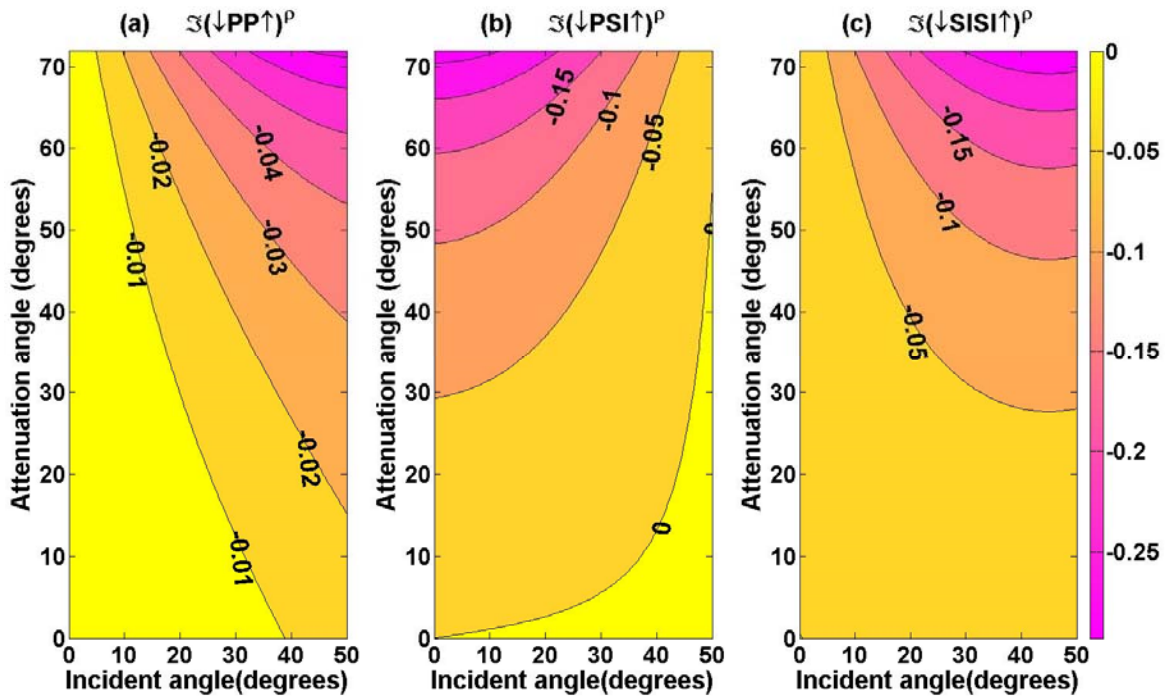


FIG. 1. The maps of imaginary part of density component of the linearized reflectivities. The vertical axis indicates the attenuation angle and horizontal axis incident angle.

A framework for full waveform modeling and imaging for CO₂ injection at the FRS project

Davood Nowroozi, Donald C. Lawton

ABSTRACT

The Field Research Station (FRS) is a project developed by CMC Research Institutes, Inc. (CMC) and the University of Calgary. It is a CO₂ injection and test site in the south east of Alberta, near Brooks. A well has been drilled to a depth of 550 m and a full set of well log data has been acquired. It is ready for the small volume of CO₂ injection in the shallow targets to be monitored using seismic and other survey types.

During the injection CO₂ in the target layer (300 m depth), dynamic parameters of the reservoir as pressure and phases saturation will change and they can be derived of fluid simulation result. For the project, strategy is five years' injection with constant mass of CO₂ equal to 1000 t/yr. In this case, the CO₂ saturation increases to a maximum of 70% in the injection zone adjacent to the well but is generally between 10 to 50 percent; the CO₂ plume shape is an ellipsoid with radius of 120 m radius and a thickness of 12 m. Based on well log data and dynamic reservoir parameters (CO₂ and brine saturation, and reservoir pressure) the P-wave velocity and density were determined through fluid substitution methods. The bulk modulus of dry rock, fluids, minerals and density after injection was calculated and saturated bulk modulus extracted using Gassmann's equation. Fluid substitution causes a change in acoustic impedance value in injection zone of reservoir.

Time-lapse seismic analysis of reservoir was assessed by seismic finite difference time domain (FDTD) modeling based on an acoustic velocity-stress staggered leapfrog scheme. The FDTD is 2nd order in time and 4th order in space on Central Finite Difference (CFD). The boundary conditions are set on all edges except surface, based on a perfectly matched layers (PML) approach. The effect of CO₂ substitution is a time delay in time domain seismic data under the reservoir because of velocity reduction and also a change in amplitude of reservoir reflections. Bases on synthetic models, the difference between base model and time-lapse model after 5 years of CO₂ injection reveals a significant seismic result, because it is a near-surface reservoir. Given that the seismic resolution is high because of the shallow target depth and acquisition parameters, it is expected to improve that seismic monitoring will be an effective method to monitor the CO₂ injection.

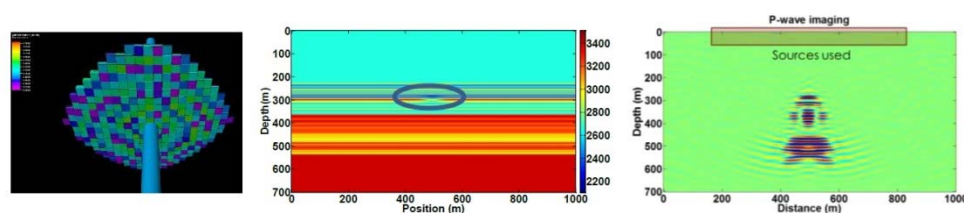


FIG. 1. Left: simulation showing CO₂ saturation; Centre - velocity change in the reservoir zone calculated using the Gassmann equation; Right – difference of migrated images between baseline and monitoring survey.

Full-waveform inversion in the frequency-ray parameter domain

Wenyong Pan, Kristopher Innanen

ABSTRACT

Full-waveform inversion (FWI) promises high-resolution estimates of the subsurface model properties by iteratively minimizing the difference between modeled and observed data. Its computational cost remains an obstacle in practical applications, and research is active in developing efficient FWI implementations. We describe an efficient frequency-ray parameter (f-p) domain FWI equipped with linear phase-encoding in this paper. The linear phase-encoding is performed by constructing the super-gathers by summing densely distributed individual shots with linear phase shifts. A slant update strategy with varied ray parameters is proposed to further reduce the computation burden. The proposed strategies can reduce the computation burden significantly but also unfortunately introduce strong cross-talk artifacts. We demonstrate that a partial overlap-frequency strategy is important to suppress these cross-talk artifacts. The frequency-ray parameter domain FWI is implemented with gradient-based methods, quasi-Newton L-BFGS method and a truncated Gauss-Newton method. The f-p domain FWI is then enacted on a Marmousi-II model to demonstrate the effectiveness and efficiency of the combined strategies on reconstructing the velocity model. Different optimization methods with the proposed strategies are examined and compared. The resistivity to noisy data is finally analyzed and discussed.

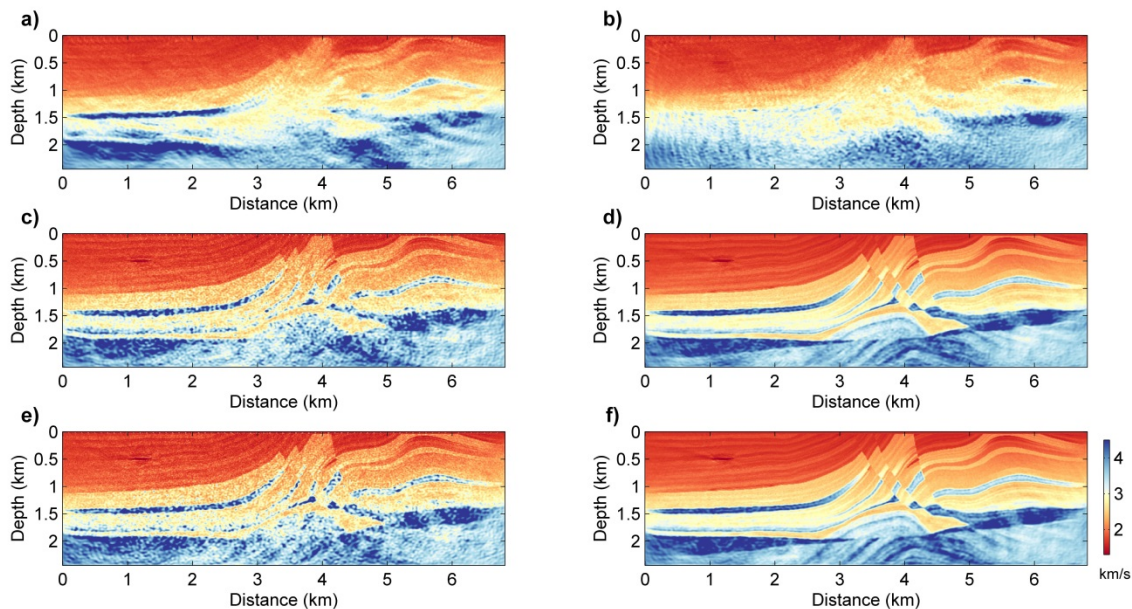


FIG. 1. (a) Mono-frequency slant update with $p = -0.01$ s/km; (b) Mono-frequency slant update with $p = -0.03$ s/km; (c) Mono-frequency random slant update; (d) Partial overlap-frequency random slant update ($\epsilon = 0.4862$); (e) Mono-frequency sequential slant update; (f) Partial overlap-frequency sequential slant update ($\epsilon = 0.4596$).

FWI numerical test using Hussar dataset

Wenyong Pan, Kristopher Innanen, Gary Margrave, Nassir Seed

ABSTRACT

Full-waveform inversion (FWI) promises high-resolution estimates of subsurface model parameters by iteratively minimizing the difference between the modelled data and observed data. While FWI also suffers from a lot of difficulties, one of which is the cycle-skipping problem resulting from lack of low-frequency and inaccurate initial model. CREWES acquired Hussar low-frequency data set for inversion methods tests. In this paper, we carry out full-waveform inversion tests using the Hussar low-frequency data set.

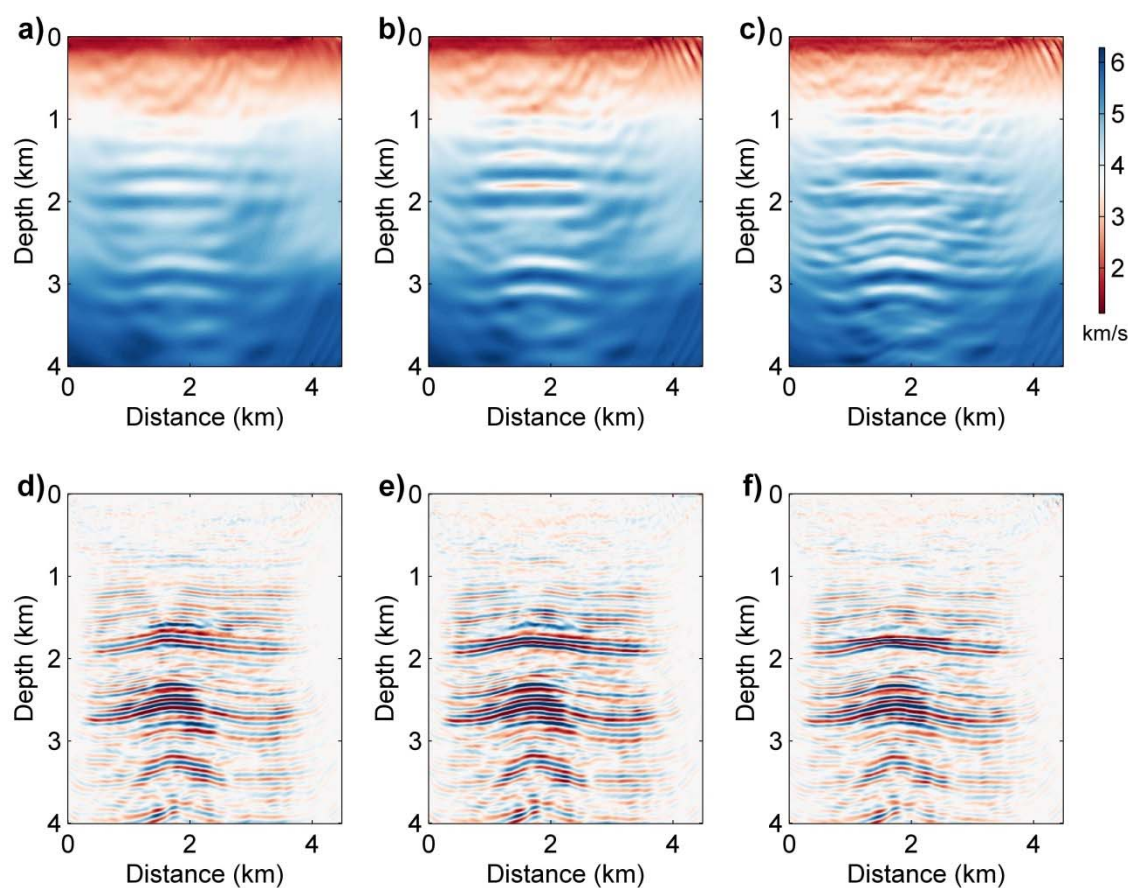


FIG. 1. (a), (b) and (c) show the inversion results at 4th, 6th and 10th iterations. (d), (e) and (f) show the reverse time migration images using the corresponding inverted models.

Preconditioning for the Hessian-free Gauss-Newton full-waveform inversion

Wenyong Pan, Kristopher Innanen, Wenyuan Liao

ABSTRACT

Full-waveform inversion (FWI) has emerged as a powerful strategy for estimating the subsurface model parameters by iteratively minimizing the difference between the synthetic data and observed data. The gradient-based methods promise to converge globally but suffer from slow convergence rate. The Newton-type methods provide a quadratic convergence, but the computation, storage and inversion of the Hessian are beyond the current computation ability for large-scale inverse problem. The Hessian-free (HF) optimization method represents an attractive alternative to these above-mentioned optimization methods. At each iteration, it obtains the search direction by approximately solving the Newton linear system using a conjugate-gradient (CG) algorithm with a matrix-free fashion. One problem of the HF optimization method is that the CG algorithm requires many iterations. The main goal of this paper is to accelerate the HF FWI by preconditioning the CG algorithm. In this research, different preconditioning schemes for the HF Gauss-Newton optimization method are developed. The preconditioners are designed as Hessian approximations (e.g., diagonal pseudo-Hessian and diagonal Gauss-Newton Hessian) or its inverse approximations. We also developed a new pseudo diagonal Gauss-Newton Hessian approximation for preconditioning based on the reciprocal property of the Green's function. Furthermore, a quasi-Newton l-BFGS inverse Hessian approximation preconditioner with the diagonal Hessian approximation as initial guess is proposed and developed. Several numerical examples are solved to demonstrate the effectiveness of the preconditioning schemes. It is concluded that the quasi-Newton l-BFGS preconditioning scheme with the pseudo diagonal Gauss-Newton Hessian as initial guess shows the best performances in speeding up the HF Gauss-Newton FWI, improving the convergence rate and reducing the computation burden.

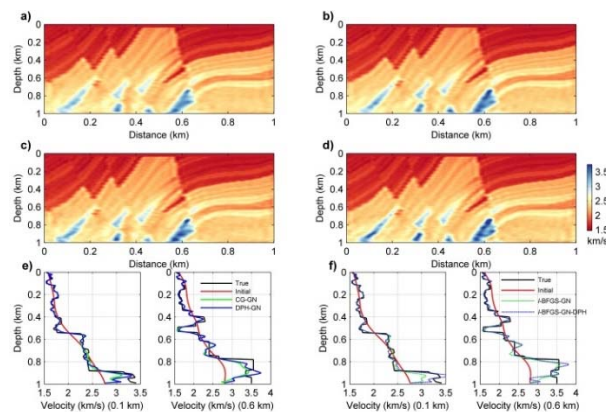


FIG. 1. (a) CG-GN method ($\phi = 4.1e-3$); (b) l-BFGS-GN method ($\phi = 1.1e-3$); (c) DPH-GN method ($\phi = 4.4e-3$); (d) l-BFGS-GN-DPH method ($\phi = 1.1e-3$); (e) and (f) show the comparison of well log data at 0.1 km and 0.6 km. In (e), the green and blue lines indicate the inverted models by CG-GN and DPH-GN methods. In (f), green-dash and blue-dash lines are the inverted models by l-BFGS-GN and l-BFGS-GN-DPH methods.

Recover low-frequency for full-waveform inversion via band-limited impedance inversion and projection onto convex sets

Wenyong Pan, Kristopher Innanen, Gary Margrave, Scott Keating

ABSTRACT

Full-waveform inversion (FWI) provides high-resolution estimates of the subsurface properties by iteratively minimizing an l_2 norm misfit function, which measures the difference between the modelled data and observed data. FWI suffers from cycle-skipping difficulty arising from inaccurate initial model and lack of low frequency information in the seismic data. In this paper, we aim at recovering low frequency information from well log data through band-limited impedance inversion. Projection-onto-convex-sets (POCS) algorithms are generally used to infill the missed traces in seismic data reconstruction. In this paper, we also consider to recover the low frequency information by spectral extrapolation with POCS algorithm. The reflectivity estimate is first generated. The frequency spectrum is then extrapolated with POCS algorithm. The band-limited impedance inversion is then performed with the reflectivity section and interpolated well log data. Through this process, we build an enhanced initial model for full-waveform inversion with low frequency information. We illustrate with numerical examples that the inversion results can be improved with the enhanced initial velocity model.

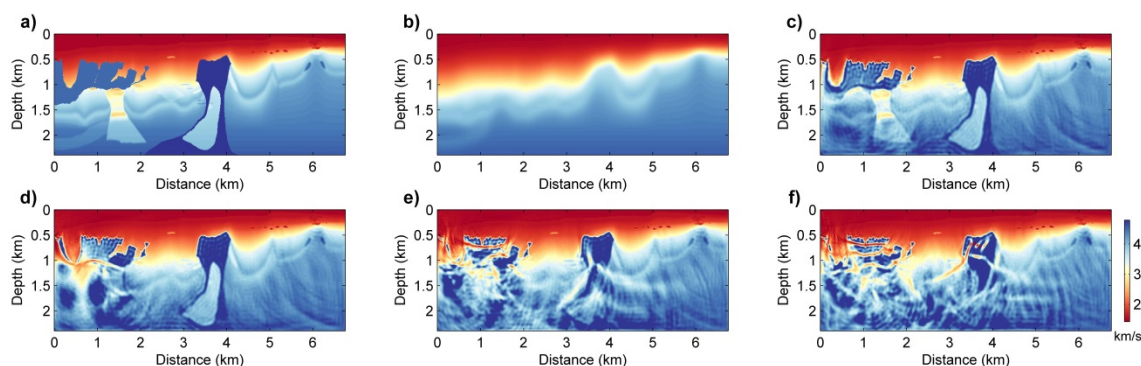


FIG. 1. (a) The true P-wave model; (b) The initial P-wave model; (c) The inverted model with frequency band (1-25 Hz); (d) The inverted model with frequency band (3-25 Hz); (e) The inverted model with frequency band (6-25 Hz); (f) The inverted model with frequency band (8-25 Hz).

Source-independent Hessian-free Gauss-Newton full-waveform inversion

Wenyong Pan, Kristopher Innanen

ABSTRACT

Full-waveform inversion (FWI) is a powerful and promising technique for estimating the subsurface model parameters by minimizing an l_2 norm misfit function which measures the difference between the modelled data and observed data. While FWI still suffers from a lot of difficulties, one of which being the lack of source information. The estimation of source wavelet is important for successful implementation of full-waveform inversion (FWI). Many FWI algorithms estimate the source signature iteratively in the inversion process. In this paper, a source-independent method is adopted with a data calibration process. Furthermore, the gradient-based methods for FWI suffer from slow local convergence rate. A Hessian-free (HF) Gauss-Newton method is implemented in this research by solving the Newton system with a conjugate-gradient (CG) method. The Hessian-free optimization method only needs Hessian-vector products instead of constructing the Hessian matrix explicitly. In this paper, the Hessian operator in HF Gauss-Newton method is modified by combining with the source-independent strategy. We demonstrate with numerical examples that the proposed strategies can improve the convergence rate and reduce the computational burden.

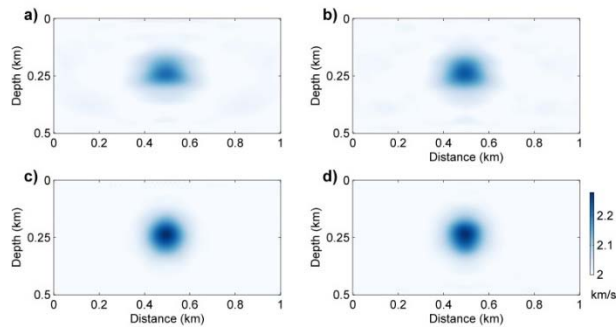


FIG. 1. (a) SD method; (b) L-BFGS method; (c) HF-GN method; (d) SI-HF-GN method.

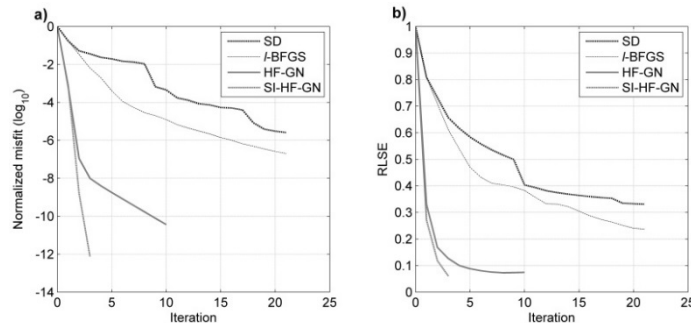


FIG. 2. (a) Normalized misfit (\log_{10}) vs. Iteration; (b) RLSE vs. Iteration. The bold-dash-dot, thin-dash-dot, bold-solid and bold-dash lines indicate SD, L-BFGS, HF-GN and SI-HF-GN methods respectively.

Suppressing cross-talk for elastic FWI with multi-parameter approximate Hessian and its parameter-type approximation

Wenyong Pan*, Kristopher Innanen

ABSTRACT

Full Waveform Inversion (FWI) method becomes popular in recent years for estimating subsurface parameters by iteratively minimizing the difference between the modelled data and observed data. Inverting isotropic and elastic parameters using multi-parameter FWI has been studied by many researchers. While updating multiple parameters is still a challenging problem for increasing the nonlinearity of the inverse problem. One difficulty for multi-parameter FWI is known as cross-talk problem rising from the coupling effects between different physical parameters. It is known that the strong coupling effects between P-wave velocity and density make it difficult to recover density. In this research, we examine the ability of multi-parameter approximate Hessian and its parameter-type approximation in suppressing cross-talk and de-coupling the elastic parameters. We also show that they can be calculated using adjoint-state technique efficiently. Compared to the multi-parameter approximate Hessian, the parameter-type approximation can be inverted trivially and its storage requirement is reduced greatly.

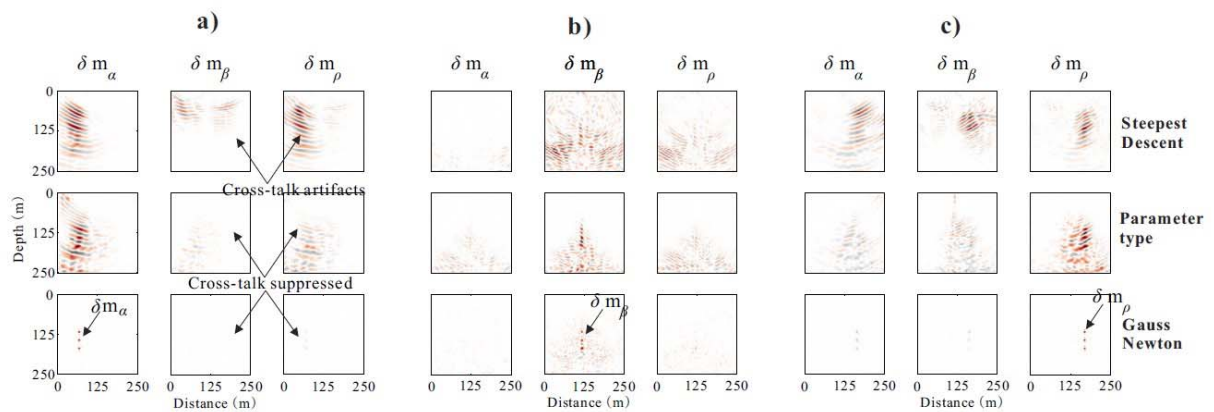


FIG. 1. The estimated model perturbations using steepest descent method (the first row), parameter-type preconditioning method (the second row) and Gauss-Newton method (the third row) with data residuals $\Delta \mathbf{d}_\alpha$ (a), $\Delta \mathbf{d}_\beta$ (b) and $\Delta \mathbf{d}_\rho$ (c) respectively.

Effects of available long offset and random noise on simultaneous-AVO inversion

Sergio Romahn and Kris Innanen

ABSTRACT

The purpose of this work is to understand how the maximum offset available and the level of noise impact together the performance of simultaneous-AVO inversion. A low 30-m-thick gas sand reservoir, with a Class-III AVO anomaly, constitutes the geological framework. The evaluation is focused on the ability of separating the gas reservoir from the background (shale layers and brine sands) in a P- vs S-impedance plot. We took the original logs from the well as reference to measure the root mean square error (RMSE) of the inverted P- and S-impedance logs. The combined error in a P- vs S-impedance crossplot is represented by the multiplication of the inverted P- and S-impedance errors. We plotted the error as a function of noise and maximum angle in order to observe the combined effect of these two factors. Based on the reservoir discrimination, we classified the combined effect of maximum offset available and noise in four categories: best, acceptable, risky and non-acceptable results. The best results are produced with S/N greater than 7 and maximum angles between 40 and 45 degrees. Acceptable results arise for a S/N between 3 and 7 and maximum angles greater than 30 degrees; and with maximum angles between 30 and 40 with S/N greater than 7. Risky results are produced with S/N lower than 3 and angles smaller than 30 degrees. The results are not acceptable if we have maximum angles of incidence smaller than 25 degrees. We also observed that angles greater than 45 degrees may deteriorate the inversion result.

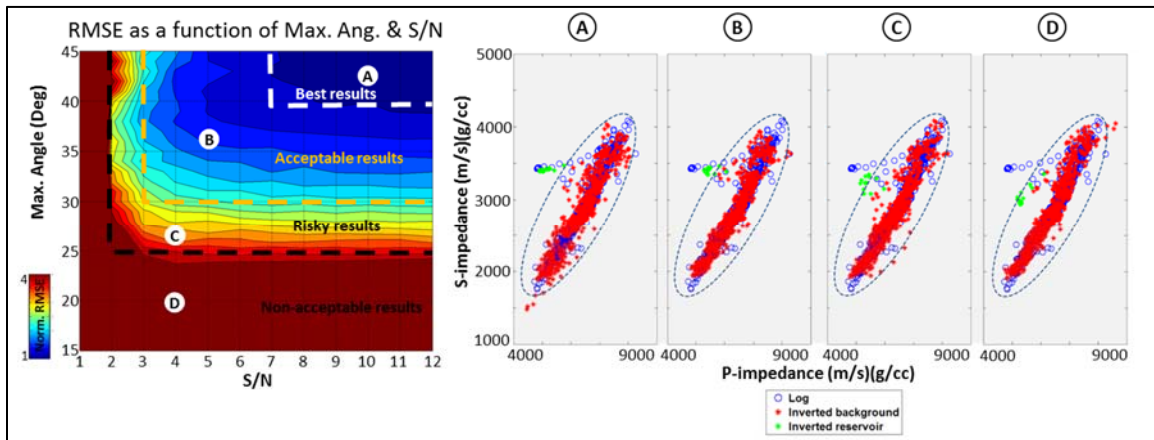


FIG. 1. Combined RMSE of inverted S- and P- impedances (on the left). Four zones were defined based on the reservoir discrimination. Examples of P-vs S-impedance plots from the four zones are shown on the right.

Repercussions of available long offset, random noise and impedance contrast on AVO analysis

Sergio Romahn and Kris Innanen

ABSTRACT

The amplitude variation with offset (AVO) or angle of incidence (AVA) is sensible to several factors that may affect the feasibility of doing this kind of analysis. This work measures how the available long offset, level of random noise and impedance contrast affect the estimation of the AVO parameters (intercept, gradient and curvature). A low impedance oil sand, with a class-III AVO anomaly, constitutes the geological framework. Fluid replacement modelling was used in order to extent the analysis to three different impedance contrast scenarios: gas, oil and water filling the pore space. Firstly, we analyzed the AVO response with no noise and offsets related to angle of incidence up to 45 degrees. This case was taken as reference to measure the error and standard deviation in the AVO-parameter estimation when decreasing the available offset and varying the level of noise. The results show that the intercept is minimally impacted by the reduction of offset and is slightly affected by the level of noise. On the other hand, the gradient and curvature are strongly affected by these two factors, being the curvature the most affected. When comparing the gas, oil and water scenarios, we observe that the error increases as the impedance contrast decreases. This information may be relevant when designing a seismic survey or for time-lapse seismic studies.

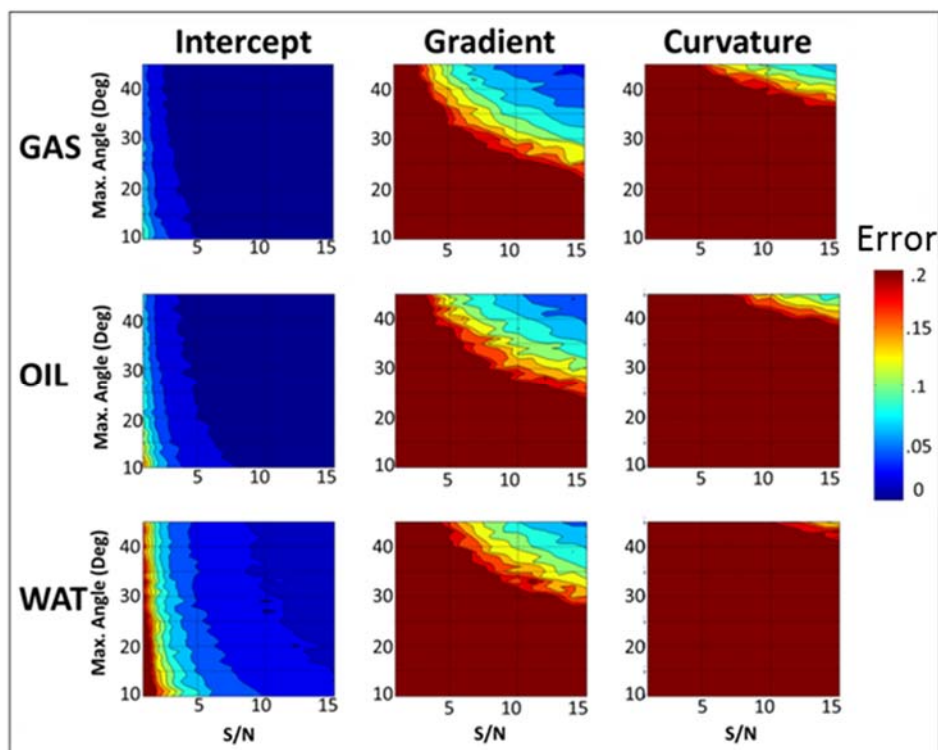


FIG. 1. Concurrent error produced by noise and maximum available angle (or offset) in AVO-parameter estimation for gas, oil and water scenarios. We applied a cut-off of 20%, the smallest error that produces stable estimations.

Predicting heavy oil viscosity from well logs - testing the idea

Eric A. Rops* and Laurence R. Lines

ABSTRACT

Viscosity is a critical parameter in selecting the best recovery method to exploit a heavy oil reservoir. While heavy oil viscosities can be measured in the lab from well samples, it would be very useful to have a method to reliably estimate heavy oil viscosity from well logs. In this study, data from thirteen wells were obtained from the Athabasca region of northern Alberta. Each well has laboratory oil viscosity measurements, as well as dipole sonic logs, and a full suite of the standard well log curves.

Multi-attribute analysis enables a target attribute to be predicted using other known attributes. In this study, the available well log curves were used to predict viscosity. Five wells were used to train the relation to blindly predict the viscosity of the remaining wells. Four out of the seven remaining wells successfully predicted the viscosity comfortably below an error bound of 25%. The remaining three wells predicted the viscosity above the error bound of 25%. It was found that the shear sonic is the most important viscosity predictor. Further observations suggested that viscosity predictions are most accurate when there is separation between the deep, medium, and shallow resistivity curves.

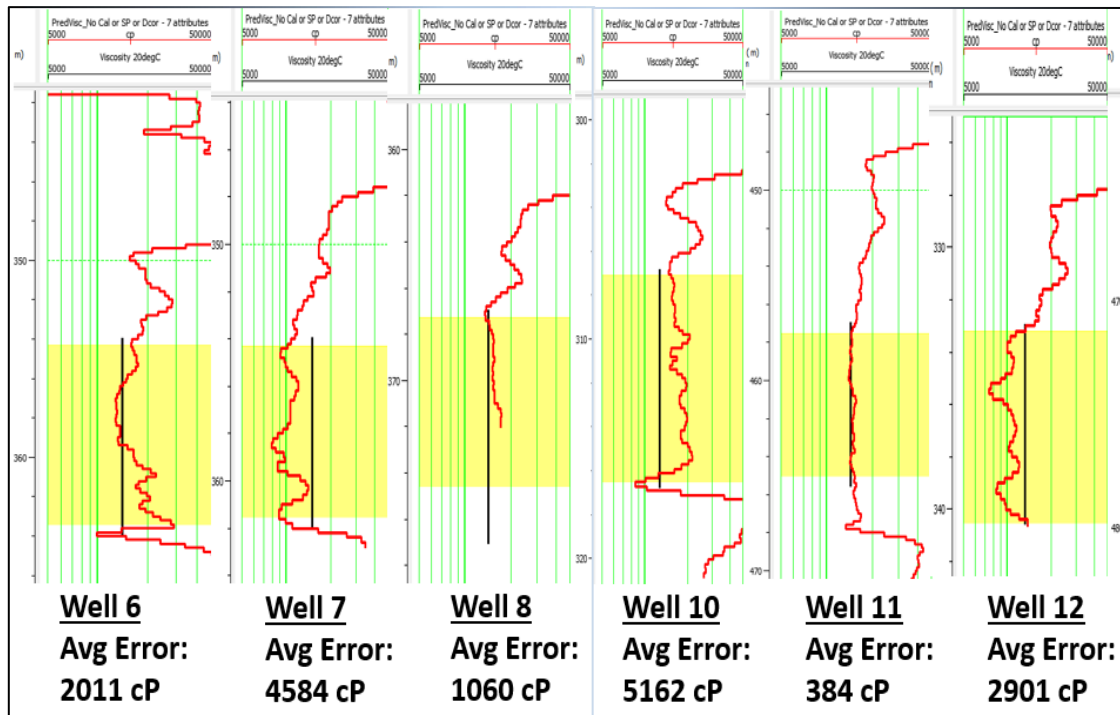


FIG. 1. Blind viscosity prediction results displayed on a logarithmic scale from 5,000 to 50,000 cP. The black lines are the viscosity lab-measured values and the red curves are the predicted viscosities. Note that the black lines (true viscosities) only cover the producing depth intervals highlighted in yellow, which is the only interval we care about.

Predicting oil sands viscosity from well logs using an industry provided dataset

Eric A. Rops and Laurence R. Lines

ABSTRACT

This study is an expansion of the work the first author did in the previous CREWES report (Rops & Lines 2015), where it was demonstrated that heavy oil viscosity could be predicted directly from well logs within 25% error using a limited dataset. To further explore this idea, Nexen – CNOOC has generously provided viscosity data from their Long Lake and Kinosis oil sands development projects, with multiple measurements per well.

Multi-attribute analysis enables a target attribute (viscosity) to be predicted using other known attributes (the well logs). In the Long Lake area, *P-wave sonic* and *Density porosity* were used to predict viscosity and the average validation error was 147,000cP, or 19% of the total viscosity range. In the Kinosis area, *medium resistivity*, *gamma ray*, and *P-wave sonic* were used to predict viscosity and the average validation error was only 70,000 cP, or 13% of the total viscosity range. Figure 1 shows the prediction results for two wells in Kinosis, plotted alongside the logs used in the viscosity prediction. In the viscosity tracks on the left, the black curves are true viscosities and the red curves are the predicted viscosities.

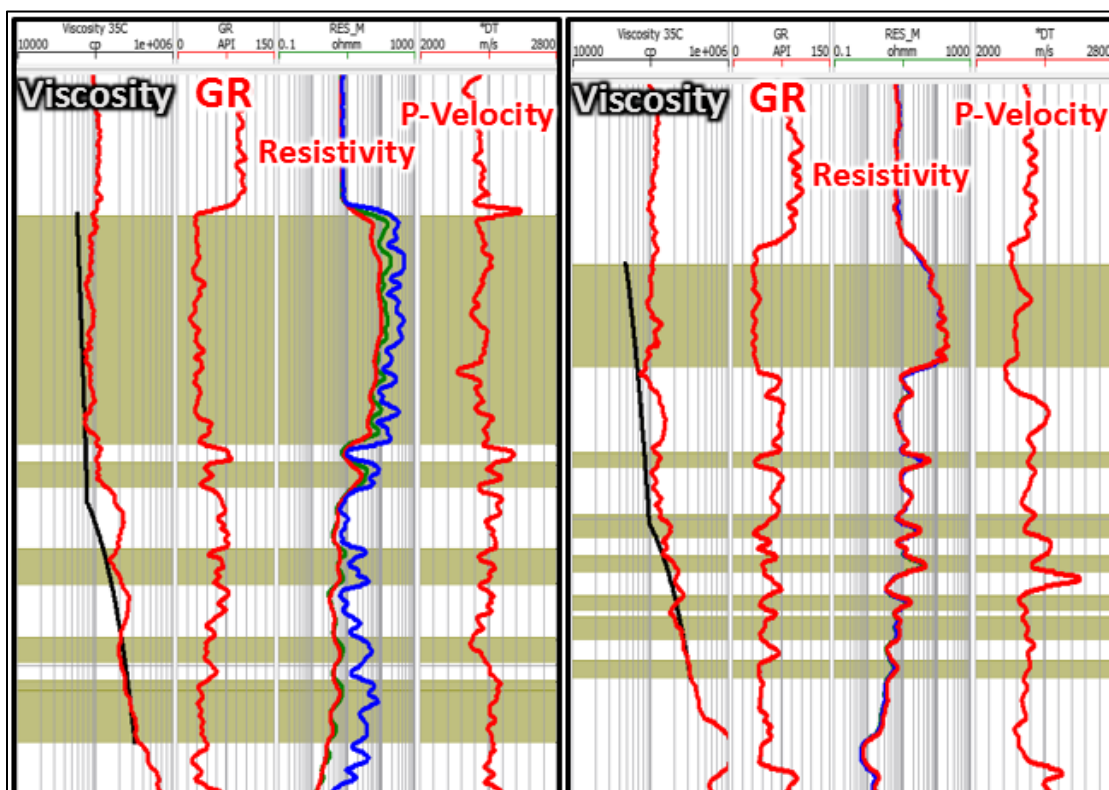


FIG. 1. Viscosity prediction (validation) results for two Kinosis wells. The black curves in the viscosity tracks are the true viscosities and the red curves are the predicted viscosities. The logs used to predict viscosity are also plotted. The yellow areas highlight the reservoir intervals.

Visualizing inversion results with rock physics templates

Brian Russell*¹

ABSTRACT

In this report, I discuss several new approaches for linking rock physics to the seismic reservoir characterization process. I will first discuss a deterministic rock physics approach and show how we can project the results of rock physics modeling onto a cross-plot of V_P/V_S ratio versus P-impedance that has been extracted from the results of simultaneous pre-stack seismic inversion. From this cross-plot interpretation we can then project the results directly onto the seismic volume itself. Having identified the hydrocarbon zone using this deterministic approach I will then discuss a statistical clustering and classification approach applied to the data cross-plot which will allow us to develop a probabilistic interpretation of the extent of the hydrocarbon anomaly. This approach will go beyond the normal approach using bivariate Gaussian pdf functions and will introduce the concept of mixture-Gaussian pdfs. As with the deterministic method, the pdf classification functions can then be projected onto the seismic volume. I will illustrate the various approaches with examples from a gas sand example in Alberta. The figures below illustrate the mixture-Gaussian approach.

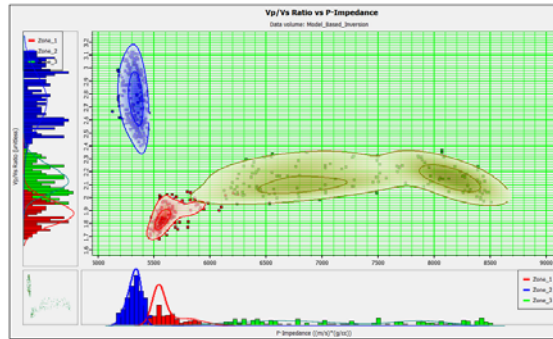


FIG. 1. Mixture-Gaussian pdfs applied to wet sand (blue), gas sand (red) and cemented sand (green) clusters.

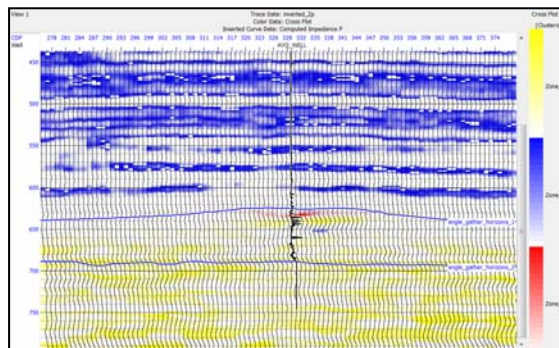


FIG. 2. Probabilistic interpretation of the three sand types from Figure 1 projected onto the seismic section.

¹ Hampson-Russell, A CGG Company, Calgary, Alberta, brian.russell@cgg.com

1.5D internal multiple prediction: physical modelling results

Jian Sun, Kristopher A.H. Innanen, Pan Pan

ABSTRACT

There are few obstacles of seismic processing remain to be solved, multiple elimination is one of them. Inverse scattering series algorithm has been verified theoretically as a wise way to eliminate internal multiples both for marine and land datasets. In this paper, we presented internal multiple predictions in plane wave domain using inverse scattering series on synthetic and physical modeling data generated in marine environment. The physical modeling experiment indicates that this algorithm can be efficient and reliable of internal multiple prediction on real seismic marine dataset. Spiking deconvolution would be suggested before internal multiples attenuation applied based on the discussion of the influence of wavelet reverberation. And the synthetic test demonstrates that plane wave domain algorithm has a good ability for internal multiple prediction on thin-layer case. Those results exemplified the relevant and practical benefits can be achieved using inverse scattering series algorithm in plane wave domain.

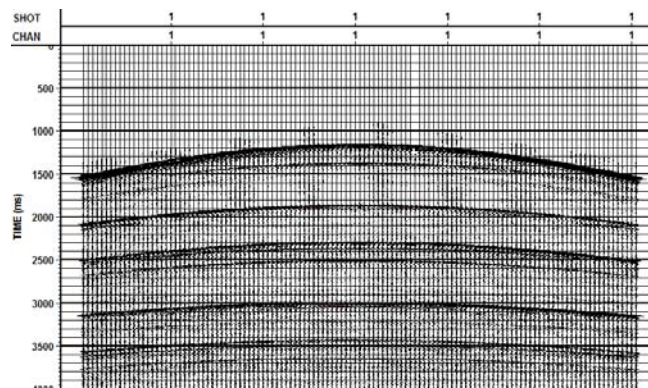


FIG. 1. Physical modelling data after direct muting, AGC, bandpass filter of 10-20-70-90 Hz, and spiking deconvolution of operator length 80ms.

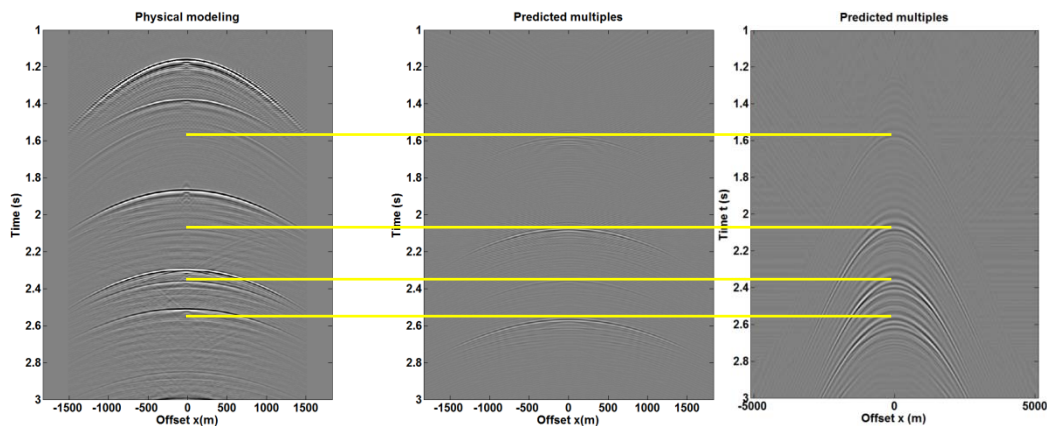


FIG. 2. Physical modelling data, predicted internal multiples on physical modelling data and on synthetic data using plane wave inverse scattering series algorithm. Four first order internal multiple are indicated in yellow at zero-offset traveltimes.

2D internal multiple prediction in coupled plane wave domain

Jian Sun*, Kristopher A.H. Innanen

ABSTRACT

Internal multiples can be constructed by primary events based on inverse scattering series (ISS) algorithm. More benefits can be achieved in plane wave domain, such as improved numerical accuracy, no large offset artifacts, and less computing time. In view of that, the plane wave domain ISS algorithm can be a promising way to eliminate internal multiples on a full 2D case. We presented 2D internal multiple predictions using ISS algorithm in coupled plane wave domain. The coupled $\tau - p_g - p_s$ transform offers a straightforward approach to obtain the input. Some preliminary results are achieved and further research is ongoing. Be that as it may, those preliminary results still exemplify ISS algorithm in the coupled plane wave domain can provide much more relevant and practical profits.

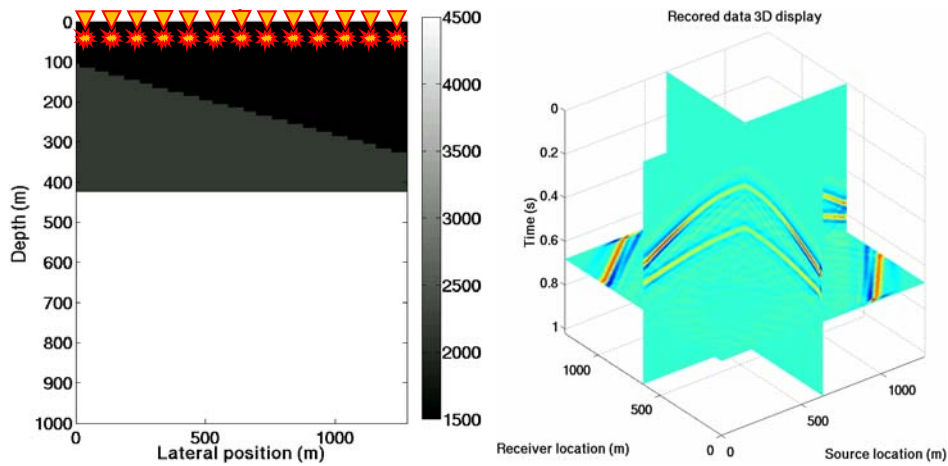


FIG. 1. Velocity model and 3D views of 128 shot gathers in source-receiver coordinates

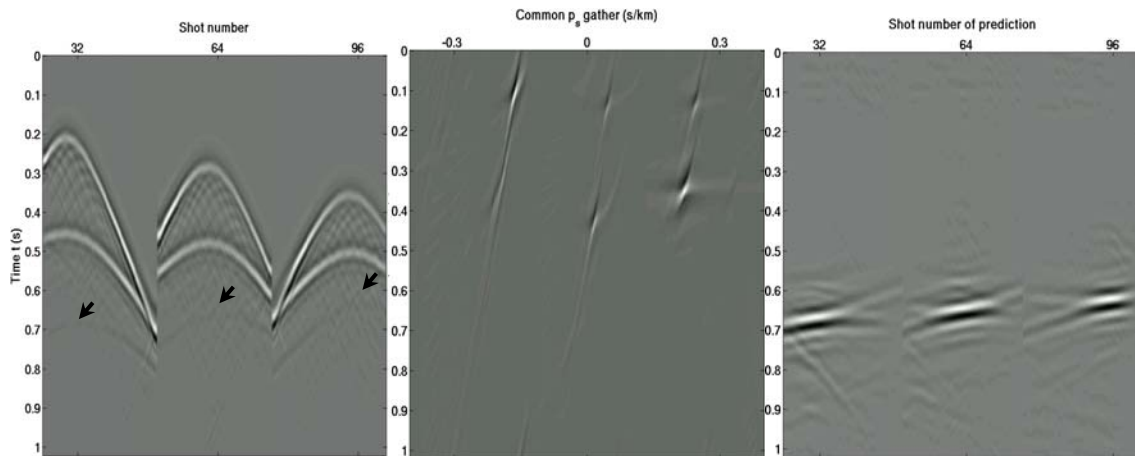


FIG. 2. Shot gathers shown in (p_s, p_g, τ) domain (left) and (x_s, x_g, t) domain (medium). Prediction of shot gathers at same location.

AVO inversion with a combination of series reversion and Gauss-Newton iteration

Jian Sun, Kristopher A.H. Innanen

ABSTRACT

Fluid-property discrimination is always an important goal we desired in seismic exploration, and one of interested ways to achieve that is related to AVO/AVA analysis. Several non-linear AVO/AVA approximations were derived directly from Zoeppritz equation with the comparison discussed. Non-linear AVO inversion with a combination of series reversion and Gauss-Newton iteration is introduced at the end of the paper, and one of those approximations we derived is applied into non-linear AVO inversion on synthetic data using well-log. Ultimately, the comparison between non-linear inversion method and linear inversion was discussed.

$$R_{pp}^{(1)} = A_1 d_M + B_1 d_\mu + C_1 d_\rho;$$

$$R_{pp}^{(2)} = A_2 d_M^2 + B_2 d_\mu^2 + C_2 d_\rho^2 + D_{M\mu} d_M d_\mu + D_{M\rho} d_M d_\rho + D_{\mu\rho} d_\mu d_\rho;$$

$$R_{pp}^{(3)} = A_3 d_M^3 + B_3 d_\mu^3 + C_3 d_\rho^3 + D_{2M\mu} d_M^2 d_\mu + D_{M2\mu} d_M d_\mu^2 + D_{2M\rho} d_M^2 d_\rho$$

$$+ D_{M2\rho} d_M d_\rho^2 + D_{2\mu\rho} d_\mu^2 d_\rho + D_{\mu2\rho} d_\mu d_\rho^2 + D_{M\mu\rho} d_M d_\mu d_\rho;$$

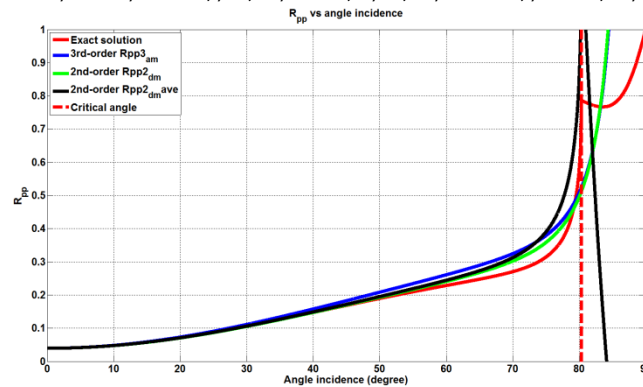


FIG. 1. Comparison of R_{pp} both in perturbation and ratio form in incidence angle.

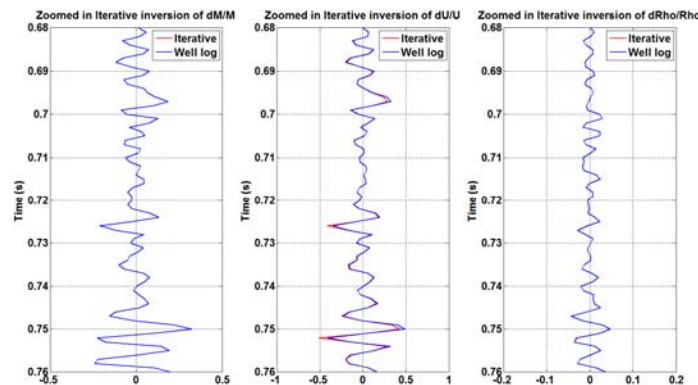


FIG. 2. Inversed P-wave modulus, S-wave modulus and density using non-linear AVO approach

Internal multiple prediction in the tau-p domain: 1.5D synthetic results

Jian Sun, Kristopher A.H. Innanen

ABSTRACT

Internal multiples on land data can be predicted in an efficient way using inverse scattering series approach, and more elegant results could be achieved in plane wave domain than in wavenumber-pseudo depth domain. With a view to the feasibility of this algorithm on land data with thin layers and large offset, we carried out a complex model using Hussar well-log, and implemented 1.5D algorithm with a constant epsilon value in plane wave domain. Two different type taper windows were suggested to remove bright-spot artifacts caused by $\tau - p$ transform. After that, a quite elegant internal multiple predicts is obtained without any large offset artifacts and impacts of thin-layer.

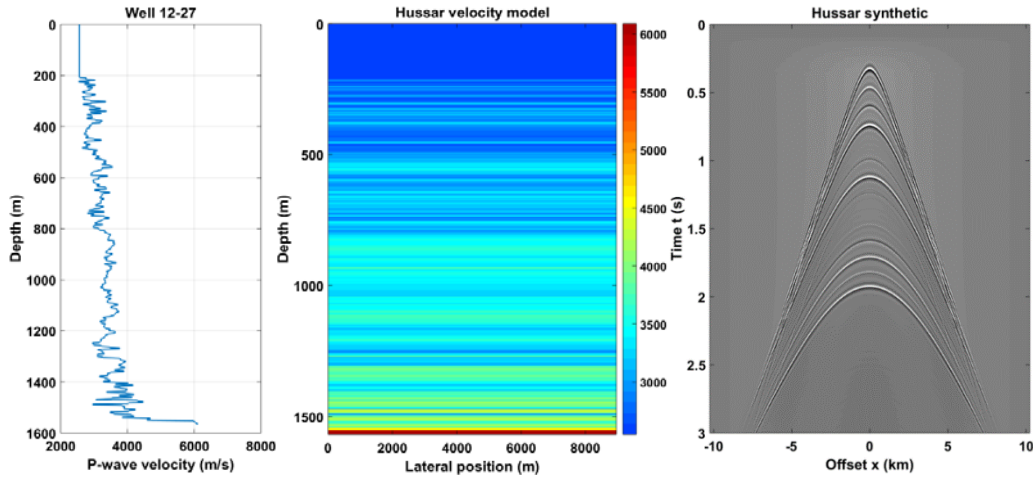


FIG. 1. Sampled well-log of P-wave velocity, 2D velocity model and finite difference synthetic data.

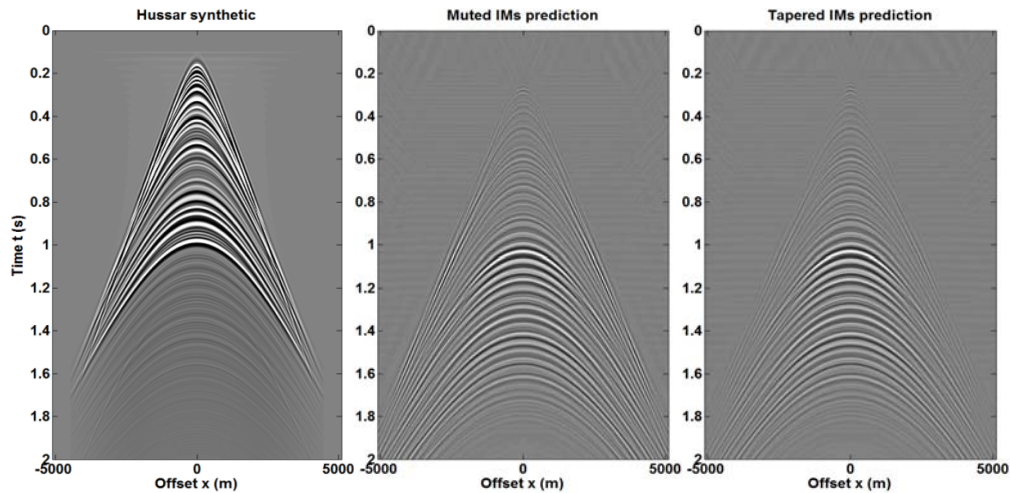


FIG. 2. Comparisons between non-block Hussar synthetic (left), IM predictions with muted directly (medium), and IM predictions with cosine taper (right).

The Borga transform and some applications in seismic data analysis

Todor I. Todorov and Gary F. Margrave

ABSTRACT

Signal transforms form the bases for many seismic data processing and analysis algorithms. We present the adjoint of the Gabor transform, which we call the Borga transform. Figure 1 is a flow chart of the computational steps. The Gabor transform uses the operations of first windowing and then Fourier transform while the Borga transform reverses the order so that the window is applied in the frequency domain. The result is a real-valued time-frequency decomposition that is essentially a complete set of filter slices. When summed, the frequency slices exactly recreate the original signal.

The Borga transform can be used in a various processing steps. Since surface noise is predominantly low-frequency and high-amplitude, one can separate it from the signal in a raw shot gathers. Other types of noise can have a band-limited nature and anomalous amplitudes as well. By assuming local linear behavior of the amplitudes in a CMP NMO-corrected gathers, we can design a noise attenuation algorithm, based on Borga frequency slices. The process can lead to better results in AVO analysis and inversion. The transform can be a natural choice for time-variant spectral whitening as well. By applying an amplitude gain function to frequency slices, one can compensate for time and frequency dependant amplitude attenuation.

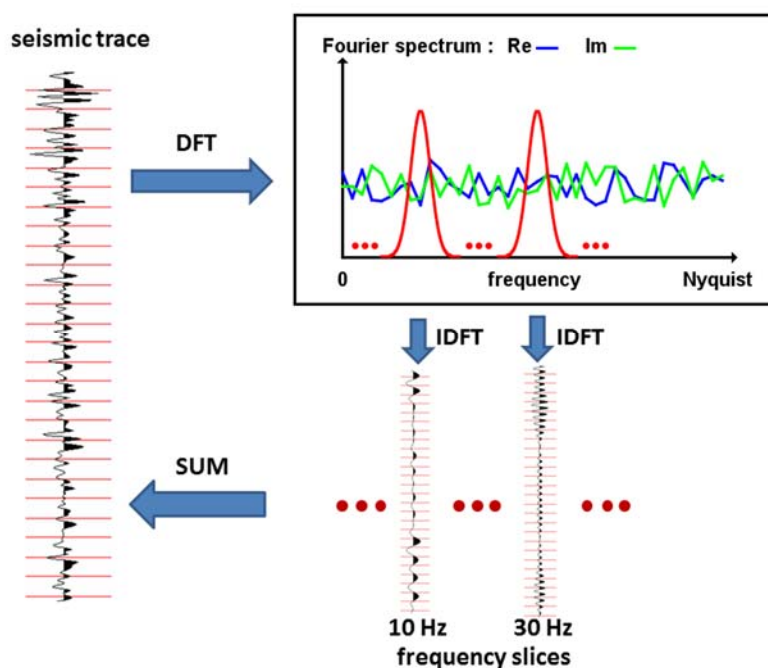


FIG. 1. Flow chart of the Borga transform. A seismic trace can be decomposed into frequency slices by performing DFT, windowing the complex spectrum with a Gaussian window and applying IDFT. The inversed Borga transform is performed by summing all the frequency slices.

Field and numerical investigation of filtered m-sequence pilots for vibroseis acquisition

Joe Wong and David Langton

ABSTRACT

We conducted field tests to evaluate the effectiveness of time-domain filtered m-sequences used as pilots for driving land vibrators in simultaneous multi-sourcing. Common-source gathers extracted from the blended field data for two and four simultaneous vibrators indicate that the time-domain filtered pilots produced seismograms somewhat degraded by crosstalk interference originating from large-amplitude arrivals produced by adjacent and nearby vibrators. We conducted numerical simulations to show that, by carefully filtering pure m-sequences in frequency domain instead of in time domain, we obtain an improved set of quasi-orthogonal pilots for which crosstalk interference is reduced. The improvement comes from retaining as much spectral energy as possible between 4 and 250 Hz.

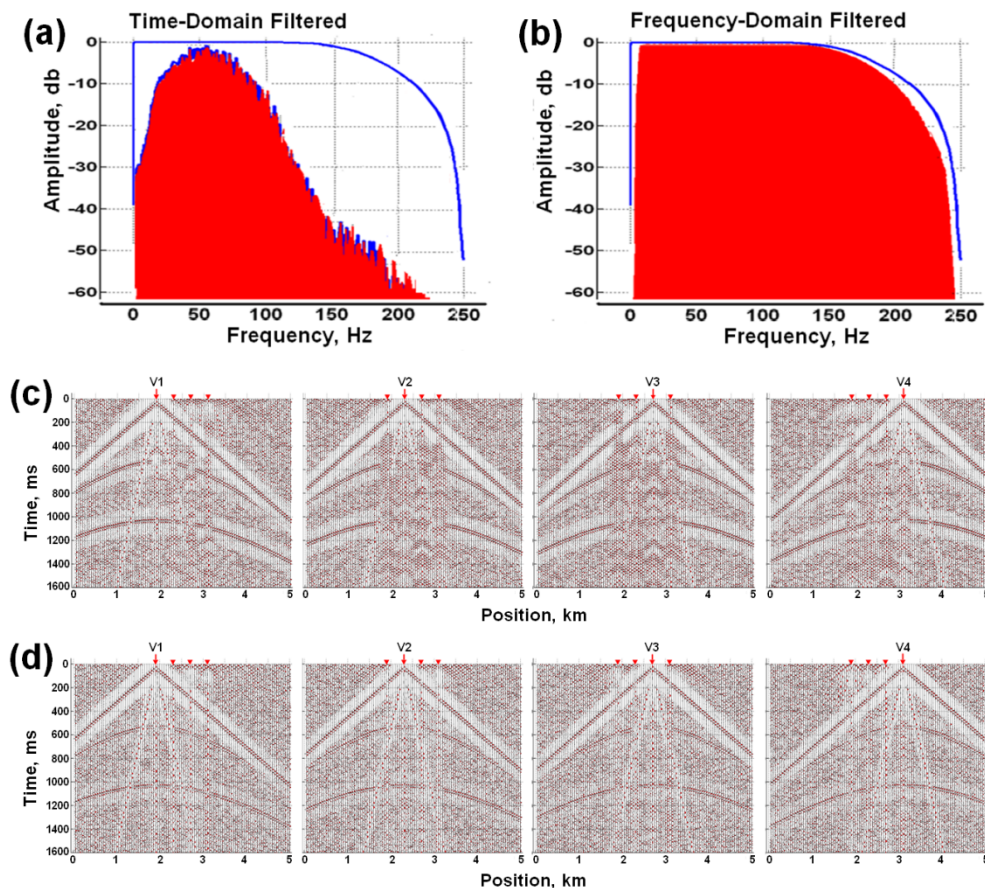


FIG. 1. (a) Spectrum of time-domain filtered m-sequences; (b) spectrum of frequency-domain filtered m-sequences. Extracted CSGs from numerical simulations of four-vibrator simultaneous sourcing using m-sequences pilots filtered in (c) time domain; (d) filtered in frequency domain.

Upgrading the CREWES seismic physical modeling facility

Joe Wong*, Kevin Bertram, and Kevin Hall

ABSTRACT

From 2008 to 2015, the CREWES Seismic Physical Modeling Facility utilized acquisition software and hardware that executed under the Windows XP operating system. With Windows XP no longer being supported, CREWES has taken the prudent step of upgrading software and hardware to be compatible with the replacement operating systems (i.e., Windows 7, 8, and/or 10). Also, the growing emphasis in industry on high-resolution 3D surveys motivated us to add capabilities enabling the completion of physically-modeled 3D surveys within reasonable time frames. To this end, we replaced the old single-channel A/D module with faster two- and eight-channel A/D modules. Employing multi-channel data acquisition as well as multiple source transducers firing simultaneously (supported by efficient post-survey deblending algorithms), the upgraded modeling facility is expected to be able to complete a 3D survey with over 10 million deblended seismograms within 240 hours.

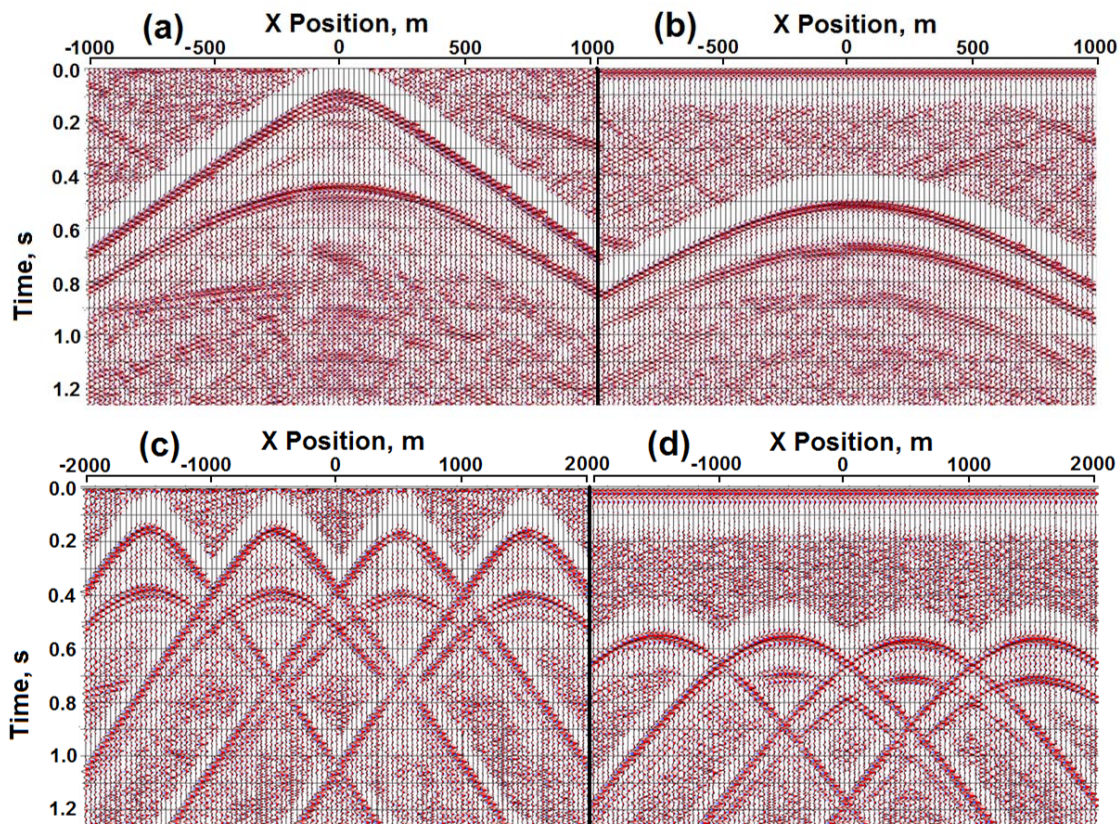


FIG. 1. Common source gathers for two receiver lines, recorded with upgraded two-channel A/D module. Single source acquisition, receiver line offset = (a) 140m; (b) 740m. Simultaneous four-source acquisition, receiver line offset = (c) 200m; (d) 800m.

Interpretation of a multicomponent walkaway vertical seismic profile data

Bona Wu*, Don C. Lawton, and Kevin W. Hall

ABSTRACT

A multicomponent walkaway VSP data was processed to study the AVO response. Inversion and AVO modeling were conducted on PP wave data. The data show a Class I AVO response at the top of reservoir and a Class IV water-sand AVO response at the bottom of the study reservoir. There were no obvious gas effects in the study interval. The observations were validated by production data. Post stack PP-PS joint inversion was completed and compared to only P-wave inversion. Overall, they showed good consistency and the joint inversion added value to lithology prediction and fluid identification. This case study demonstrated that the multicomponent VSP is an effective tool to predict rock properties, characterize the reservoir and monitor production.

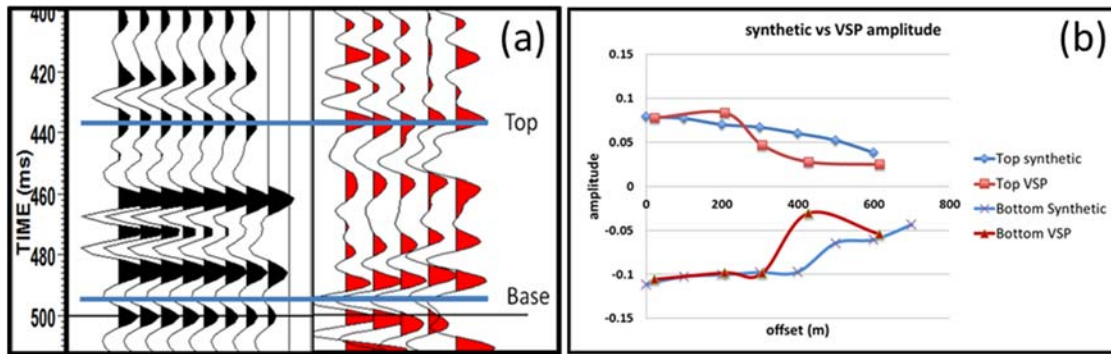


FIG. 1. (a) Tie of synthetic offset gather (shown in black) and VSP reflectivity gather (shown in red). Top and base of the target reservoir are picked and highlighted by blue lines. (b) AVO responses at the top and base of the study reservoir. Red lines are amplitudes from VSP and blue lines are amplitudes from synthetic seismogram.

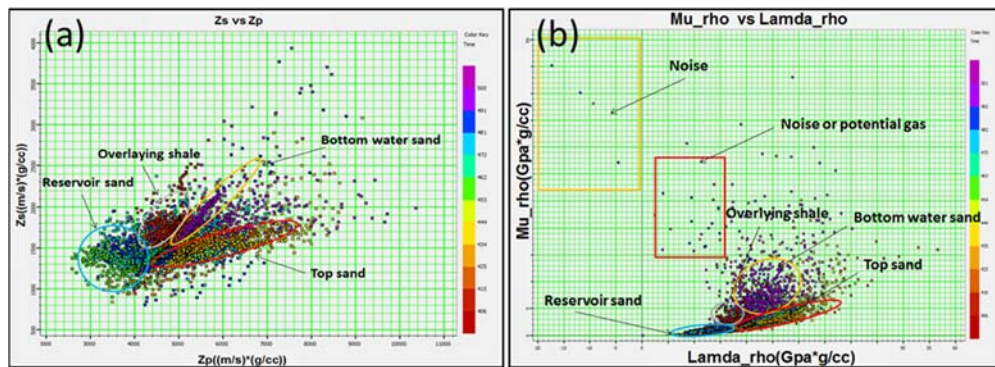


FIG. 2. (a) Crossplot of Z_s vs Z_p inverted from Joint PP-PS inversion. (b) Crossplot of μ_{ρ} vs λ_{ρ} .

Porosity prediction using cokriging with multiple secondary datasets

Hong Xu*, Jian Sun, Brian H. Russell, and Kris A. Innanen

ABSTRACT

Porosity is always a productive indicator for hydrocarbon detection, oil and gas exploration, and many useful algorithms, such as multiple attributes analysis and cokriging porosity prediction, has been developed to implement the porosity prediction in subsurface. Somewhat differently of multiple attributes analysis, the porosity prediction using cokriging algorithm might be more effective and accuracy by combining the well-log data and seismic attribute. However, the traditional cokriging porosity estimation system only involves one seismic attribute with well-log data, which might get us in trouble as we know that the porosity are related to more than one seismic attribute. To solve that and improve the accuracy of prediction, we develop a new cokring system with more than one seismic attribute involved during the estimation. The Blackfoot seismic data from Alberta is applied into the new cokriging system and the final estimation map is encouraging. Finally, the Leave-one-out cross-validation is employed to evaluate the accuracy of porosity prediction both for the traditional cokriging and the new cokriging algorithm. Compared to the traditional cokriging, an improved predicted result with higher lateral resolution and decreased error can be obtained using the new cokriging algorithm. We believe that the new cokriging system can be considered for porosity prediction.

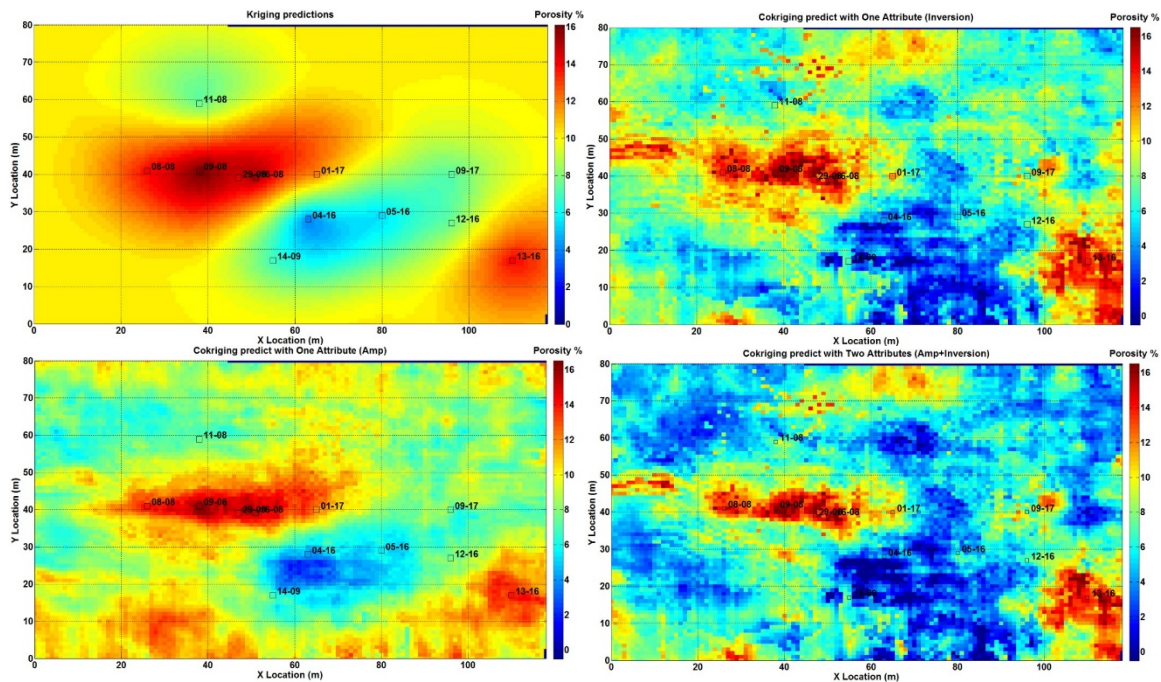


FIG. 1. Porosity predictions using kriging or cokriging. Kriging result is shown in upper left panel. Traditional cokriging results with amplitude slice or impedance slice are shown in upper right and lower left respectively. Prediction using new cokriging system with amplitude and impedance slices are shown in lower right panel.

Explosion source data analysis from a Jordanian quarry

Matthew Yedlin^{*1}, Gary F. Margrave², and Yochai Ben Horin³

ABSTRACT

This seismic case study is a preliminary analysis of a unique seismic data set of 1805 quarry blasts detonated in a phosphate quarry of the Jordan Phosphate Mines Company (JPMC). Three component recordings of these blasts at the broadband station, HRFI, Israel, are analyzed to determine source similarity. Presented herein are the singular value decomposition and reconstruction of the z component of the recorded data. The noisy quality of the original records is evident in the reconstruction, as the L2 norm of the reconstruction error has the same log-linear dependency as the singular value spectrum.

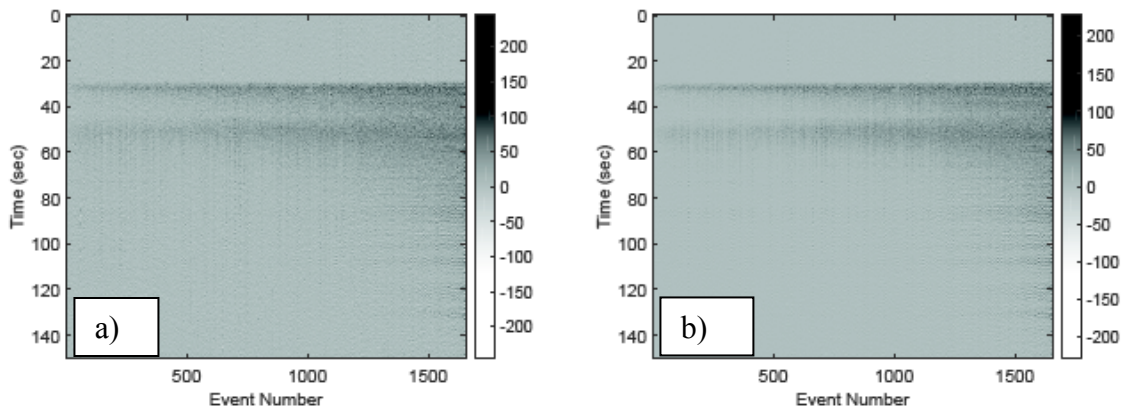


FIG. 1. a) Z component of 1654 quarry blasts. b) Reconstruction of the Z component using 10% of the singular values.

¹ Department of Electrical and Computer Engineering, UBC

² Geoscience, University of Calgary

³ SOREQ, Yavneh, Israel